INFORMATION TO USERS

This manuscript has been reproduced from the microfilm master. UMI films the text directly from the original or copy submitted. Thus, some thesis and dissertation copies are in typewriter face, while others may be from any type of computer printer.

The quality of this reproduction is dependent upon the quality of the copy submitted. Broken or indistinct print, colored or poor quality illustrations and photographs, print bleedthrough, substandard margins, and improper alignment can adversely affect reproduction.

In the unlikely event that the author did not send UMI a complete manuscript and there are missing pages, these will be noted. Also, if unauthorized copyright material had to be removed, a note will indicate the deletion.

Oversize materials (e.g., maps, drawings, charts) are reproduced by sectioning the original, beginning at the upper left-hand corner and continuing from left to right in equal sections with small overlaps. Each original is also photographed in one exposure and is included in reduced form at the back of the book.

Photographs included in the original manuscript have been reproduced xerographically in this copy. Higher quality 6" x 9" black and white photographic prints are available for any photographs or illustrations appearing in this copy for an additional charge. Contact UMI directly to order.

University Microfilms International
A Bell & Howell Information Company
300 North Zeeb Road, Ann Arbor, MI 48106-1346 USA
313/761-4700 800/521-0600

Order Number 9302206

Femtosecond and quasi-steady-state optical nonlinear physics of GaAs/AlAs type-II quantum wells

Fu, Winston Su-Kee, Ph.D.

Stanford University, 1992

Copyright ©1992 by Fu, Winston Su-Kee. All rights reserved.

U·M·I
300 N. Zeeb Rd.
Ann Arbor, MI 48106

FEMTOSECOND AND QUASI-STEADY-STATE OPTICAL NONLINEAR PHYSICS OF GaAs/AlAs TYPE-II QUANTUM WELLS

A DISSERTATION

SUBMITTED TO THE DEPARTMENT OF APPLIED PHYSICS

AND THE COMMITTEE ON GRADUATE STUDIES

OF STANFORD UNIVERSITY

IN PARTIAL FULFILLMENT OF THE REQUIREMENTS

FOR THE DEGREE OF

DOCTOR OF PHILOSOPHY

by

Winston Su-Kee Fu

August 1992

© Copyright by Winston S. Fu 1992

All Rights Reserved

I certify that I have read this dissertation and that in my opinion it is fully adequate, in scope and quality, as a dissertation for the degree of Doctor of Philosophy.

James S. Harris, Jr. **(Principal Advisor)**
James and Ellenor Chesebrough Professor
of Electrical Engineering

I certify that I have read this dissertation and that in my opinion it is fully adequate, in scope and quality, as a dissertation for the degree of Doctor of Philosophy.

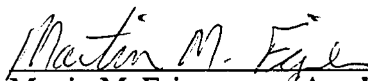

Martin M. Fejer **(Applied Physics)**
Assistant Professor

I certify that I have read this dissertation and that in my opinion it is fully adequate, in scope and quality, as a dissertation for the degree of Doctor of Philosophy.

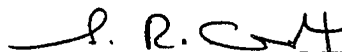

Gregory R. Olbright **(Ph.D.)**
President, Photonics Research Inc.

Approved for the University Committee on Graduate Studies:

Abstract

The linear and nonlinear optical properties of GaAs/AlAs type-II quantum wells (QWs), under femtosecond and continuous-wave excitation are presented in this thesis. The photoluminescence (PL) spectra in type-II QWs exhibit an additional line due to the radiative recombination of spatially separated electrons and holes. This additional information is utilized to develop a new spectroscopic technique which allows a direct measurement of the quantum-confinement energy (QCE) shifts in the valence band, independent of the QCE shifts in the conduction band. The QCE shifts are used to determine the conduction- and valence-band discontinuities without the use of any fitting parameters. In addition, the interfacial roughness responsible for the inhomogeneous broadening of the optical transitions is determined.

The nonlinear optical properties of type-II QWs are dramatically influenced by the spatial separation of the electrons and holes. The nonlinear effects of many-body interactions on the absorption spectrum with femtosecond and nanosecond optical pulses were investigated. Under extremely high excitation conditions, optical gain and an ultrafast nonlinear response in type-II GaAs/AlAs MQWs were observed. In addition, the dependence of the optical gain and absorption nonlinearities on the distribution of electrons between the GaAs and AlAs layers were investigated by applying a longitudinal static electric field.

Acknowledgments

I am grateful to Professor James S. Harris for his patience and enthusiasm as an educator and scientist. I thank him for giving me the freedom to seek out my own path.

I gratefully acknowledge the advice and guidance of Greg Olbright, my experimental advisor at Sandia National Laboratory. Greg is an intense experimentalist and teacher.

I thank Rolf Binder, Ian Galbraith (now at Heriot-Watt University), and Stephan Koch at the Optical Sciences Center (University of Arizona) for their theoretical support. A great deal has been accomplished through our collaboration.

This work would not have been possible without the long-term collaboration between Stanford University and Sandia National Laboratory in Albuquerque. I would like to thank Dr. Del Owyoung for his support of the collaboration and for helping me with my technical writing in the early stages. Special thanks go to John Klem and Tom Brennan for teaching me about MBE. I would also like to thank Rob Bryan, Greg Poirier (presently at NIST), Ken Bacher (Stanford), Herman Chui (Stanford), Raj Apte (Stanford), and Bill Banyai (presently at Stanford).

I would also thank Professor Marty M. Fejer, my academic advisor, for his guidance.

Gail Chun-Creech and Susan Burns deserve special mention for their assistance in working through the red tape.

Finally, I thank my family and friends for their support and encouragement.

I acknowledge the financial support of DARPA Contract Number MDA972-90-C-0046, Sandia National Laboratory under DOE Contract Number DE-ACO4-76DP00789, and the JSEP Fellowship through Army Research Contract Number DAAL03-91-C-0010.

Table of Contents

Page

Abstract....iv

Acknowledgments....v

List of Illustrations....vii

1. Introduction....1

2. Linear Optical Properties of GaAs/AlAs Type-II Quantum Wells....6
- 2.1 Excitons in quantum wells....7
- 2.2 Luminescence and absorption spectra of GaAs/Al(Ga)As type-I and type-II quantum wells....10
- 2.3 Differential Quantum-Confinement Energy Shifts....18
  - (a) Independent determination band discontinuities....22
  - (b) Inhomogeneous broadening due to atomic layer fluctuations....23
- 2.4 Effects of a static longitudinal electric field....27

3. Nonlinear Optical Properties of Quantum Wells....37
- 3.1 Many-body effects....38
- 3.2 Type-II quantum wells: spatially heterogeneous plasma....44
  - 3.2.1 Space-charge effects....44
  - 3.2.2 Generalized Wannier equation....50

4. Transient and Steady-state Spectroscopy....52
- 4.1 Generation of amplified femtosecond optical pulses....53
- 4.2 Quasi-steady-state spectroscopy....58
- 4.3 Differential transmission spectroscopy....59
- 4.4 Single-wavelength time scans....60

5. Nonlinear Absorption: Quasi-Steady-State and Femtosecond Nonlinear Optical Properties of Type-II Quantum Wells....61
- 5.1 Quasi-steady-state absorption nonlinearities....62
- 5.2 Femtosecond nonlinearities in the absorption spectra....72
  - 5.2.1 Hole-plasma cooling in a heterogeneous Fermi gas....72
  - 5.2.2 Effects of a static longitudinal electric field....78

6. Optical Gain and Ultrafast Nonlinear Response in Narrow GaAs/(Al,Ga)As Quantum Wells....85
- 6.1 Gain in narrow type-I GaAs/(AlGa)As quantum wells....85
- 6.2 Gain in type-II GaAs/AlAs quantum wells....90
  - 6.2.1 Effects of AlAs X-valley "reservoir"....91
  - 6.2.2 Effects of a static longitudinal electric field....94
- 6.3 Ultrafast nonlinear optical response: 95

7. Conclusion and Future Work....103

References....105

List of Illustrations

Page

Figure 1.1 Nested (type-I) and staggered (type-II) band alignment....................2

Figure 1.2 Band diagram of a type-II quantum well....................................3

Figure 2.1 Energy band diagram of a type-II quantum well in real space and in momentum space..11

Figure 2.2 Phase diagram for type-I and type-II quantum wells........................13

Figure 2.3 Experimental and fitted absorption spectra for a narrow GaAs/AlAs type-II multiple quantum well samples..........................16

Figure 2.4 Schematic of the two heterojunction interfaces..............................25

Figure 2.5 Schematic of a type-II MQW photodiode. The potential energy diagram of type-II quantum wells in a static longitudinal electric field. Effects of a strong longitudinal electric field on the linear optical properties of type-II quantum wells.................................30

Figure 2.6 Photoluminescence spectra versus applied field strength. Peak position versus applied field strength. Upper and lower voltage of "kink-1" versus excitation power.............33

Figure 2.7 Stark shift of X-like electronic state..35

Figure 3.1 Band bending due to spatial separation of electrons and holes.............45

Figure 3.2 Schematic band diagram of asymmetric type-II QWs in real and momentum space..46

Figure 3.3 Photoluminescence spectra of the asymmetric type-II QW shown in Fig. 3.2..49

Figure 3.4 Schematic band diagram depicting energy shifts due to the Hartree potential and Coulomb exchange-correlation effects................50

Figure 4.1 Block diagram of the femtosecond optical pulse generation system........53

Figure 4.2 Schematic of the Balanced Colliding Pulse Modelocked (CPM) Ring Dye Laser..54

Figure 4.3 Pump/probe experimental configuration......................................56

Figure 4.4 Cross-correlation trace..57

Figure 5.1 Blue shift of the cw PL and absorption in type-II quantum wells in the quasi-steady state....63

Figure 5.2 Nonlinear absorption spectra for three type-II samples having different Γ-X splitting....64

Figure 5.3 Heavy hole blue shift versus excitation power....65

Figure 5.4 Power dependence of the (10/30) sample using 7-*ns* pump and probe pulses....67

Figure 5.5 Absorptive ($\Delta\alpha L$) and dispersive (Δn) changes for the changes in absorption shown in Fig. 5.4....68

Figure 5.6 Low-temperature solutions to the generalized Wannier equation. Density-dependent absorption spectra....72

Figure 5.7 Femtosecond absorption and differential transmission spectra for the (10/30) sample....73

Figure 5.8 Transfer rate diagram....76

Figure 5.9 Temperature-dependent solutions to the generalized Wannier equation...77

Figure 5.10 Temporal behavior of the absorption spectra for the flat-band case and the indirect-to-direct crossover region....79

Figure 5.11 The shift of the heavy-hole exciton before (+200 *fs*) and after (+500 *fs*) electrons have transferred from the GaAs Γ-band to the AlAs X-band....80

Figure 5.12 Solutions to the generalized Wannier equation, where the electrons contribute only to screening....82

Figure 6.1 The femtosecond gain development and decay....87

Figure 6.2 Single-wavelength time scan showing the fit for the 10-*ps* time-constant due to stimulated emission....88

Figure 6.3 Condition for gain in type-II quantum wells....90

Figure 6.4 Comparison of gain in type-I and type-II structures....93

Figure 6.5 Optical gain versus E-field....95

Figure 6.6 Power-dependent single-wavelength time scans....96

Figure 6.7 Temperature-dependent single-wavelength time scans of the type-I sample below and above the unexcited bandgap....97

Figure 6.8 Spatially resolved single-wavelength time scans....99

Figure 6.9 Solutions to the semiconductor Bloch equations....101

1 Introduction

The study of highly excited semiconductors remains one of the most active areas in semiconductor research. During the last decade a number of new optical and transport phenomena, such as the integral and fractional Hall effects, have been discovered in semiconductor heterostructures (a structure made of more than one material; e.g. quantum wells). The application of heterojunction electronic and optical devices (e.g. quantum-well laser diodes, high-electron-mobility transistors, resonant tunnel diodes) continues to grow rapidly. These structures are grown by modern epitaxial techniques, such as molecular beam epitaxy or chemical vapor deposition, which can control semiconductor layer thicknesses to within an atomic monolayer.

In the history of highly excited semiconductors, optical experiments have played a key role, and most of our knowledge in this field is based upon the richness of information provided by these methods. It is the spectral sensitivity combined with the high temporal and spatial resolution which makes optical methods so powerful. Linear spectroscopic techniques, such as absorption and luminescence, are routinely used for material characterization. For example, the energy gap for bound-state and free-carriers in quantum well structures can be directly measured, and both interface and material quality can be inferred from the optical transition linewidths.

The study of optical nonlinearities in semiconductors is motivated to a great extent by the current interest in semiconductor diode lasers and optoelectronic devices. Gain enhancement by the quantum confinement in ultrathin layers has sparked practical interest

in quantum-well lasers. Optical nonlinearities of bulk semiconductors and quantum wells have been studied extensively [see e.g. Haug, 1984; Zimmermann, 1987; Haug, 1988; Schmitt-Rink, 1989; Haug and Koch, 1990]. The rapid advances in short-pulse lasers have allowed the study of hot-carrier dynamics in heterostructures at fundamental time scales (e.g. carrier-phonon scattering takes place on the order of 100 *fs*). [For a review of ultrafast spectroscopy, see Shah, 1989.] Short-pulse lasers provide an excellent tool for studying nonlinearities due to excitonic and electron-hole (*e-h*) plasma effects in semiconductors. A good qualitative understanding of the many-body effects in bulk and QW semiconductors has been achieved in recent years. Most of the nonlinearities in bulk and conventional (type-I) QW structures are caused by a homogeneous *e-h* plasma. This thesis addresses the nonlinearities caused by a *heterogeneous e-h* plasma in GaAs/AlAs "type-II" QWs. In general, type-II QWs or superlattices are formed when the *e* and *h* are confined in different layers by the potential offsets [see Fig. 1.1].

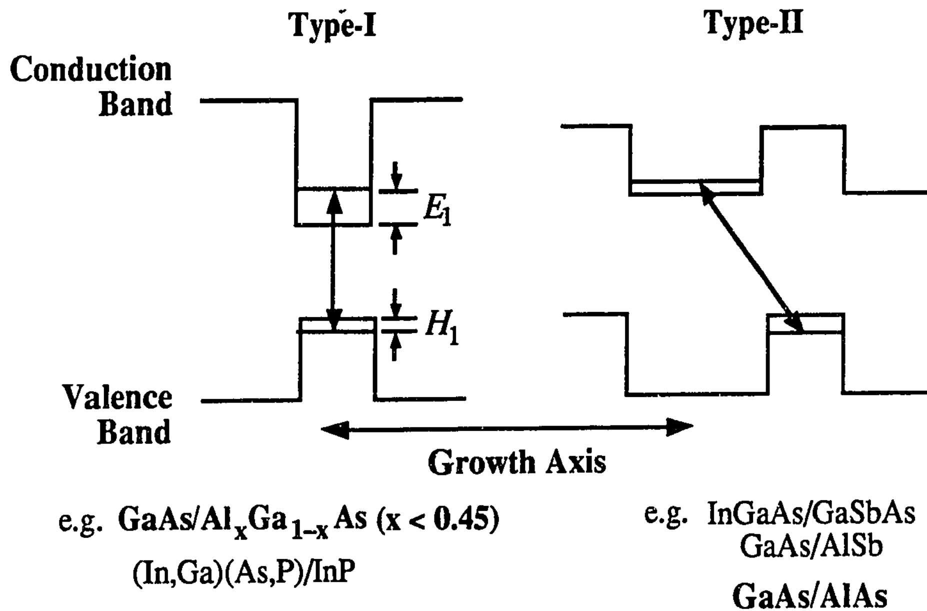

Figure 1.1 Schematic showing (a) conventional type-I and (b) type-II quantum wells. E_1 and H_1 are the effects of quantum confinement.

The binary GaAs/AlAs heterostructures can form type-II QWs. The lowest-lying conduction-band state for AlAs resides at its X-point (i.e. AlAs is an indirect material). Thus, for GaAs layer thicknesses less than 35 Å, the quantum confinement pushes the GaAs Γ-band above the AlAs X-band, and the structure becomes type-II [Danan, 1987a; Finkman, 1987; Ihm, 1987]. The spatial separation of *e* and *h* arises in narrow GaAs/AlAs quantum wells because the quantum-well maximum for the holes (which are at the Γ-point of the Brillioun zone) is in the GaAs layer (i.e. the AlAs layer is the barrier), whereas the quantum-well minimum for the electrons is in the AlAs layer [at the X-point; see Fig. 1.2]. Furthermore, type-II QWs can be formed using $Al_xGa_{1-x}As$/AlAs heterostructures for $x \geq 0.25$ [neglecting quantum confinement; see e.g. Wilson *et al.* 1986].

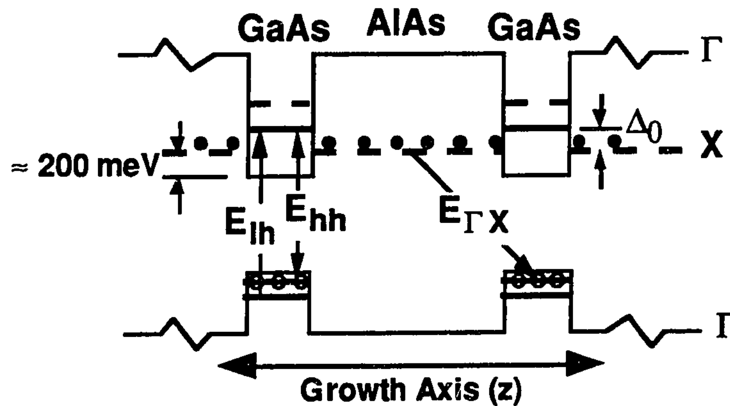

Figure 1.2 Energy band diagram of a GaAs/AlAs type-II quantum well. Upward arrows show optical absorption transitions and downward arrows show transitions for radiative recombination. Light solid (dashed) line represent the Γ-valley (X-valley) for bulk (3d). The dark solid line shows the effect of quantum confinement. Here the effect of quantum confinement on the X-valley is neglected.

Because AlAs offers a large band discontinuity and index change relative to GaAs, GaAs/AlAs heterostructures are prevalent in devices such as resonant tunnel diodes [see e.g. Boykin et al.], modulation-doped field-effect transistors [see e.g. Kugler, 1988], and heterojunction bipolar transistors [see e.g. Ezis *et al.*, 1989], light modulators [e.g. see

Pezeshki *et al.*, 1991] and laser diodes [Jewell, 1991; Lee *et al.*, 1991]. Many of these devices operate with the semiconductor layers in a regime known as the highly excited state where heterogeneous *e-h* plasmas are formed. Thus, further impetus for this work is provided by the widespread application of GaAs/AlAs heterostructures. In addition, type-II quantum wells mimic systems which support space-charge layers (e.g. modulation-doped structures and *n-i-p-i* structures).

In the past, many-body effects, such as the bandgap reduction due to Coulomb exchange-correlation interactions, have been studied in modulation doped structures [see e.g. Livescu *et al.*, 1988; Schmitt-Rink *et al.*, 1989]. Nonlinearities in *n-i-p-i* superlattices (i.e. doping superlattices) have been investigated by Dohler and co-workers (1983, 1985). The type-II QWs are similar to *n-i-p-i* structures in that the electrons (*e*) and holes (*h*) are spatially separated. One advantage of studying type-II QWs, is that an intense optical pulse can be used to precisely create carrier densities over a broad range (10^{11} to 10^{13} cm^{-2}), and thus, avoid problems inherent with dopants. Furthermore, the *n-i-p-i* structures revert back to a flat band structure under high excitation conditions.

Early continuous-wave (cw) linear photoluminescence (PL) studies revealed direct evidence of the spatially separated *e* and *h* plasmas in GaAs/AlAs type-II QWs [Danan, 1987a; Finkman, 1987; Moore 1986, 1987]. The lifetime of the indirect luminescence has been found to be very long (~1 μs) and strongly dependent upon temperature [Wilson *et al.*, 1988] and layer thickness [Meynadier *et al.*, 1988]. Danan *et al.*, (1987) and Meynadier *et al.* (1988) have reported on the effects of an electric field on the linear PL. Feldmann *et al.* (1989, 1990) have reported the subpicosecond spatial transfer rate of electrons from the GaAs layer to the AlAs layer.

The spatial separation of the *e* and *h* plasmas in the type-II system produces a richness in nonlinear optical properties distinct from those observed in conventional type-I MQWs. The fast transfer rate (~500 *fs*) relative to the long radiative lifetime (~1 *μs*) allows

the carriers to thermalize deeper into the distribution of localized states in type-II QWs compared to in type-I or bulk systems. Olbright *et al.* (1990a) have investigated the nonlinear space-charge (Hartree) and many-body effects on the PL transitions in type-II MQWs. These competing effects are reviewed in Chapter 3. One consequence of the spatial separation is the inhibition of carrier inversion (i.e. optical gain) in type-II heterostructures. The sensitivity of *absorption* and *gain* nonlinearities to carrier loss resulting from the spatial separation of *e* and *h* plasmas is investigated in this thesis.

This thesis is organized as follows: In Chapter 2 the linear optical properties of GaAs/AlAs type-II quantum wells is presented. In particular, a spectroscopic technique which allows the direct measurement of the quantum-confinement energy shift of the valence band independent of the shift in the conduction band is presented. This technique allows independent determination of the conduction- and valence-band discontinuities without the use of any fitting parameter. In addition, inhomogeneous broadening due to the unavoidable atomic-layer fluctuations in heterostructure interfaces is quantified. In Chapter 3, both the macroscopic (space-charge) and local (many-body) effects in heterostructures are reviewed. The amplified femtosecond laser system and the time-resolved spectroscopic techniques employed in performing these experiments are described in Chapter 4. The physics of nonlinear absorption due to a single-component hole plasma in type-II structures is discussed in Chapter 5. The observation of gain in type-II quantum wells and the femtosecond nonlinear optical response under extremely high excitation conditions is discussed in Chapter 6. Furthermore, the ability to control the absorption nonlinearities (Chapter 5) and gain amplitude (Chapter 6) by the application of a static longitudinal electric field is demonstrated. Finally, the results and conclusions are summarized in Chapter 7.

2 Linear Optical Properties of Type-II GaAs/AlAs Quantum Wells

Linear spectroscopic techniques, such as absorption and photoluminescence (PL), have been vital tools in understanding the basic physics of semiconductor materials. In this chapter linear absorption and PL spectra are used to characterize the samples. The PL spectra of type-II quantum wells (QWs) provide direct evidence of the spatial separation of electrons and holes. As in three dimensional (3d) semiconductors, the optical spectra of QWs near the bandgap energy are greatly influenced by the *e-h* correlation that induces excitonic resonance below the bandgap and enhancement above. This has been experimentally verified by several groups [Dingle *et al.*, 1974; Chemla, 1985; Chemla and Miller, 1985; Miller and Kleinmann, 1985]. Although this thesis largely addresses the nonlinearities caused by a dense heterogeneous *e-h* plasma, the concept of excitons is key to the physics of the optical properties of semiconductors. Therefore, our discussion begins with a brief review of the basic properties of excitons and linear absorption in III-V layered semiconductors. The linear PL and absorption spectra of GaAs/AlAs type-II MQWs are then presented in the following section. In Section 2.3, linear PL and absorption spectroscopy are utilized to accurately measure the quantum confinement energy shifts and the band discontinuities. In addition, the QW layer thickness fluctuations responsible for the inhomogeneous broadening of the exciton resonance are determined. Finally, the effects of an electric field on the linear spectra of type-II MQWs are presented.

2.1 Excitons in quantum wells

Quantum wells have properties intermediate between 2d and 3d materials. It is therefore instructive to compare excitonic effects in pure 2d and 3d systems. It has been shown that single-particle states are well described within the effective mass approximation (EMA) [see e.g. Haug and Koch, 1990]. The theory of excitons in 3d semiconductors is well documented [see e.g. Elliot, 1957]. It has been shown that, within the EMA, the 3d theory of excitons can be extended to Wannier excitons with a pure 2d motion and the Coulombic (1/r) *e-h* attraction [Shinada and Sugano, 1966]. In QWs the electrons (*e*) and holes (*h*) are free to move in the plane of the layers (x,y) but their motion normal to the layers (z) is controlled by the potential discontinuities at the interfaces [Dingle *et al.*, 1974]. The wavefunctions are plane waves for the in-plane motion. The energy for the continuous spectrum of the ionized states is given by $E_{k_\parallel} = \frac{\hbar^2 k_\parallel^2}{2\mu}$. The quantization normal to the layers gives rise to "particle-in-a-box" wave functions, which are sinusoidal in the well and exponential outside. The low-energy states form a discrete set of two-dimensional (2d) valence and conduction subbands with a step-like density of states. These states can be labeled by quantum numbers, $n_z = 1, 2, 3, ...$

For simplicity, let us consider the ideal case of a semiconductor of bandgap E_g with two isotropic conduction and valence bands having masses m_e and m_h, respectively. The solution to the Wannier equation (i.e. the 2d Schoedinger equation) [see e.g. Haug and Koch, 1990, pp.157-66] yields a series of bound states with binding energies

$$E_n^{2d} = -\frac{R_0}{(n-\frac{1}{2})^2}, \qquad n = 0, 1, 2, \ldots \qquad (2.1)$$

as compared to the 3d result

$$E_n^{3d} = -\frac{R_0}{n^2} \qquad n = 1, 2, 3, \ldots \tag{2.2}$$

where

$$R_0 = \frac{e^4 \mu}{2\hbar^2 \varepsilon_0^2} \tag{2.3}$$

is the 3d ground-state exciton Rydberg energy and

$$a_0 = \frac{\hbar^2 \varepsilon_0}{e^2 \mu} \tag{2.4}$$

where a_0 and is the 3d ground-state (n = 1) exciton Bohr radius. [$\mu^{-1} = m_e^{-1} + m_h^{-1}$ is the reduced *e-h* mass and ε_0 the dielectric constant.] In 2d, the ground-state exciton binding energy and Bohr radius are $R_{2d} = 4R_0$ and $a_0/2$, respectively. The larger binding energy in 2d can be understood by considering quantum well structures with decreasing width. The wavefunction tries to conserve its spherical symmetry as much as possible since admixture of s- and p-wavefunctions is energetically unfavorable. Consequently, the Bohr radius decreases in the direction of confinement (perpendicular to the layers). The Bohr radius for a bulk gallium arsenide (GaAs) exciton is ~150 *Å* while the typical 2d exciton is ~75 *Å*.

Schmitt-Rink *et al.* (1989) and Bastard (1988) have discussed the shortcomings of the above analysis; for example, the treatment of the complicated mixing of the heavy-hole (*hh*) and light-hole (*lh*) bands for $k \neq 0$. The above analysis is physically appealing because it makes several physical parameters transparent. For example, one sees that the exciton Bohr radius scales inversely with effective mass. The Bohr radius increases in materials with smaller effective masses (e.g. InSb, InAs, etc.). Consequently, the excitons

in these materials will experience greater confinement. The trade-off, of course, is that the binding energy is diminished quadratically by the effective mass.

Of course, real semiconductor QWs have finite thickness and depth, which introduces many complications. For example, the penetration of the wavefunctions into the barriers requires the effective mass to change at the interface [see e.g. Morrow *et al.*, 1987]. Also, the motion of holes in III-V compounds is complicated because the quantum confinement lifts the degeneracy of the light- (*lh*) and heavy-hole (*hh*) bands at the Γ-point. The "heavy-hole" and "light-hole" bands are anisotropic. Although the "heavy-hole" mass is larger than the "light-hole" mass perpendicular to the layers, in the plane of the layers, the *hh* mass is smaller than the *lh* mass at the zone center (i.e. $\mathbf{k} = \mathbf{0}$). Furthermore, away from the zone center, the *hh* and *lh* bands couple [Chang and Schulman, 1983] and acquire a highly non-parabolic dispersion so that a constant effective mass can no longer be defined for the holes [see e.g. Bastard, 1988; Broido and Sham, 1986]. Several approximations have been attempted to make the problem tractable [Lee and Lin, 1979; Miller *et al.*, 1981; Bastard *et al.*, 1982; Greene *et al.*, 1984]. The non-parabolicity of the valence band does not play a significant role until the quasi-chemical potential of the hole distribution becomes greater than several milli-electron-volts below the valence-band maximum.

Experimental verification of various models utilize the richness of information provided by optical measurements. For example, the selection rule for interband optical transitions in an infinitely deep rectangular well is that transitions can only take place between valence and conduction subbands having the same quantum number (i.e. $\Delta n_z = 0$). In reality the *e* and *h* wavefunctions penetrate by different amounts into the barriers, which leads to a small but finite transition probabilities for the "forbidden transitions" (i.e. those transitions for which the wavefunctions would be orthogonal in an ideal case). In GaAs/Al(Ga)As QWs the $\Delta n_z = 0$ transitions are much stronger than any "forbidden transitions" [Bastard, 1988]. Close to $\mathbf{k} = 0$, where the *hh* and *lh* character is well defined,

the squares of the dipole matrix elements for transitions from *hh* and *lh* subbands to the *e* subbands are proportional to 3/4 and 1/4, respectively, for optical fields polarized in the plane of the QWs.

At low temperatures exciton resonances are clearly observed at the onset of each interband transition, the *hh* and *lh* doublets being well resolved. The fitted *hh*- and *lh*-exciton oscillator strengths are ≈3:1, as expected. The exciton lines in QWs are broad compared to other exciton lines at low temperature. The primary broadening mechanism is due to the unavoidable fluctuations in the QW thickness [Weisbuch *et al.*, 1981; Deveaud *et al.*, 1986], and is therefore an inhomogeneous broadening. The best samples have interfaces with an island-like structure with steps one monolayer high. For well-widths less than ~100 *Å* the absorption profile is well fitted by exciton peaks with Gaussian line shape and 2d Coulomb-enhanced continua [Chemla *et al.*, 1984].

2.2 Luminescence and absorption spectra of GaAs/AlAs type-II quantum wells

Gallium arsenide (GaAs) is a direct bandgap material with a low-temperature bandgap of 1.51 electron volts (*eV*). Type I QWs formed by GaAs and $Al_xGa_{1-x}As$ layers are the best understood QW system [see Fig. 1.1]. The $Al_xGa_{1-x}As$ alloy becomes indirect for $x > 0.45$ [Casey and Panish, 1976], with its X-valley being the lowest-lying conduction-band state. The X-valley in AlAs is about 0.89 *eV* below the Γ-valley in the conduction band [see Fig. 2.1(a)]. The staggered band alignment of type-II QWs occurs for narrow GaAs layers bound by AlAs layers.

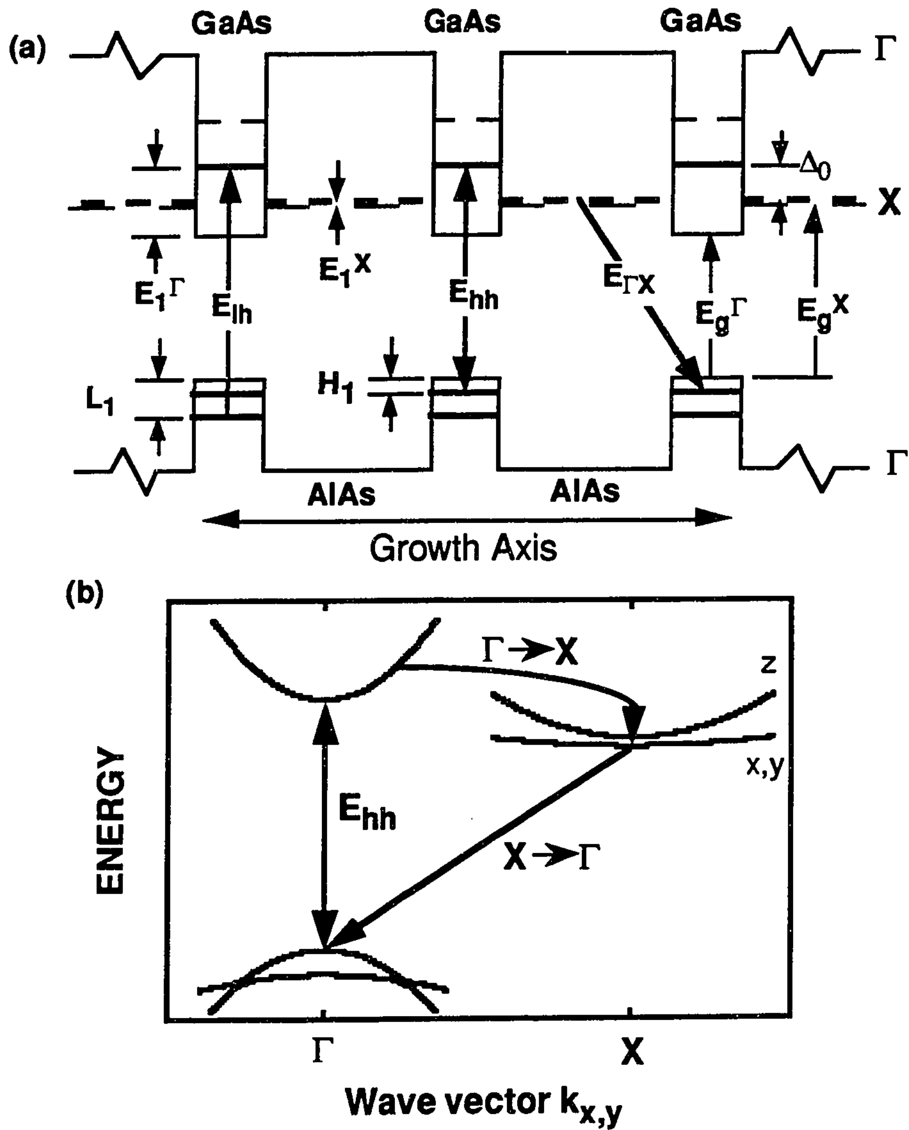

Figure 2.1 (a) Type-II band diagram in real space. The up arrows labeled E_{hh} and E_{lh}, refer to the heavy-hole (hh) and light-hole (lh) resonances in the absorption spectrum, respectively. The down arrow labeled $E_{\Gamma\text{-}X}$ corresponds to the indirect luminescence peak. E_g^{Γ} and E_g^{X} are the direct- and indirect-bandgap energies; and E_1^{Γ}, E_1^{X}, H_1^{Γ}, and L_1^{Γ} are the direct-electron, indirect-electron, hh and lh quantum-confinement energies, respectively. Δ_0 is the flat-band Γ-X splitting. (b) Schematic in-plane band structure in momentum-space of a type-II structure.

Fig. 2.1(a) shows the potential energy diagram of a typical GaAs/AlAs type-II heterostructure in real space. The lowest direct transitions are the GaAs *hh*- and *lh*-exciton lines, which are given by:

$$E_{hh} = E_g{}^{\Gamma} + E_1{}^{\Gamma} + H_1 - E_R{}^{hh} \tag{2.5}$$

and

$$E_{lh} = E_g{}^{\Gamma} + E_1{}^{\Gamma} + L_1 - E_R{}^{lh}, \tag{2.6}$$

respectively, where $E_g{}^{\Gamma}$ is the direct bulk bandgap for GaAs, and $E_1{}^{\Gamma}$, H_1, and L_1 are the electron, *hh* and *lh* confinement energies, respectively. $E_R{}^{hh}$ and $E_R{}^{lh}$ are the binding energies for the *hh* and *lh* excitons, respectively. The lowest indirect transition is given as:

$$E_{\Gamma\text{-}X} = E_g{}^{X} + H_1{}^{\Gamma} + E_1{}^{X} - E_R{}^{\Gamma\text{-}X} \tag{2.7}$$

where $E_g{}^X$ is the effective indirect bandgap§ for the heterostructure (see Fig. 2.1), $E_R{}^{\Gamma\text{-}X}$ is the binding energy of the indirect exciton [Finkman *et al.*, 1986], and $E_1{}^X$ is the confinement energy of the AlAs X-state. The difference between $E_g{}^{\Gamma}$ and $E_g{}^X$ is less than 200 *meV*. This difference can be easily surmounted by the quantum confinement energy (QCE) of the GaAs electron, which are very light ($m^* \approx 0.067 m_o$). Thus, for narrow GaAs/AlAs heterostructures having GaAs layer thickness < 35 Å quantum confinement pushes the lowest GaAs conduction-band state above the AlAs X-valley [Ihm, 1987; Danan *et al.*, 1987; Finkman *et al.*, 1987; Moore *et al.*, 1987]. Consequently, the lowest-energy radiative transition becomes spatially indirect ($E_{\Gamma\text{-}X}$ in Fig. 2.3). This is the case for the so-called type-II QW, where the *e-h* pairs separate spatially after optical excitation. Thus, the holes are confined to the GaAs layer (at the Γ-point of the Brillioun zone), whereas the electrons are confined to the AlAs layer (near the X-point; see Fig. 2.1). A phase diagram

---

§ $E_g{}^X$ is not to be confused with the indirect bandgap for bulk AlAs.

as a function of layer thicknesses is shown in Fig. 2.3. The QCE of the AlAs X-electrons is not as sensitive to thickness changes because of the larger effective masses. This is reflected in the phase diagram (Fig. 2.3) where the thickness of the GaAs layer dictates the "type" of QW.

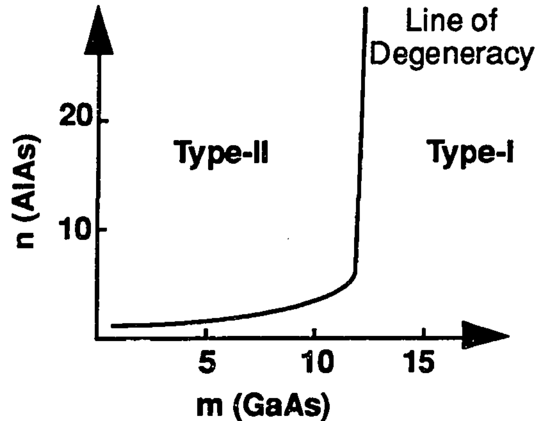

Figure 2.2 Phase diagram for type-I and type-II quantum wells. m = number of monolayers of GaAs. n = number of monolayers of AlAs. The line of degeneracy was calculated by Ihm (1987), and refined experimentally [Danan 1987a, Finkman, 1987].

A comment on nomenclature may be helpful before proceeding. Most of the samples (both type-I and type-II QWs) considered in this thesis are composed of narrow GaAs layers and wide (Al,Ga)As layers. Consequently, the GaAs wavefunctions decay rapidly outside the GaAs layer making the structures "multiple quantum wells" from this point of view. However, in the type-II structures the AlAs X-like electrons penetrate significantly into the GaAs layers. Thus, from the perspective of the AlAs electron, the type-II structures are more accurately described as "superlattices." To avoid confusion, both the type-I and the type-II structures well be referred to as multiple quantum wells (MQWs). Furthermore, the type-II samples will be distinguished from each other by the number of monolayers of GaAs and AlAs in each period. For example, the spectra in Fig.

2.3(a) are taken for the (10/30) type-II sample which refers to a MQW sample with m = 10 monolayers of GaAs and n = 30 monolayers of AlAs per period.‡

Sample Preparation

All of the samples were grown by molecular beam epitaxy (MBE), and the GaAs substrates were removed in order to allow optical transmission measurements to be made. Special attention was given to eliminating reflectance by anti-reflection coating the structures with quarter-wave index-matching layer of titanium dioxide (TiO_2). Prior to removing the GaAs substrate, the top side of the samples were anti-reflection coated. When necessary, the reflectance was further suppressed by anti-reflection coating the back side after substrate removal. The GaAs substrate was removed as follows: First, a ~ 3 x 3 x 0.5 mm^3 sample was mechanically polished down to approximately 25 μm in thickness. Then a 500-ml solution of 100:1 hydrogen peroxide:ammonium hydroxide provided a relatively fast etch rate (~1 μm/min.) for GaAs with adequate selectivity (~1000:1 GaAs:$Al_xGa_{1-x}As$, $x \geq 0.3$) [LePore, 1980]. A commercial vertical-jet etching machine (South Bay Technologies, Model 550D) produced a continuous flow of the etch solution over the sample. After the etching was completed, the sample was transferred onto a sapphire substrate using only surface tension from the semiconductor film. The sapphire substrate was in turn mounted to a cryostat cold-finger with a conductive grease. Both low temperature and room temperature data were taken.

Linear spectra

The linear PL and absorption spectra for the (10/30) type-II MQW sample are plotted in Fig. 2.3(a). The absorption spectra in type-II QWs look very much like that for type-I QWs because the absorption takes place only in the direct-gap GaAs layer.* The *hh*-

‡ Each monolayer is 2.83 Å.

* The absorption coefficient for the indirect transition in AlAs is three orders of magnitude less than the absorption coefficient for the direct transition.

and *lh*-exciton doublet and the combined *hh*- and *lh*-contiuum states are observed in the absorption spectrum. The PL spectra, however, are very different for the two cases. In the type-I case there exists only one PL peak which arises from direct recombination of electrons and holes in the GaAs layers. In the type-II PL spectrum, two peaks are observed: The small high-energy PL peak at the absorption edge arises from direct recombination in the GaAs layer. The prominent low-energy PL peak [labeled "Γ-X" in Fig. 2.3] corresponds to indirect/interlayer recombination of X-like electrons from the AlAs layer with Γ-like holes from the GaAs layer. The difference between the direct Γ-Γ peak and the indirect Γ-X peak is called the Γ-X splitting and denoted as $\Delta_{\Gamma\text{-}X}$. [For the 30-Å GaAs/80-Å AlAs type-II sample $\Delta_o \approx 80$ meV.] The recombination lifetime of the indirect/interlayer Γ-X peak has been measured to be around one microsecond (~3 orders of magnitude longer than the direct recombination lifetime) [Meynadier *et al.*, 1988; Wilson *et al.*, 1988]. Furthermore, the lifetime of the X-like electrons has been reported to be strongly dependent on the Γ-X splitting [Meynadier *et al.*, 1988; Olbright *et al.*, 1990a]. The PL spectra are mainly determined by the relative occupation and carrier lifetimes of the various levels, with the shorter lifetime states dominating the signal. The relative population of the AlAs X-state and the GaAs Γ-state is estimated from the linear PL spectra in Fig. 2.3(a) to be greater than 10^6.**

** Note: $\frac{n_X}{n_\Gamma} = \frac{L_X}{L_\Gamma}\frac{\tau_X}{\tau_\Gamma}$ where $L_i \equiv \int g_i(\lambda)d\lambda$ where $g_i(\lambda)$ is the PL lineshape.

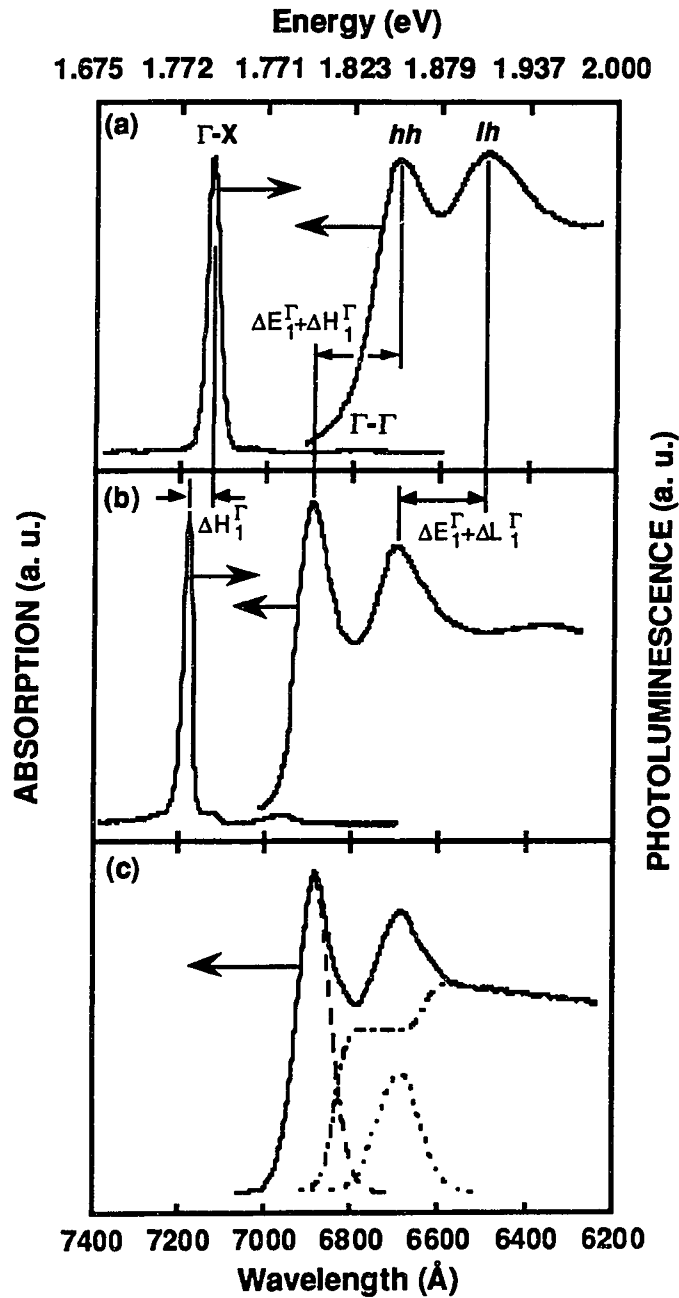

Figure 2.3 Low-temperature (15 K) absorption and PL spectra of (a) a GaAs(29 Å)/AlAs(91 Å) and (b) GaAs(32 Å)/AlAs(89 Å) type-II samples. Excitation intensity and energy for the PL spectra are 0.5 W/cm^2 and 1.959 eV, respectively. (c) The solid line shows the least squares fit of the absorption spectrum for sample B. The dashed lines represent the *hh* and *lh* excitonic functions whereas the dot-dashed line represents the sum of the *hh*- and *lh*-continuum functions.

The AlAs X-valley

In bulk AlAs the X-valley is three-fold degenerate at the Brillioun zone edge (i.e. [100] direction).† These three valleys are labeled X_x, X_y, and X_z in association with the valley in which the electrons reside. The X_x and the X_y valleys are degenerate in 2d, and they will henceforth be referred to as the $X_{x,y}$ valley. The X-valleys are also anisotropic: perpendicular to the layers, the electrons in the $X_{x,y}$ valley have an effective mass which is lighter than the X_z effective mass, however, the masses switch values in the plane of the layers. Since the confinement is perpendicular to the layers, the $X_{x,y}$ band always exhibits greater quantum confinement energy than the X_z band. Unlike quantum confinement, the strain on the AlAs layers only effects the X_z band. The strain splitting due to a 0.18% lattice mismatch between GaAs and AlAs has been estimated to be ≈ 23 meV by using the deformation potential found in GaP/GaAs [van Kesteren *et al.*, 1989]. A rigid 23-meV shift of the X_z band to higher energy causes the $X_{x,y}$ band to become the lowest-lying X-state for AlAs layers thicker than ~60 Å [van Kesteren *et al.*; 1989, Dawson *et al.*, 1990]. For AlAs layer narrower than ~60 Å the quantum confinement of the $X_{x,y}$ band overcomes the strain-induced shift, and the X_z becomes the lowest-lying state. All of the type-II samples, except one, have AlAs layer thicknesses greater than 55 Å.

Wilson *et al.* (1988a, b) have investigated temperature-dependent PL decay to determine the recombination mechanism for type-II structures. They concluded that both disorder-induced scattering and Γ-X mixing are responsible for the indirect recombination mechanism. Subpicosecond transfer of electrons from the GaAs layer to the AlAs layer has been reported by Feldmann *et al.* (1989) [also see Saeta *et al.*, 1989; Olbright *et al.*, 1990b] and will be discussed further in Chapter 5. The type-II band alignment can be continuously changed to a quasi-type-I band alignment by the application of a longitudinal electric field

† The probability distributions in k-space resemble P-like orbitals centered about each of the three axes (x, y, and z).

[Meynadier *et al.*, 1988; Olbright *et al.*, 1990b] or hydrostatic pressure [Wolford *et al.*, 1985; Drummond *et al.*, 1986]. The electric-field-dependent linear optical properties of type-II QWs will be discussed in Section 2.4, but first, the band discontinuities and the interfacial roughness in type-II QWs will be presented.

2.3 Differential Quantum Confinement Energy Shifts: Demonstration of a Novel Spectroscopic Technique

Quantum-confinement energies (QCEs) are crucial to understanding the optical-transition energies in semiconductor quantum-well structures. Numerous researchers have used experimental and theoretical methods to determine transition-energy shifts due to well-thickness changes [Dingle, 1975]. These previous studies used the measured transition energy (equal to the *sum* of the *e* and *h* QCEs and the band-gap energy minus the excitonic-binding energy) to indirectly calculate binding energies [R.C. Miller *et al.*, 1981], electron and hole QCE's, effective masses [R.C. Miller *et al.*, 1984], and energy-gap discontinuities [for a review see Duggan, 1985]. In this section a novel spectroscopic technique is employed. This technique allows an independent measurement of the *e, hh,* and *lh* QCE shifts (i.e. constituents of the transition energies) by intentionally varying the width of the narrow GaAs wells while keeping the AlAs layer thickness constant. Both low-temperature PL and absorption spectra were obtained to measure the *e*, *hh*, and *lh* QCE shifts without invoking any numerical fitting factors. These energy shifts are then used to compute the valence-band discontinuity (ΔE_v) independent of the conduction-band

discontinuity (ΔE_c) using an effective-mass Hamiltonian for abrupt heterojunctions. Using the measured *e* and *h* QCE shifts and the inhomogeneously broadened linewidths from the absorption data in conjunction with the GaAs well widths (obtained from x-ray rocking curve analysis), the well-width fluctuation is determined to be half a monolayer.

This spectroscopic technique utilizes the additional information provided by the indirect PL transition in GaAs/AlAs type-II heterostructures. As discussed in the previous section, the lowest radiative transition in these heterostructures involves the indirect/interlayer recombination of X-valley electrons in AlAs with Γ-valley holes in GaAs and is the primary focus of the PL analysis. The existence of both intra-layer (GaAs-GaAs) and inter-layer (AlAs-GaAs) transitions in these structures affords the opportunity to monitor QCE shifts separately in the valence and conduction bands by making changes only in the GaAs (or AlAs) layer of separate samples. Thus, for example, by examining two samples in which only the GaAs well widths are varied, indirect-PL energy shifts will only reflect *hh* QCE shifts in the GaAs valence band since the X-valley electron energy in AlAs is unaffected by the GaAs layer thickness.

First, consider two type-II heterostructures. Sample A has a GaAs well-thickness L_Z, and sample B has well-thickness $L_Z+\delta$. However, the AlAs X-valley minimum is a stationary-energy point since the two samples have the same AlAs barrier thickness. The energetic positions for the *hh*- and *lh*-exciton lines are given by eqns. (2.5) and (2.6), respectively, and the energetic position for the Γ-X indirect/interlayer luminescence line is given by eqn. (2.7). One final note: the AlAs X-valley electrons for the two structures considered in this section have negligible quantum confinement (i.e. $E_1^X = 0\ meV$).

As seen by examination of Fig. 2.1 and/or eqn. (2.7), the shift of the Γ-X PL line between the two samples is a direct measure of the *hh* QCE shift (ΔH_1^Γ). Here the change in exciton binding energy for the 4-Å change in GaAs well thickness is neglected because the change in binding energy is ~ 0.1 *meV* [R. C. Miller *et al.*, 1981]. In contrast, the *hh*-

(*lh*-) exciton absorption-peak energy shift is equal to the *sum* of the *e* and *hh* (*lh*) QCE shifts. Therefore, the shift of the *e* QCE ($\Delta E_1{}^{\Gamma}$) is obtained by subtracting the shift of the Γ-X PL line from the total shift of the *hh*-exciton absorption line. Finally, the shift of the *lh* QCE ($\Delta L_1{}^{\Gamma}$) is obtained by subtracting $\Delta E_1{}^{\Gamma}$ from the total shift of the *lh* exciton absorption peak. Expressions for the QCE shifts in eqns. (2.8)–(2.10) are obtained from analytic expressions for the direct and indirect transition energies given in eqns. (2.5)–(2.7). These energy shifts are given by,

$$\Delta H_1{}^{\Gamma} = \Delta E_{\Gamma X}, \tag{2.8}$$

$$\Delta E_1{}^{\Gamma} = \Delta E_{hh} - \Delta H_1{}^{\Gamma}, \tag{2.9}$$

$$\Delta L_1{}^{\Gamma} = \Delta E_{lh} - \Delta E_1{}^{\Gamma}, \tag{2.10}$$

where $\Delta E_{\Gamma X}$ is the shift of the Γ-X PL peak while ΔE_{hh} and ΔE_{lh} are the shifts of the *hh*- and *lh*-exciton absorption peaks.

The two samples were grown sequentially in a MBE chamber. Growth interruption was not employed in order to mimic the most common growth conditions. Seventy-five (75) QWs were grown in each case. The AlAs layers were nominally 90 Å thick, thus providing substantial isolation of the GaAs wavefunctions. Sample A had a GaAs layer thickness of d_{GaAs}= 28±1 Å and an AlAs layer thickness of d_{AlAs}= 91±1 Å, whereas sample B had d_{GaAs}= 32±1 Å and d_{AlAs}= 89±1 Å. [The period and layer thicknesses were determined by x-ray double-crystal rocking curve analysis as described by Speriosu and Vreeland (1984).] The small, 2-Å difference in the AlAs layer thicknesses, between samples A and B produced a negligible QCE shift of the AlAs X-point states because the AlAs layers are relatively wide and the X-valley effective mass is relatively large ($\frac{\delta E_X}{\delta L}$ < 0.1 *meV*/monolayer).

Each sample was anti-reflection coated, etched (to remove the substrate) and transferred to a sapphire substrate in a cryostat as described in Section 2.2. Low-temperature (15 *K*) cw absorption and PL measurements were performed using a tungsten-filament white-light source and a helium-neon (He-Ne) laser ($E_{exc.}$ = 1.959 eV and $I_{exc.} \approx$ 0.5 W/cm^2), respectively. Absorption, PL, and x-ray diffraction spectra were taken from the same 100-μm-diameter spot on each sample.

In Fig. 2.3 the absorption and PL spectra for samples A and B are presented. The low-temperature PL spectra reveal two peaks: a high-energy peak corresponding to direct *e*-*h* recombination at the Γ-point in GaAs (see Fig. 2.3; PL peak labeled Γ-Γ), and a low-energy peak corresponding to indirect/interlayer recombination of X-like *e* in AlAs with Γ-like *h* in GaAs (see Fig. 2.3; PL peak labeled Γ-X). From these spectra, the shifts of the Γ-X, *hh*-exciton, and *lh*-exciton features are measured to be 13.3 *meV*, 48.5 *meV* and 55.6 *meV*, respectively. Of course, the same *hh*-exciton shift was also obtained using the Γ-Γ PL line shifts. Using equations (2.8)-(2.10) above, QCE shifts of are obtained

$$\Delta H_1^{\Gamma} = 13.3\ meV,$$

$$\Delta L_1^{\Gamma} = 20.4\ meV,$$

and

$$\Delta E_1^{\Gamma} = 35.2\ meV,$$

resulting from the 4-Å change in the GaAs average layer thickness between the two samples. The QCEs increase as the effective masses decrease, consistent with effective-mass considerations [i.e. $\Delta H_1^{\Gamma} < \Delta E_1^{\Gamma} < \Delta L_1^{\Gamma}$; $m_{hh}^* = 0.403m_o$, $m_{lh}^* = 0.087m_o$, $m_e^* = 0.067m_o$].

Band Discontinuities

The energy shifts obtained from the spectra provide a means to separately determine the conduction-band and valence-band offsets. These shifts in conjunction with a simple effective mass Hamiltonian were used to calculate the GaAs-Γ-point to AlAs-Γ-point conduction- and valence-band offsets of $\Delta E_c = 1036\ meV$, and $\Delta E_v = 542\ meV$, respectively. These values are consistent with other reports [Finkman *et al.*, 1987; Duggan, 1985]. However, no pre-determined band-offset parameter in this calculation. This is made possible by the experimental separation of the *h* QCE shift from the *e* QCE shift. In addition, a simple model could be used to calculate the QCE shifts because the high AlAs barriers strongly confine the GaAs wavefunctions. The primary source of uncertainty for this method is the thickness determination (± 1 Å), however the additional information provided by the indirect transition allows a more thorough comparison of experimental and numerical results.

In previous calculations the electron and hole QCE shifts were coupled and the band-offset parameter had to be inferred [R.C. Miller *et al.*, 1984; Duggan, 1985]. One notable exception is a two-photon absorption experiment reported by Tai *et al.* (1989). By using polarization-dependent selection rules for two-photon absorption (in the wave-guide geometry) they independently determined the conduction and valence band discontinuities for a GaAs/AlGaAs QW structure. Tai *et al.* (1989) reported a conduction-band to valence-band offset ratio of 75/25. The discrepancy in the two results could arise from several sources. As mentioned above, the primary source of error here arises from the determination of the layer thicknesses. In addition, the ternary sample of Tai and co-workers may indeed have a different band offset than the binary structures presented above [see e.g. Duggan, 1985]. However, the linear spectroscopic technique described above is the much simpler to implement, in general, than the two-photon absorption measurement.

Inhomogeneous Broadening

The linewidths of absorption and PL spectra in narrow-well heterostructures such as those examined in this study are known to be inhomogeneously broadened primarily by layer-thickness variations [Weisbuch *et al.*, 1981; Deveaud *et al.*, 1986]. The quantum mechanical solution to the infinite-well problem tells us that the energy levels are discrete and scale inversely with the square of the well width. In other words, $E_n \propto L^{-2}$. By differentiating, one finds $\delta E_n \propto L^{-3}\, \delta L$. Therefore, an increase in all of the optical-transition linewidths is expected (and observed) for a decrease of the GaAs layer thickness. [See Fig.2.2 compare the spectra in (a) and (b).] Since inhomogeneous broadening of the Γ-X PL transition arises primarily from the variation in the *hh* level, its linewidth is considerably narrower than that of the *hh*- (*lh*-) absorption line whose width is broadened by the distribution of both the *hh* (*lh*) and *e* QCEs in the GaAs layer.

The well-width fluctuations are determined to be half a monolayer using only experimentally measured absorption, PL, and x-ray spectra. First, the *e, hh,* and *lh* QCE shifts are divided by the difference of the GaAs layer thickness between sample A and B to obtain the average differential energy shift, $\delta E/\delta L_z$. Then the linewidths from the absorption resonances are extracted by performing a least-squares fit on each spectrum using two Gaussians and two densities of states. The two Gaussians account phenomenologically for well-width-variation broadening. The two densities of states, one for each hole, consist of Fermi functions that include the appropriate 2d Coulomb-enhancement factors [see e.g. Haug and Koch, 1990; Chemla *et al.*, 1984; Shinada and Sugano, 1966]. The two different continuum contributions from the *hh* and *lh* subbands are included, since they are decoupled. The separation between each Gaussian and its respective continuum function is set equal to the binding energy of the exciton. Binding energies of 13 and 16 *meV* were used for the *hh* and *lh* excitons, respectively, ≈ 1-2 *meV* higher than the values reported in R.C. Miller *et al.* (1981) for GaAs/AlGaAs wells. The

slightly higher binding energies could reflect the greater confinement due to the pure AlAs barriers [Moore *et al.*, 1986].

The linewidths obtained from the best fits to the absorption spectra are listed in Table I, along with the Γ-X-PL linewidths. Impurity broadening of ≈1 meV is taken into account in the tabulated values. The average linewidths are divided by the average differential-energy shift and a calculated well-width fluctuation of 0.6 ± 0.1 monolayers, full width at half maximum (FWHM) is obtained. The same value are obtained by numerically calculating the differential-energy shifts ($\delta E/\delta L_z$) about GaAs well-widths of 28 Å and 32 Å (see Table I). The inhomogeneous broadening that is observed in the PL and absorption measurements is in excellent agreement with half-monolayer well-width fluctuations.

Table I. First three columns are: the *hh* absorption, *lh* absorption and Γ-X luminescence linewidths, respectively. The last three columns are the first three columns divided by the measured dispersions. The dispersion is given by the spectral peak shift divided by the spectral peak shift divided by the difference in the well widths of samples A and B.

Sample	$FWHM_{hh}$ (meV)	$FWHM_{lh}$ (meV)	$FWHM_{\Gamma X}$ (meV)	$\frac{FWHM_{hh}}{(\delta E_{hh}/\delta L_z)}$	$\frac{FWHM_{lh}}{(\delta E_{lh}/\delta L_z)}$	$\frac{FWHM_{\Gamma X}}{(\delta E_{\Gamma X}/\delta L_z)}$
A	28.4	37.1	6.8	0.6 a_0	0.6 a_0	0.6 a_0
B	20.5	27.1	5.0	0.5 a_0	0.5 a_0	0.6 a_0

a_0 = 2.83 Å, the length of one monolayer of GaAs in the [001] direction.

Observation of a one-half monolayer well-width fluctuation does not imply that the semiconductor interfaces are composed of sub-monolayer steps. Rather, it implies that the FWHM of the distribution function of the GaAs well widths for these multiple-quantum-well structures are one-half monolayer. The two interfaces which compose the quantum well are not symmetric. In other words the (a) AlAs:GaAs interface roughness and (b) GaAs:AlAs interface roughness are dissimilar (see Fig. 2.4). Negligible contribution from

the AlAs:GaAs interface is expected since termination of AlAs epitaxial growth results in atomically flat islands much smaller than the exciton Bohr radius (~75 Å), so the exciton wavefunction is averaged over these fluctuations. Consequently, the AlAs:GaAs interface is *pseudo-smooth*, and the inhomogeneous broadening is due primarily to the GaAs:AlAs interface [Tanaka and Sakaki 1987]. The non-integral value of 0.6 monolayers is due to the quasi-continuous distribution function which arises from sampling of a very large number of atomically flat islands and a large number of quantum wells.

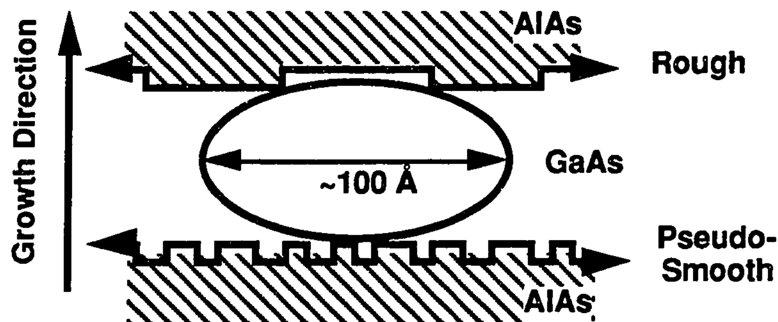

Figure 2.4 Schematic of heterojunction interfaces illustrating the difference in the two interfaces.

The main effect of the layer thickness fluctuation is simply a change of the confinement energies [$\Delta E(L)$; corresponding to a shift of the in-plane bands]. If the scale of the atomically flat islands is on the order of the exciton Bohr radius, one can assume that the averaging of well thicknesses follows effectively a continuous distribution although the actual thickness variations are always multiple integers of the lattice constant. This assumption is valid in the case of multiple-quantum wells because the inhomogeneities occur both within each layer (i.e. as a function of the x, y coordinates for fixed z) and in the growth direction (z). Thus, the inhomogeneous broadening can be obtained from a superposition of homogeneously broadened spectra $\alpha_{\mathrm{hom.}}(\hbar\omega)$

$$\alpha_{in\,\mathrm{hom.}}(L) \propto \int \exp\left[\frac{-(L-L_0)^2}{\sigma^2}\right]\alpha_{\mathrm{hom.}}[\hbar\omega + \Delta E(L)]\; dL \qquad (2.11)$$

where L_0 is the average well width and σ is the variance of the Gaussian distribution of well widths. The numerical evaluations have yielded good agreement with these experimental results [as will be seen in Chapter 5].

Discussion

Essentially, the exciton is being used to probe the heterojunction interfaces. Several parameters can be varied during MBE growth to better understand the interfacial roughness on a scale of the exciton radius. For example, the island sizes can be increased significantly by providing the Ga atoms more time to move about the surface and minimize the bonding energies. Tanaka and Sakaki (1987) have shown that by interrupting the growth at the GaAs interface, the inhomogeneous broadening can be reduced by a factor of ≈2.5. They attributed the reduction in the inhomogeneous broadening to an increase in the island size of the GaAs interface (i.e. termination of a GaAs layer) with respect to the exciton radius [Tanaka and Sakaki, 1987].

Another approach would be to decrease the exciton radius with the application of a magnetic field perpendicular to the layers. However, a field of 10 Tesla reduces the cyclotron radius, $R_c = (c/eH)^{1/2}$, to only ~100 Å. Stark *et al.* (1990) observed a ≈20% increase in the oscillator strength in the *hh*-exciton absorption peak in a magnetic field of ≈12 T (R_c = 70 Å). Fields in excess of 20 T are required to reduce the cyclotron radius below the mean GaAs island size. One final variation would be to preferentially sample one interface by applying an electric field perpendicular to the layers. However, a simultaneous change in the exciton binding energy (due to the field-induced change in wavefunction overlap) complicates the interpretation of such data.

In conclusion, a method for direct measurement of the quantum-confinement-energy shifts of the heavy-hole, light-hole and electron levels in narrow type-II GaAs/AlAs MQWs has been presented. The experimental results are consistent with values obtained from an effective-mass Hamiltonian model. In addition, the inhomogeneous broadening in 30-Å-wide quantum wells grown by uninterrupted molecular beam epitaxy arises from half-monolayer well-width fluctuations. Finally, the spectroscopic technique described above affords a method to calculate the valence-band discontinuity independent of the conduction-band discontinuity. The experimental technique described above is generally applicable to type-II heterostructures that exhibit photoluminescence from spatially indirect transitions. Examples of other such systems are GaAs/AlSb, InP/AlSb, and AlSb/AlP.

2.4 Effects of a static longitudinal electric field

In the previous section, the Γ-X splitting was reduced by growing samples which had different GaAs layer thicknesses. The application of hydrostatic pressure [Wolford and Bradley, 1985; Drummond *et al.*, 1986] can continuously vary the Γ-X splitting, however, cumbersome equipment is required for large changes in pressure. The application of an electric field is a much more attractive means to vary the Γ-X splitting since it may have device applications. Danan *et al.* (1987b) first showed that the Γ-X luminescence peak shifts to higher energy as an electric field is applied normal to the plane of the layers. [In other words, an electric field effectively reduces the Γ-X splitting.]

Meynadier *et al.* (1988) showed that the indirect (Γ-X) PL peak can be pushed above the direct PL peak by the application of moderate electric fields (0–6x10^4 V/cm). The sample studied by Meynadier *et al.* had layer thicknesses of 35 Å (GaAs) and 80 Å (AlAs), and a flatband Γ-X splitting (Δ_o) of only $\approx$ 15 meV. This sample is referred to as "weakly type-II" because it is near the type-II–to–type-I crossover region in the phase diagram shown in Fig. 2.2. They estimated that the GaAs Γ-state and the AlAs X-state exhibit an anti-crossing with a mixing potential ~1 meV. [This implies a switching rate on the order of 1 *ps*.] They also determined the effective mass of the X-valley to be $m_X^* \approx 1.2m_o$ from the quadratic Stark shift of the X-like wavefunction in the applied electric field. This result contradicts the findings of van Kesteren *et al.* (1989) [see Sec. 2.2].

Sample Preparation

A type-II MQW sample was grown in the intrinsic region of a *p-i-n* structure using MBE. The sample consisted of 30-Å GaAs layers and 80-Å AlAs layers repeated ninety (90) times. This sample had a low-temperature (30 K), flat-band Γ-X splitting of $\approx$75 meV. The *p* and *n* regions were composed of highly doped $Al_xGa_{1-x}As$ having $\approx$35% Al so that these contact regions would be transparent to both the pump and probe beams. The as-grown structure was fabricated into individually isolated and contacted mesa photodiodes. The photodiodes were also anti-reflection coated before cw and time-resolved optical measurements were performed.

Linear spectra

The field strength was varied between 0-3x10^5 V/cm. Fig. 2.5(c) shows the steady-state linear PL and absorption spectra for the two extreme field settings.[††] The high-field linear absorption spectrum exhibited a small red shift of both exciton peaks

[††] By fitting the linear absorption spectrum we determined the inhomogeneous broadening of the *lh* and *hh* absorption peaks of the structure under consideration to be 28 *meV* and 20 *meV* (FWHM), respectively.

relative to the zero-field spectrum, evidence of a small quantum-confined Franz-Keldysh or quantum-confined Stark shift in these narrow GaAs QWs [Mendez *et al.*, 1982; Miller *et al.*, 1984, 1985]. The Stark shift is suppressed in these narrow (≈ 30-Å) GaAs QWs because the wavefunctions in the GaAs conduction and valence bands cannot be spatially pulled apart as the electric field distorts the square wells into triangular wells.

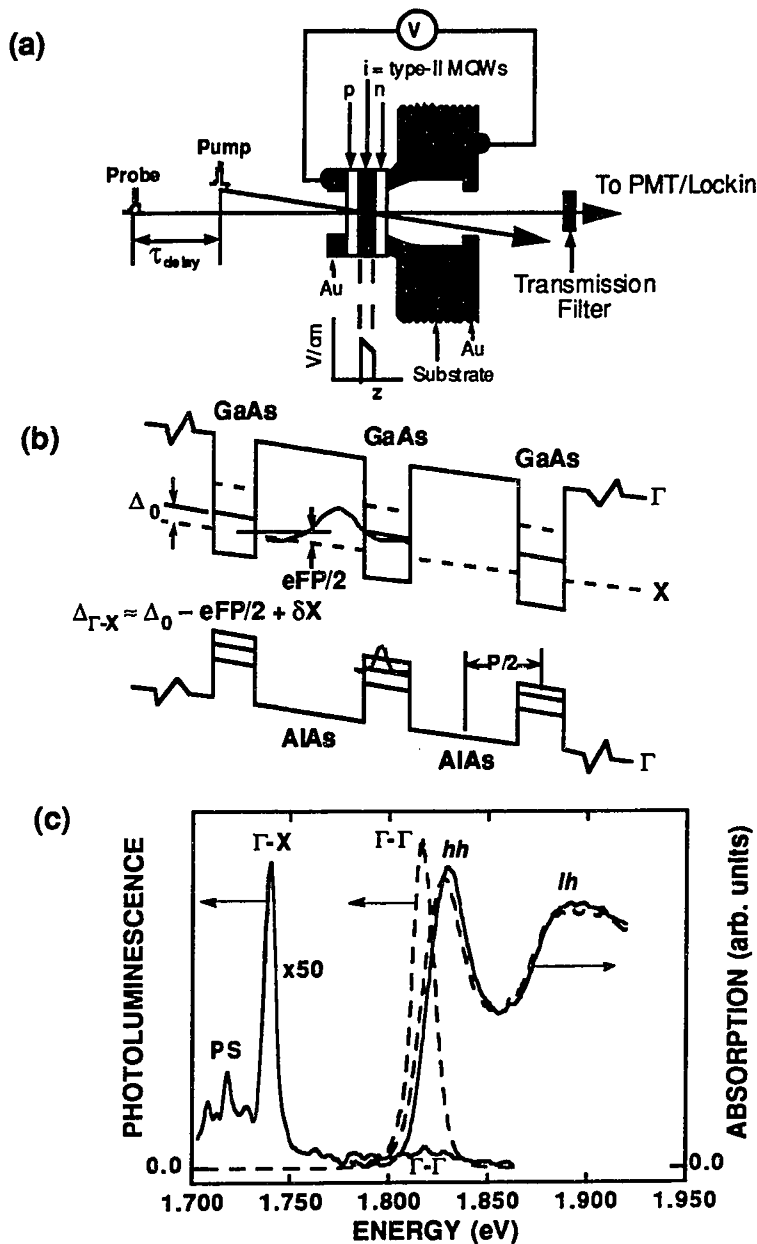

Figure 2.5 **(a)** Experimental configuration of electric-field-dependent PL and absorption measurements. The clear aperture of the p-type contact is 100 µm in diameter. **(b)** Type-II structure in a longitudinal electric field. The case shown is the high-field case near the indirect-to-direct crossover region. Δ_0 is the flat-band Γ-X splitting, P is the length of one period, and F is the field strength. **(c)** CW linear-optical absorption and PL spectra of the p-i-n quantum-well photodiode for flat-band (solid lines) and a field strength of 3×10^5 V/cm (dashed lines). The i-region consists of a 90-period (11/30) type-II structure. The pump energy and intensity were 1.96 eV and 1 W/cm^2, respectively. T = 30 K.

The low-field PL spectrum reveals both the indirect Γ-X and direct Γ-Γ lines, verifying the type-II band alignment and the Γ-X splitting of 75 meV. In contrast, the high-field (3×10^5 V/cm) PL spectrum in Fig. 2.5(c) illustrates the effect of Γ-X alignment: the presence of only one PL peak, and a ~100-fold increase in the integrated PL intensity. Actually, two indirect transitions are associated with each *hh* level [see Fig. 2.5(b)], however, they are degenerate at flatband. When a field is applied, this degeneracy is broken and two indirect Γ-X PL peaks appear.

In Fig. 2.6(a) the electric-field-dependent PL spectra are presented. The sample was photoexcited with a He-Ne laser while monitoring the applied bias and photo-current on a curve tracer. At the lowest field strengths the Γ-X peak is observed to be the prominent PL line and the Γ-Γ peak to be relatively small, similar to that in the intrinsic type-II samples. As a reverse bias is applied to the type-II MQW photodiode, the relative intensity of the Γ-X peak to the Γ-Γ peak is observed to decrease rapidly. At a relatively low bias level, a discontinuity is observed in the photocurrent. This discontinuity will be henceforth referred to as "kink-1." Simultaneously, a splitting of the indirect Γ-X PL peak into two smaller peaks is observed. The energy splitting between these two peaks slowly increase with the applied field. These two peaks correspond to the indirect transitions between adjacent layers, whose degeneracy is broken by the application of an electric field. Accordingly, these oblique transitions are labeled Γ-X^+ and Γ-X^- (see Fig. 2.6). As the Γ-X^- peak shifts to lower energy, its intensity decreases until it is finally lost in the background. The Γ-X^- oscillator strength is diminished by the field because the X-electron wavefunction is pulled away from the Γ-like *hh* wavefunction. On the other hand, the tilted potential pulls the X^+ electron wavefunction toward the Γ-like *hh* wavefunction [see Fig. 2.5(b)], and consequently, the intensity of the Γ-X^+ peak increases with field.

As the reverse bias is increased further, yet another discontinuity is observed in the photocurrent (referred to as "kink-2"). The spectral change is more subtle this time: the intensity of the Γ-X^+ indirect PL peak increases and it shifts onto the shoulder of the direct Γ-Γ PL line. The Γ-X^+ peak eventually aligns with the Γ-Γ peak at a field strength of $\approx$ 280 *kV/cm*. The excitation-power dependence of kink-1 is plotted in Fig. 2.6(c).

Danan *et al.* (1987) actually observed the two oblique transitions, however, they avoided discussion of the low-energy transition (Γ-X^-). Meynadier *et al.* did not report any observation of two indirect transitions in their weakly type-II sample. The primary interest here is to control the spatial separation of the *e* and *h* wavefunctions.

The electric-field effectively decreases the Γ-X splitting, and at high field it is given by

$$\Delta_{\Gamma\text{-}X}(F) = \Delta_O - eFP/2 + \delta X, \qquad (2.12)$$

where $\Delta_O \approx 75\ meV$ is the flat-band Γ-X splitting, $eFP/2$ is simply the potential drop from the center of the GaAs layer to the center of the AlAs layer, and δX is the quantum-confined Stark shifts for the X-electron and *hh* wavefunctions. Finally, *e* is the electronic charge, *F* is the magnitude of the applied electric field, and *P* is the quantum-well period [see Fig. 2.5(b)].

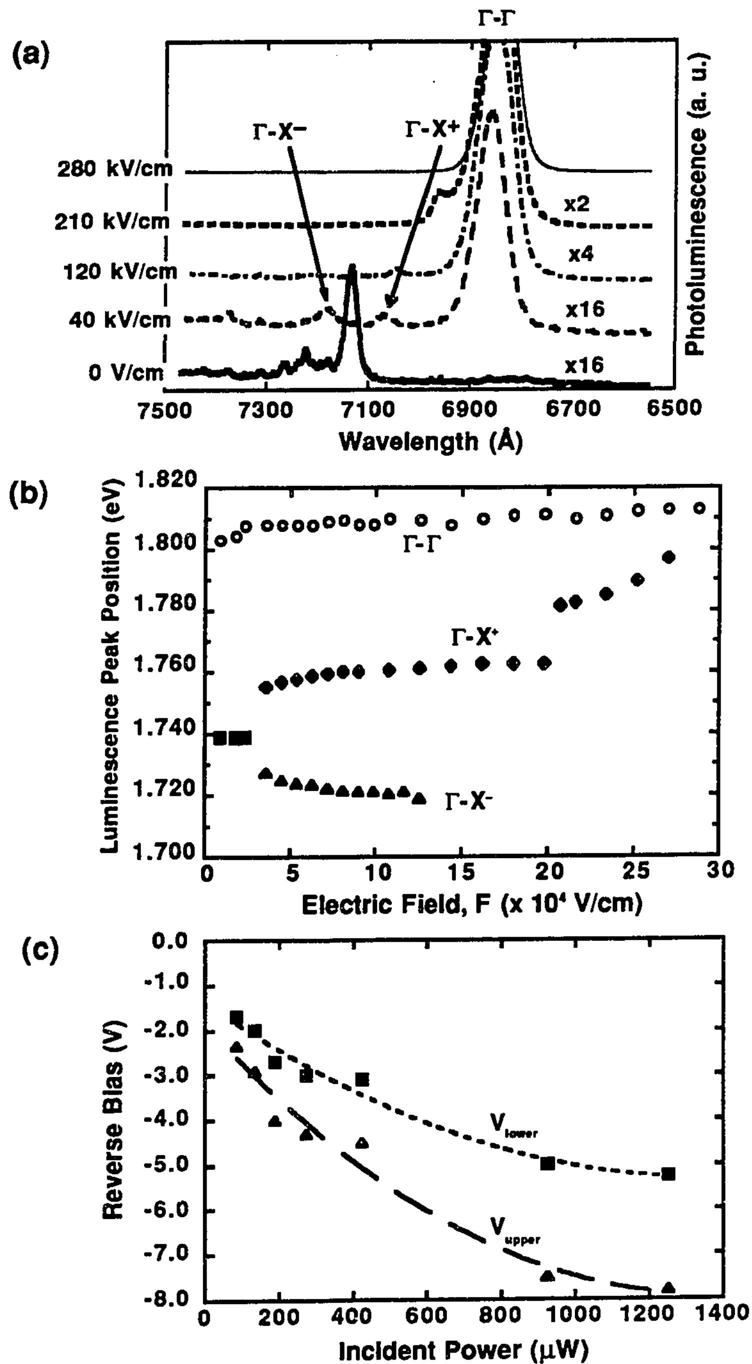

Figure 2.6 (a) Photoluminescence spectra and (b) peak position versus electric field. (c) Upper and lower voltage of "kink-1" as a function of electric field. The two curves are quadratic fits and intersect at -1.2 ± 0.4 V.

The measured shift of the high-energy Γ-X transition is given by

$$\Delta E_{\Gamma\text{-X}}(F) \; = \; eFP/2 - \delta X - \delta H, \qquad (2.13)$$

where δH is the Stark shift of the *hh* wavefunction. As seen in Fig. 2.5(c), the δH term is small relative to the other terms in eqn. (2.13). The Stark shift can be viewed as a second-order perturbation, proportional to the square of the dipole matrix element, and inversely proportional to energy, hence,

$$\delta X \sim m_x^* \, F^2 \, d^4 \qquad (2.14)$$

where m_x^* is the effective mass of the X-state and d is the layer thickness. The GaAs well is much narrower than the AlAs layer ($d_{AlAs}/d_{GaAs} \approx 2.5$) and the masses are approximately the same, which implies that $\delta X >> \delta H$.

The Stark shift is a negative shift and it is determined from the spectra by

$$\delta X \; = \; eFP/2 - \Delta E_{\Gamma\text{-X}} \qquad (2.15)$$

The quadratic regime of the Stark shift ($F \leq 50$ *kV/cm*) has been investigated by Meynadier *et al.* (1988). The Stark shift, δX, in the field regime between "kink-1" and "kink-2" (i.e. $50 < F < 220$ *kV/cm*) exhibits a linear dependence on the field [see Fig. 2.7]. At fields greater than 220 *kV/cm*, the dependence becomes sub-linear. For further discussion on the Stark shift, the reader is referred elsewhere [Bastard, 1988; Mendez *et al.*, 1982; Miller *et al.*, 1985].

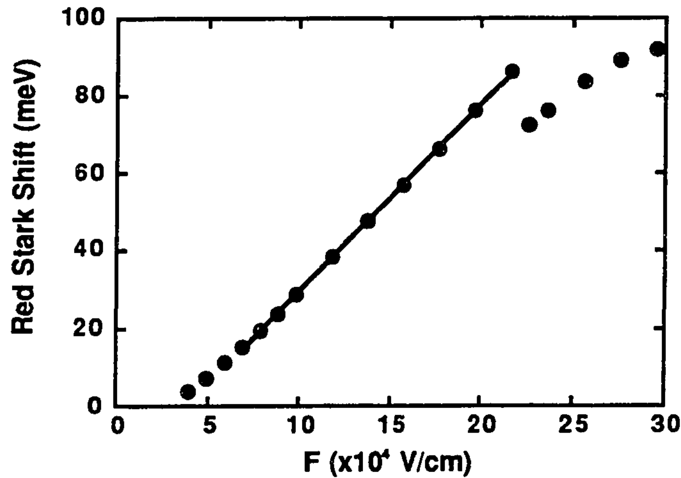

Figure 2.7 The Stark shift of the X-like electronic state (δX; see eqn. 2.15). The line is a least squares fit of the data from 50 to 220 kV/cm. The slope of the linear fit is 0.4736 eV/kV/cm with a correlation coefficient of r = 0.9999.

Summary

In this chapter the linear optical properties of type-II MQWs has been discussed. A novel spectroscopic technique has been used to independently determine the individual quantum-confinement energy shifts of electrons and holes. The use of these energy shifts to determine the conduction- and valence-band offsets independent of each other has been demonstrated. Finally, the interfacial roughness responsible for the inhomogeneous broadening of optical transitions in the heterostructures has been determined to be ≈ one-half monolayer.. The simplicity and accuracy of the spectroscopic technique described above makes it attractive for general application to other material systems which support type-II band alignment.

The luminescence spectra of type-II MQWs exhibit a low-energy peak which arises from the recombination of spatially separated electrons and holes. The application of an

electric field breaks the degeneracy of the indirect transition between adjacent layers, and consequently, two oblique transitions are observed. The higher-energy indirect transition is favored because the *e* and *h* wavefunction are pulled closer together by the electric field. This effective reduction of the Γ-X splitting will be used to control the spatial distribution of electrons and the associated nonlinearities (see Chapters 5 and 6).

3 Nonlinear Optical Properties of Quantum Wells

Due to the strong absorption in GaAs, photoexcitation above the band edge generates large populations of excited carriers, which in turn cause changes in the optical properties of the material. These changes or nonlinearities induced in the optical spectra can be caused by bound states (such as excitons) or by unbound states (such as an *e-h* plasma). For the case of ultrafast photo-excitation, non-thermal distributions of *e* and *h* are created. The excited *e* (and *h*) reach a thermal distribution through several relaxation processes. Two relaxation times should be distinguishable. First, the excited *e* and *h* should reach a quasi-thermodynamic equilibrium (i.e. a temperature can be assigned to each distribution) among themselves through carrier-carrier scattering ($< 1\ ps$), then the carriers cool to the lattice temperature through inelastic lattice scattering (~100 picoseconds). It has been experimentally determined that the physical parameters which are most important are: the carrier density (n), the temperatures of the carrier distributions (T_e and T_h), and the bath temperature (not necessarily the same as the carrier distribution temperatures). Theoretical models for optical absorption in bulk and type-I QW semiconductors are well documented [see e.g. Haug and Schmitt-Rink, 1984; Zimmermann, 1987; Chemla *et al.*, 1988; Schmitt-Rink *et al.*, 1989; Haug and Koch, 1990]. In this chapter simple physical interpretations of the many-body effects of an *e-h* plasma are presented. First, a general overview of many-electron effects is presented in Section 3.1. Then the nonlinear effects due to the space-charge separation in type-II quantum wells is presented in Section 3.2.

3.1 Many-body effects

The general mechanisms by which the *e-h* plasma cause nonlinear effects are: (i) direct plasma screening of the Coulomb interaction between the charge carriers (particularly the attractive potential between *e-h* pairs); (ii) Coulomb exchange-correlation interaction; and (iii) phase-space filling (PSF: also referred to as Pauli "blocking" or exclusion). The potential energy felt by the carrier consists of several parts:

$$V_{tot} = V_0 + V_H + V_{xc} \tag{3.1}$$

where V_0 is the crystal potential. The Hartree potential (V_H) describes the electrostatic potentials and is non-zero only for a non-uniform distribution of charge (as is the case in type-II QWs; see Sec. 3.2.1). The final term in eqn. (3.1) arises from Coulomb exchange interaction and correlation (generalized Coulomb hole) effects.

Screening

Direct screening is the primary mechanism which reduces (or bleaches) the excitonic absorption in a bulk (3d) material. In other words, the Mott transition can extinguish the exciton state before phase-space filling (PSF) becomes strong. Screening by a plasma is extremely effective compared to the screening by excitons because the plasma's excitation spectrum has no energy gap. Intraband transitions in a plasma do not consume energy, whereas excitons can only screen by transitions from their ground state to some excited state. Thus, the energy gap in the exciton excitation spectrum requires some energy so that screening by excitons is much weaker than screening by plasmas. In the static long-wavelength limit, the presence of a plasma transforms the Coulomb potential into a Yukawa potential and the condition for the disappearance of bound states is the famous Mott

criterion $\kappa_{3d}a_0 \sim 1$, where a_0 is the bulk exciton radius and κ_{3d} is the 3d screening wavenumber [see e.g. Haug and Koch, 1990].

Femtosecond experiments in QWs have shown that screening is diminished in 2d [Knox *et al.*, 1986]. Various arguments can be given for the weakening of screening in 2d versus 3d. The plasma screening is determined by the number of carriers that can undergo intraband transitions and thus is proportional to the density of states (DOS). In 2d the DOS is constant, whereas in 3d, the DOS is proportional to $E^{1/2}$. In fact, the static 2d screening wavenumber becomes constant in the low temperature and high-density limit [see e.g. Haug and Koch, 1990] due to the constant DOS.

Exchange and correlation

In an interacting electron gas the Pauli exclusion principle forbids electrons with the same spin to occupy the same k-state. In a non-interacting electron gas electrons with opposite spin do not even "see" each other. However, a reduction in the correlation of electrons with opposite spin occurs in an interacting many-electron system. Within the random phase approximation [see e.g. Schmitt-Rink *et al.*, 1989] the self-energy (Σ) can be split into a screened exchange (sx) and a correlation (Ch) term

$$\Sigma(k) = \Sigma_{sx}(k) + \Sigma_{Ch}(k) \tag{3.2}$$

where

$$\Sigma_{sx}(k) = \sum_{\vec{k}'} V_s(\vec{k} - \vec{k}', \varepsilon_k - \varepsilon_{k'}) \; f(k') \tag{3.3}$$

and

$$\Sigma_{Ch}(k) = \sum_{\vec{k}'} \int_{-\infty}^{\infty} \frac{\hbar d\omega}{\pi} \frac{\mathrm{Im}\, V_s(\vec{k} - \vec{k}', \hbar\omega) g(\hbar\omega)}{\varepsilon_k - \varepsilon_{k'} - \hbar\omega + i\delta} \tag{3.4}$$

where $V_s(\vec{q}, \hbar\omega)$ is the screened Coulomb interaction, $\varepsilon_k = \dfrac{\hbar^2 k^2}{2m_{e,h}}$ + constant are the Hartree energies and $f(\mathrm{k})$ is the Fermi distribution,

$$N = 2\sum_k f(k) = 2\sum_k \frac{1}{\exp\left(\frac{\varepsilon_k - \mu}{k_B T}\right) + 1} \tag{3.5}$$

and $g(\hbar\omega)$ is the Bose distribution,

$$g(\hbar\omega) = \frac{1}{\exp(\hbar\omega / k_B T) - 1} \tag{3.6}$$

The expressions in eqns. (3.3) to (3.4) are both negative and therefore lead to a lowering of the single-particle energy. Physically, one can view the electron as having an "exchange hole," which indicates that the mean separation between electrons with parallel spin is larger than it would be without the Pauli principle. The existence of the exchange hole reduces the overall Coulomb repulsion and consequently, reduces the energy of the system. Similarly, the reduction in Coulomb correlation effects described by eqn. (3.4) can be viewed as a generalized "Coulomb hole." Σ_{Ch} describes the energy gain due to charge polarization of the medium. The exchange term dominates at high densities because $\Sigma_{Ch} \sim -n^{1/3}$ while $\Sigma_{sx} \sim -n^{1/2}$ in their asymptotic limits [Schmitt-Rink *et al.* 1989].

The renormalized single-particle energy is now given by,

$$\varepsilon_{e,k} + \varepsilon_{h,k} \rightarrow \varepsilon_{e,k} + \varepsilon_{h,k} + \Sigma_e + \Sigma_h \tag{3.7}$$

This energy shift can be viewed as a rigid shift of the bandgap, and is often referred to as bandgap renormalization (BGR) or shrinkage. In general, the renormalization for electrons and holes and different subbands are unequal. This is a particularly important point when considering a single-component plasma. For example, in an n-type material, electrons experience exchange and correlation effects, while holes experience only correlation effects [Schmitt-Rink *et al.*, 1989].

To gain further physical insight, the exact solution to the Hartree-Fock exchange term in 2d is given below [Pan, 1988]:

$$V_{exc}(k) = -\frac{e^2 k_F}{4\pi\varepsilon_0}\frac{2}{\pi}\mathrm{E}\left(\frac{k^2}{k_F^2}\right) \tag{3.8}$$

where k_F is the Fermi wavenumber, ε_0 is the dielectric constant and e is the electronic charge. The elliptic integral $\mathrm{E}(x)$ decreases monotonically from $\pi/2$ to 1 as x varies from 0 to 1. Of course, the carrier density, n, is proportional to k_F^2 in 2d (see below). Therefore,

$$E_{\mathrm{exc}}(k) \sim -n^{1/2}. \tag{3.9}$$

The short-coming of the above model is of course the improper treatment of screening and correlation effects, however, it provides a simple starting point for estimating experimental results. According to Eqn. 3.8, for $\boldsymbol{k = 0}$ the average shift is given by $-\frac{e^2 k_F}{4\pi\varepsilon_0}\frac{8}{3\pi}$; for $n = 5\mathrm{x}10^{11}\ \mathrm{cm}^{-2}$, the average shift will be $\langle E_{\mathrm{exc}}(k)\rangle \approx -20\ meV$.

Phase-space filling

The phase-space filling (PSF) by an *e-h* plasma are well-known. As stated above, the Pauli exclusion principle "blocks" absorption transitions into an occupied state in k-space. This occurs only for fermions with the same spin, and is most efficient at short distances. The distribution functions, $f_{\mathrm{e}}(k)$ and $f_{\mathrm{h}}(k)$, describe the occupied states. Since absorption can only take place into unoccupied states, absorption is proportional to $(1 - f_{e,h})$ and the effective energy gap equals the sum of the e and h quasi-Fermi levels $(\varepsilon_{e,F} + \varepsilon_{h,F})$. Consequently, the effects of PSF on absorption transitions are most effective at low plasma temperatures. A cold plasma is especially efficient when the thermal spread of the Boltzmann distribution in k-space is much less than the inverse exciton radius.

Phase-space filling in the simplest form (T = 0 K) is often referred to as band filling. The areal density in 2d is given by

$$n = 2g\frac{k_F^2}{4\pi} \tag{3.10}$$

where g is the band degeneracy (g = 2 for the GaAs Γ-band). The Fermi energy is given by

$$E_F = \hbar^2 \frac{k_F^2}{2m^*}, \tag{3.11}$$

which implies that

$$E_F = \hbar^2 \frac{\pi}{m^*}\frac{n}{g} \tag{3.12}$$

Thus, the band filling is proportional to the carrier density. Eqn. (3.12) shows that a +9 meV bandwidth is expected for $n = 5\text{x}10^{11}\ cm^{-2}$.

Energy shifts

The difference due to Pauli exclusion between the perturbed and unperturbed *e-h* relative motion Hamiltonians in momentum space is

$$\left\langle \bar{k} \middle| \delta H \middle| \bar{k}' \right\rangle_{sx} = -\delta_{\bar{k},\bar{k}'} \sum_{\bar{k}''} V_s(\bar{k}-\bar{k}'')[f_e(k'')+f_h(k'')] \\ +V_s(\bar{k}-\bar{k}')[f_e(k)+f_h(k)] \tag{3.13}$$

where $V_s(q)$ is the screened Coulomb interaction. The first term in eqn. (3.13) is a self-energy correction that encompass the *e* and *h* exchange self-energies. The second term is the corresponding vertex correction, which describe the weakening of the *e-h* interaction due to the exclusion principle. For simplicity, the correlation term which also has a

corresponding cancellation term has been excluded. In bulk or wide (L_z > 100 Å) type-I QWs there is significant cancellation of the competing effects described by eqn. (3.13). Thus, bound-state energies are fairly constant in bulk and type-I structures. This important phenomena was first explained by Gay (1972) and put on firm ground by Zimmermann *et al.* (1978). The point is quite simple: when one brings *e* and *h* together, their opposite polarization clouds partially cancel each other, The smaller the bound state, the larger the cancellation [Schmitt-Rink *et al.*, 1989].

Alternatively, the constancy of the exciton state in type-I QWs can be viewed as a cancellation of attractive and repulsive forces. The effects of Pauli blocking, in a weakly non-ideal boson picture, can be re-interpreted as hard core repulsion of excitons and electrons. It has been argued by Schmitt-Rink *et al.* (1989) that the long-ranged Coulomb correlation between excitons can be viewed as a "poor man's Van der Waals attraction." Hard core repulsion gives rise to a blue shift, and Van der Waals attraction gives rise to a red shift. Again, excitons in 3d and wide QWs (d > 100 Å) hardly shift because a nearly exact cancellation occurs [see e.g. Zimmermann, 1987; Haug and Schmitt-Rink, 1984].

Deviations in Type-I QWs: exciton-exciton interaction

Schmitt-Rink *et al.* (1989) have extended this simple physical picture to explain the observation of an exciton blue shift in narrow GaAs/AlGaAs type-I QWs [Peyghambarian *et al.*, 1984; Hulin *et al.*, 1986; Masumoto *et al.*, 1986; Weinert *et al.*, 1987]. In 2d the effects of the long-ranged Coulomb correlation are quenched and consequently the blue shift due to Pauli blocking is no longer canceled exactly [Schmitt-Rink *et al.*, 1985]. Absorption measurements [Peyghambarian *et al.*, 1984; Hulin *et al.*, 1986; Masumoto *et al.*, 1986] performed on QWs of various thicknesses have shown this blue shift when excitons are *selectively* generated (i.e. the exciton was resonantly pumped). In addition, excitons formed ~100 ps after the interband optical excitation at low temperatures also

exhibited shifts toward higher energies [see Chapter 6]. The blue shift is difficult to observe in wide QWs because only in the 2d limit does the quenching of the long-range Coulomb correlation become significant. One final note: the *hh* and *lh* excitons both shift to higher energy in the case of exciton-exciton interactions. The conditions are quite different in type-II QWs because the nonlinear effects in the absorption spectra arise from a *heterogeneous* hole plasma, rather than from a homogeneous plasma for the type-I case.

3.2 Type-II quantum wells: spatially heterogeneous plasma

3.2.1 Space-charge effect

A space-charge potential created by the spatially separated *e-h* plasmas in type-II QWs lead to optical nonlinearities in the PL spectra. The space-charge or Hartree potential [V_H in eqn. 3.1] consists of the electrostatic potentials due to ionized impurities and free carriers. It depends on the local distribution of carriers through Poison's equation, and therefore must be determined self-consistently [see e.g. Ruden and Dohler, 1983]. The Hartree potential gives rise to the band bending shown schematically in Fig. 3.1. For most of the type-II structures considered here the Γ-X splitting is large and charge transfer can be assumed to be complete. Poisson's equation for a type-II sample is

$$\frac{d^2}{dz^2}V_H(z) = -\frac{4\pi e^2}{\varepsilon_0}[\rho_e(z) - \rho_h(z)] \qquad (3.14)$$

where ρ_e and ρ_h are the electron and hole densities, respectively. Consider a simple model where the charge distribution is uniform within each layer (and neglect image charges), then the solution to eqn. 3.14 is simply

$$V_H(z) \sim -\frac{2\pi e^2 z^2}{\varepsilon_0 L_z} n \tag{3.15}$$

(in the GaAs layer). The important physical results are: (1) the Hartree potential is proportional to n; (2) the bands in adjacent layers bend in opposite directions which results in a net increase in the indirect transition energy and net decrease in the Γ-X splitting; and (3) the bands in the same layer bend in the same direction, thus the Hartree potential has little effect on spatially direct transitions.

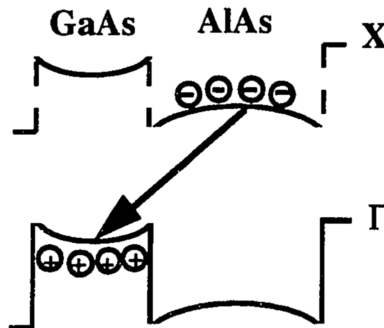

Figure 3.1 Band bending due to spatial separation of electrons and holes.

Hartree potential in asymmetric type-II MQW

The effect of the Hartree (or space-charge) potential has been investigated by Olbright *et al.* (1990a). By adding a nondegenerate AlAs layer in a novel type-II MQW structure (shown schematically in Fig. 3.2), they were able to distinguish the effects of bandgap reduction from the effects of the space-charge potential. One period of the "asymmetric" structure consisted of AlAs(50 Å)/GaAs(25 Å)/AlAs(18 Å)/GaAs(25 Å). Under cw optical excitation, the electrons distribute themselves among the three wells, Γ_1, X_1, and X_2,

according to Fermi statistics at a given temperature. The holes, on the other hand, remain at the GaAs Γ-point. The majority of the electrons are expected to reside in the X_1 well since it is the lowest-lying state. The energy splitting between the X_1 and X_2 wells was chosen such that significantly fewer electrons occupy the X_2 well. Thus, the potential drop between the 50-Å AlAs layer and the adjacent GaAs layers will be much greater than the potential drop between the 18-Å AlAs layer and the GaAs layers. The e1x→*hh* transition is therefore, analogous to the Γ-X indirect transition in a symmetric type-II structure.

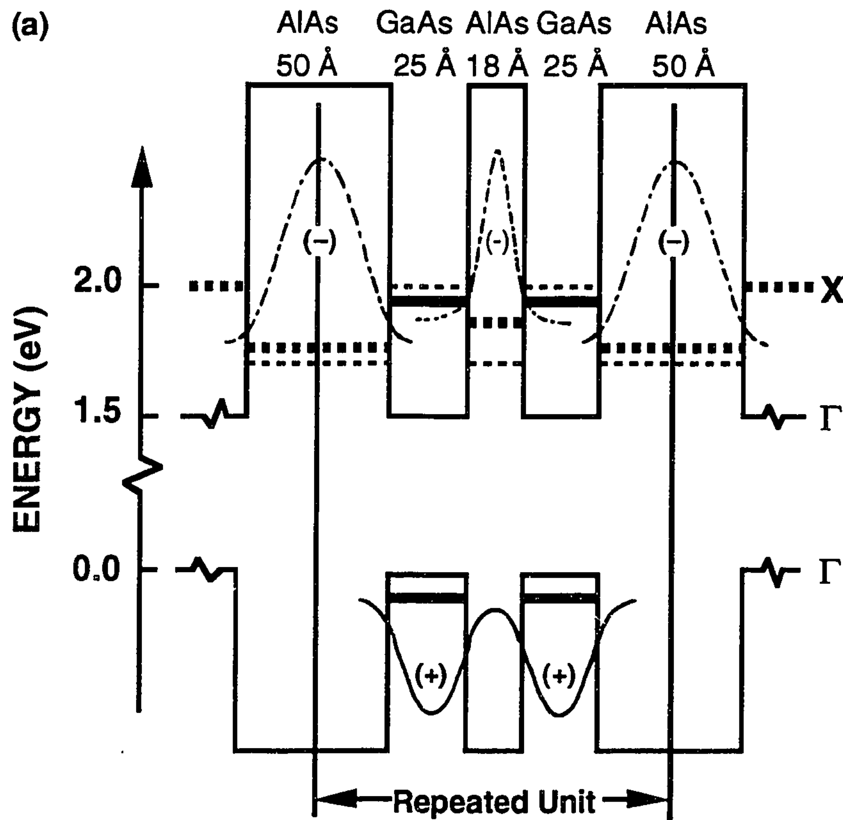

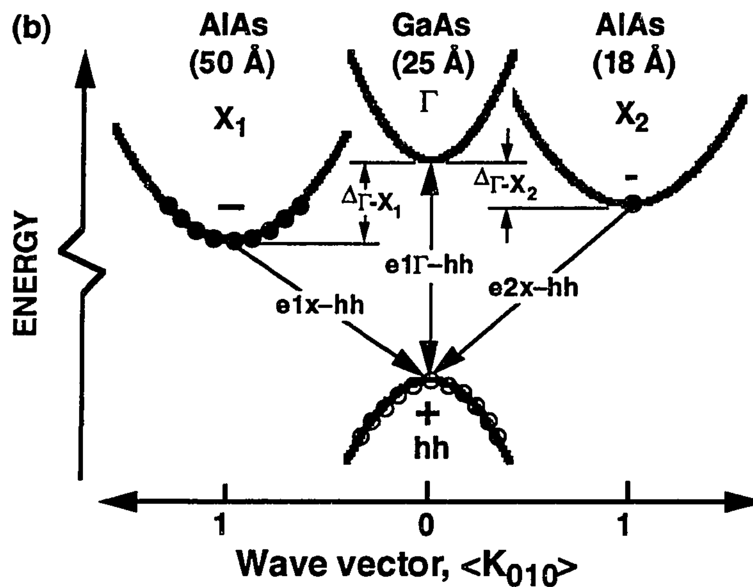

Figure 3.2 Schematic band diagram of asymmetric type-II QWs in (**a**) real and (**b**) momentum space. The light solid lines trace the Γ-band for the bulk semiconductors while the light dashed lines trace the X-band for bulk semiconductors. The respective dark lines show the effect of quantum confinement. Absorption (up arrow) occurs primarily in the GaAs layer due to momentum conservation. The three non-degenerate radiative transitions are shown by the downward arrows. The wavefunctions were calculated in the low-density limit, using a simple finite-potential -well Kronig-Penney model. The wavefunctions illustrate the overlap between the two AlAs X-like wavefunctions and the GaAs Γ-like. [After Olbright *et al.*, 1990]

cw linear and nonlinear photoluminescence

The absorption of the excitation laser occurs in the GaAs layer. The electrons then distribute themselves among the three wells, Γ_1, X_1, and X_2, according to the law of mass action while the holes remain at the GaAs Γ-point. The subsequent recombination of the carriers involves all of the electron levels as well as the two hole-levels. The linear PL and absorption spectra of this asymmetric type-II MQW structure are shown in Fig. 3.3 (solid lines). PL spectra are mainly determined by the relative occupation of the various levels and the carrier lifetimes (i.e. the overlap of the electron and hole wavefunctions). As expected, the relative intensity and lifetimes (see inset) of the PL peaks in Fig. 3.3 verify

that the majority of the electrons reside at the lowest-energy point in the conduction band (X_1).

The nonlinear PL spectrum (dashed line) in Fig. 3.3 reveals three dramatic effects: First, the lowest-energy PL peak (e1X$\rightarrow$*hh*) shifts to higher energy. Second, a small red shift of the intermediate-energy PL peak (e2X$\rightarrow$*hh*) is observed. Finally, the relative intensity of the direct PL peak (e1$\Gamma\rightarrow$*hh*) increases. In this system, the spatially separated *e* and *h* plasmas cause a shift in the bands resulting from two primary contributions: (1) the exchange-correlation interaction and (2) the macroscopic electric-field potential. The exchange-correlation interaction leads to a reduction of the energy gap which increases sub-linearly with density, as is well known from the theory of a spatially homogeneous, neutral *e-h* plasma [see Sec. 3.1]. Let us first consider the two extreme transitions: the direct e1$\Gamma\rightarrow$*hh* and indirect e1X$\rightarrow$*hh*. Using the AlAs X_1-point as a reference point, the space charge potential in the GaAs layer shifts both the conduction and valence bands down by approximately the same amount. Therefore, the spatially direct transition experiences negligible shift from the Hartree potential. At high densities the space-charge potential is roughly proportional to the carrier density (n) while the bandgap shrinkage is proportional to $n^{1/2}$. Therefore, a net blue shift of the e1X$\rightarrow$*hh* transition results because the Hartree potential overcompensates the red shift arising from bandgap shrinkage (i.e. the renormalization of the single particle states).

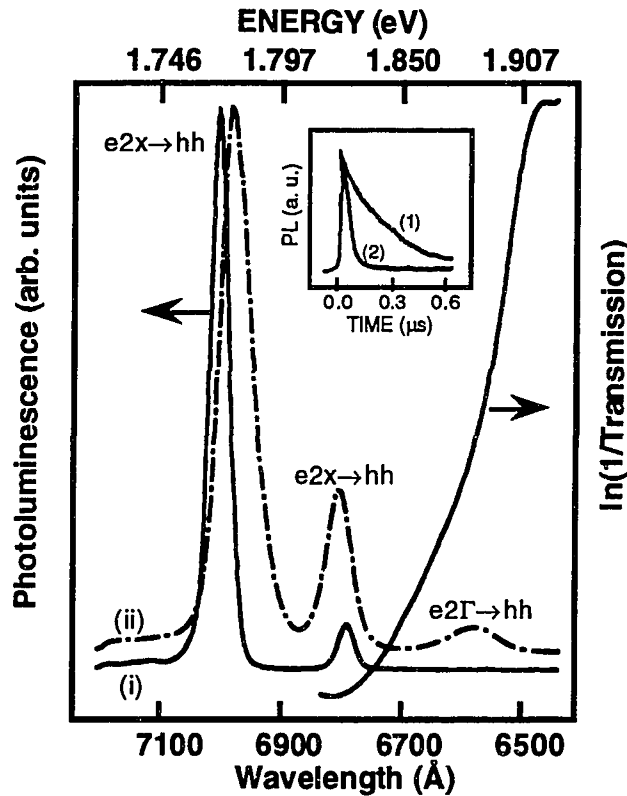

Figure 3.3 Photoluminescence spectra of the asymmetric type-II QW depicted in Fig. 3.2. (i) 1 W/cm^2 (ii) 500 W/cm^2; $E_{exc.}$ = 1.959 eV. The notation emx→hh (m = 1, 2) refers to the recombination of the *m*th-level X-like AlAs electrons with the GaAs Γ-point heavy holes. [After Olbright *et al.*, 1990]

Because most of the electrons are confined to the 50-Å AlAs layer, and all of the holes are confined to the GaAs layer, the primary potential drop due to the space-charge field occurs between these two layers. The potential drop between the 18-Å AlAs layer and the GaAs layer is much less significant, and consequently, the reduction of the bandgap dominates in the form of a red shift of the e2X→*hh* transition. Finally, the direct transition (e1→*hh*) is affected the least by the space-charge potential since the conduction and valence bands shift in parallel. Fig. 3.4 schematically illustrates the band shifts. Self-consistent solutions to the coupled Schroedinger and Poisson equations based on the δ-sheet model for the carriers confined in the asymmetric type-II heterostructure corroborate the experimental results [Olbright *et al.*, 1990; Binder *et al.*, 1991]. The additional width of

the luminescence spectra at finite densities simply reflect the occupation of *e* and *h* states according to Fermi statistics.

Finally, the blue shift of the e1X→*hh* transition results in a reduction of the Γ-X_1 splitting. This accounts for the increase in the relative intensity of the direct transition. In Chapter 2 the application of an external electric field was used to effectively reduce the Γ-X splitting in type-II MQWs. A direct analogy can be made with similar electric-field effects in *p*+-type δ-doped heterostructures [Ruden and Dohler, 1983].

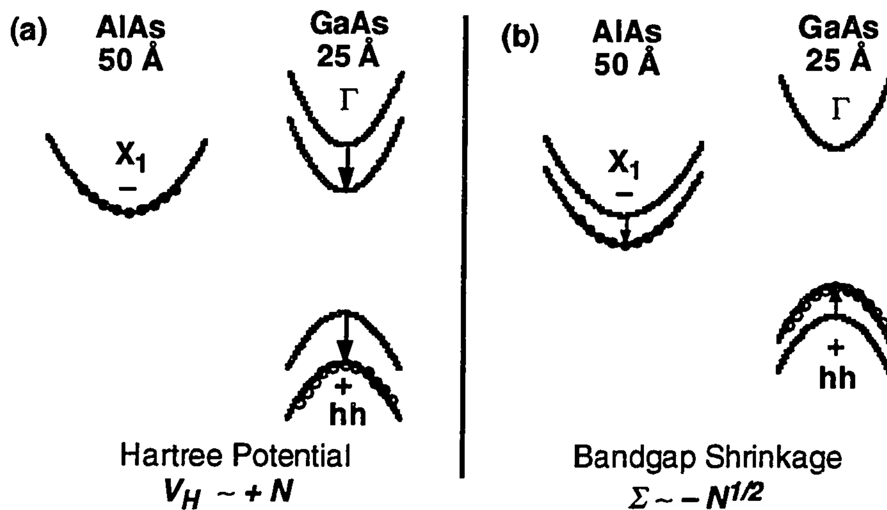

Figure 3.4 Schematic band diagram depicting energy shifts due to the (a) Hartree potential and (b) Coulomb exchange-correlation effects (i.e. bandgap renormalization).

3.2.2 Generalized Wannier equation

It is generally an extremely involved task to model a spatially inhomogeneous system like a type-II MQW structure. The spatial separation of electrons and holes creates an electric field similar to that in *n-i-p-i* structures [Ruden and Dohler, 1983]. Binder, Galbraith, and Koch (1991) have successfully modeled the experimental optical

nonlinearities of type-II MQWs presented in this thesis (see Chapter 5). They have analyzed the many-body effects through numerical solutions of a generalized Wannier equation,‡ which accounted for dynamical exchange and correlation effects as well as PSF. The generalized Wannier equation was derived by Binder *et al.* (1991) in the framework of the nonequilibrium Green's function. In order to describe the temperature-dependent damping mechanisms accurately the screening was treated dynamically. An important feature of their model is that it allows independent selection for the electron and hole densities, n_e and n_h, respectively. This has allowed the general description of type-I QWs, type-II QWs, and intermediate cases. The initial treatment was restricted to the case of thermal quasi-equilibrium. A general nonequilibrium treatment can be described by the so-called semiconductor Bloch equations.

The semiconductor Bloch equations are coupled equations of the polarization (P_k) and the population distributions (f_k) [see e.g. Lindberg and Koch, 1988; Haug and Koch, 1990]. Coulomb exchange and PSF terms are incorporated into the Bloch equations to accurately model the many-body effects associated with highly excited semiconductors [Lindberg and Koch, 1988]. Binder et al. (1990) have demonstrated the use of the semiconductor Bloch equations to study ultrafast adiabatic following (e.g. optical Stark effect) in semiconductors.

‡ As mentioned in Chapter 2, the Wannier equation is the two-particle Schroedinger equation for the relative motion of an electron and a hole interacting via the attractive Coulomb potential.

4 Transient and Steady-State Spectroscopy

The field of femtosecond spectroscopy has grown tremendously in the last fifteen years. Today, there are several dye and solid-state lasers which can generate subpicosecond pulses [Shah, 1989]. The experimental method most widely used (and most informative) is the pump and probe technique, where a strong laser beam is used to excite the sample and a weak beam which does not appreciably change the carrier density is used to probe the sample. A broad-band continuum probe is preferable for investigation of effects over a large spectral range, such as excitonic saturation and shifts. The generation of a short-pulse continuum requires the use of an optical amplifier. Among the various systems demonstrated to date, the copper-vapor-laser (CVL) amplifier system is best suited for temporal studies of type-II QW systems (see Fig. 4.1). CVLs typically operate at 8 kHz repetition rate [i.e. there is approximately 120 microseconds (μs) between pulses]. Since the radiative recombination lifetime of type-II systems are on the order of one microsecond (~ 1 μs), the CVL amplifier system allows sufficient time for the type-II samples to recover to their ground state before the next laser-excitation pulse arrives.

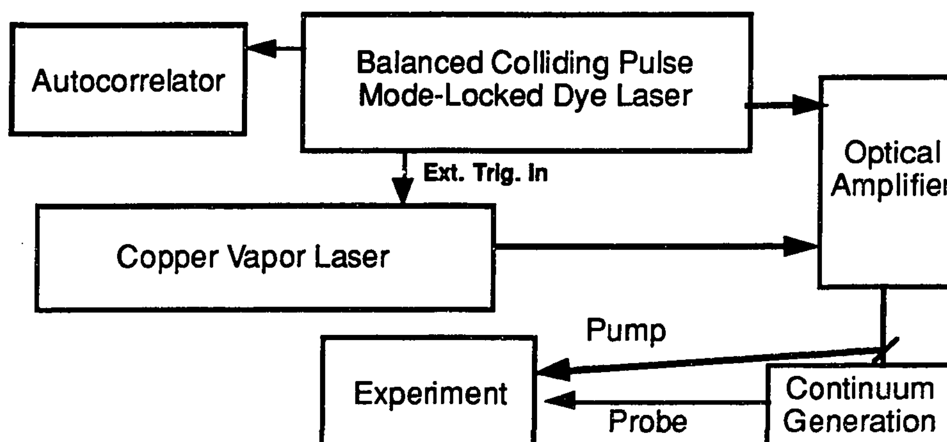

Figure 4.1 Block diagram of the femtosecond optical pulse generation system.

4.1 Generation of amplified femtosecond optical pulses

The colliding-pulse mode-locked (CPM) ring dye laser, which generates about 60-femtosecond (*fs*) pulses was built following the system described by Fork, Greene, and Shank (1981). The CPM was pumped by an argon-ion laser (see Fig. 4.2). The CPM was "balanced" by an intracavity prism assembly which introduced adjustable negative group velocity dispersion [Fork *et al.*, 1984; Bor and Racz, 1985]. The prisms allowed for continuous adjustment of optical pulse duration from 30 *fs* to 500 *fs*. The repetition rate of the ring laser was 88 megahertz (*MHz*). The lasing wavelength was centered around 6200 Å, and the frequency bandwidth was nearly Fourier-transform limited. The average power of the ring was 10-15 miliwatts (*mW*) or 200 picojoules (*pJ*) per pulse. Average power fluctuation was less than one percent (1%).

A 5-fs resolution real-time autocorrelator was used to measure the pulse duration of the CPM. A 1-fs resolution stepper-motor controlled delay line [Fork and Beiser, 1978] was used for cross-correlation measurements of the pump and probe beams.

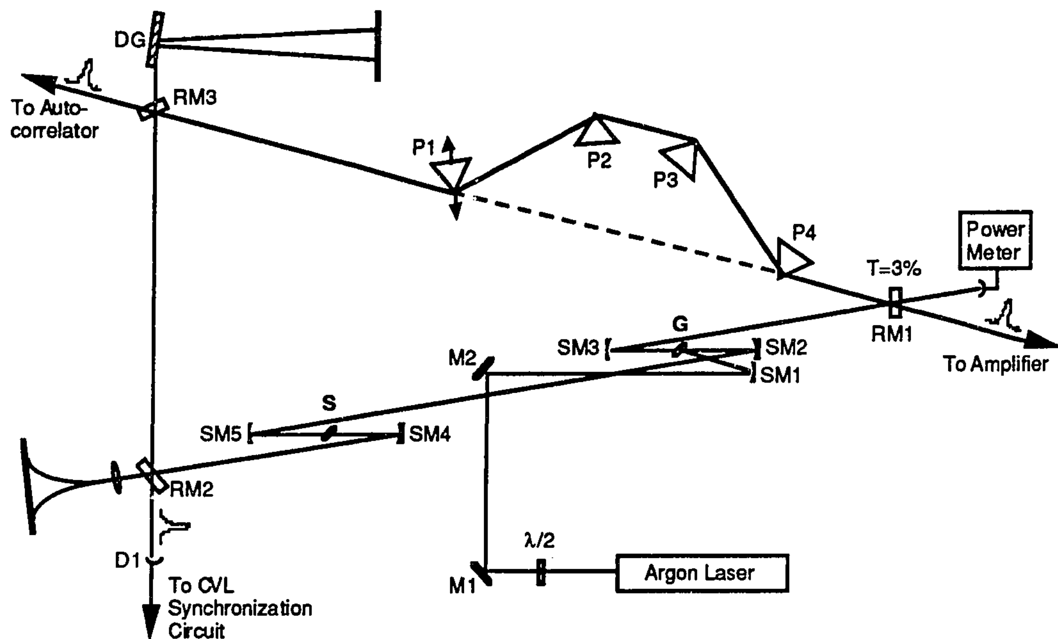

Figure 4.2 Schematic diagram of the Balanced Colliding Pulse Modelocked (CPM) Ring Dye Laser. P = prism; RM = resonator mirror; SM = sub-resonator (spherical) mirror; DG = diffraction grating; G = gain dye jet; S = saturable absorber dye jet. [see e.g. Olbright, 1987]

The CPM laser, which generated 200 *pJ* of energy per pulse at a repetition rate of 88 *MHz*, was amplified to 1 μJ per pulse at a repetition rate of 8.1 *kHz* by a CVL-pumped amplifier [Knox, *et al.*, 1984]. A fast photodiode was used to monitor the CPM laser pulses. The signal from the photodiode was fed into an electronic counter to frequency down-convert to 8.1 *kHz*. The signal from the counter in turn went to a pulse generator which synchronously triggered the CVL. The CVL pulses were seven nanoseconds (7 *ns*, FWHM) in duration. The trigger was adjusted to temporally synchronize each CVL pulse with a CPM laser pulse. A CPM pulse was passed five times through a gain jet (sulfo-rhodamine 610) which was optically pumped by the 7-*ns*-duration CVL pulse. The average gain per pass was $[1\ \mu J/200\ pJ]^{1/5} = 5.5$. The amplified stimulated emission (ASE) and the unamplified portion of the CPM pulses were suppressed with a saturable absorber (malachite green) after the fifth pass through the gain jet. Under optimal

conditions, 60-*fs* pulses from the CPM were broadened by self-phase modulation and positive group velocity dispersion to ~100 *fs*. The average power fluctuation of the amplified 8.1 *kHz* pulse train was less than 10%.

A broad-band continuum probe was generated as follows: Fifteen percent (15%) of the amplified beam was split off, and focused onto a 1-mm thick diamond single-crystal window. Focusing the beam to a 20-μm-diameter spot on the diamond window provided sufficient field intensities to generate the broad-band continuum. In the past, an ethylene glycol jet was used to generate the continuum, but the diamond window provided more efficient continuum generation (both in intensity and spectral bandwidth). Typically, intensities in excess of 10^{12} W/cm^2 are required to create a continuum in ethylene glycol.† The efficiency of the diamond window allowed nearly 85% of the amplified pulse to be reserved for the excitation pulse. The continuum had a duration of ~100 fs and a bandwidth which extends from the near ultraviolet to the near infrared ($\Delta\lambda > 4000$ Å). The continuum was collected and collimated with a lens. The collimated beam was then spectrally filtered to eliminate light with wavelengths shorter than 6300 Å. The bandwidth of the light used to probe the samples was approximately 1300 Å.

The generalized pump-probe experimental configuration is shown in Fig. 4.3. The transverse spatial extent was controlled by lenses L1 and L2. The time delay between the pump and the probe was controlled with a stepper-motor translation stage. Polarizer POL1 (POL3) allowed continuous adjustment of the pump (probe) intensity without changing the optical path difference between the pump and probe legs. Polarizers POL2 and POL4 were cross-polarized to avoid interference effects between pump and probe. The pump and probe beams were spatially and temporally overlapped on the cold-finger of the

---

† Continuum generation occurs at very high excitation intensities. The local electric field of the light at these high intensities become comparable to that experienced by core electrons. Continuum generation can be viewed classically as a perturbation of the electron orbit which results in radiation of the accelerated charge. Frequency mixing (self-phase modulation) generates harmonics which cover the optical region of the spectrum.

vibrationally isolated closed-cycle refrigerator. The cross-correlation was performed using a 300-μm thick lithium iodate crystal. The sum nonlinear signal ($\omega_1 + \omega_2$) was detected with a photomultiplier tube (PMT). The signal from the PMT was averaged by a box-car and plotted by a chart recorder as the delay line was scanned through the overlap of the pump and probe. The measured cross-correlation function [see Fig. 4.4] provided a measure of the pulse width, pulse shape, and the zero-time position. The resolution of the cross-correlation was approximately 1 fs.

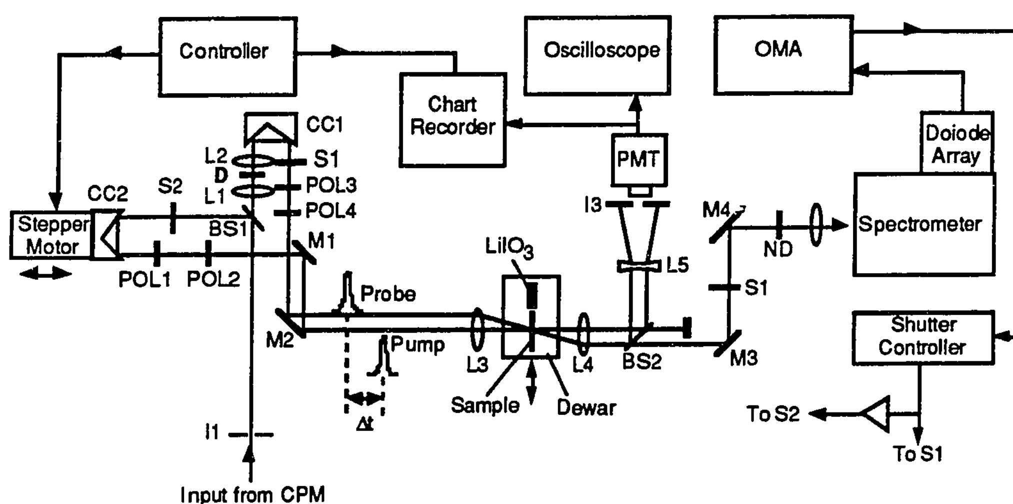

Figure 4.3 Pump/probe experimental configuration. BS = beamsplitter, CC = corner cube, D = diamond, I = iris, IF = interference filter, L = lens, $LiIO_3$ = lithium iodate, M = mirror, ND = neutral density, OMA = optical multi-channel analyzer, PMT = photomultiplier tube, POL = polarizer, S = shutter. [see e.g. Olbright, 1987]

After measuring the cross-correlation, the beam was translated off the lithium iodate crystal and onto the sample using 0.1-μm resolution stepper-motor stages (one stage for each optical axis). The spatial overlap of the pump and probe beams were verified with a 100-μm pinhole and a calibrated reading telescope. Aperture A2 spatially filtered the pump and luminescence while it allowed only the probe to pass through to the spectrometer. Aperture A2 was vital for accurate measurement of spectral features near the band edge (*e.g.* gain) because the luminescence appears at the band edge. Polarizer P5 was cross-

polarized with respect to P3 to extinguish the scattered luminescence pump light. The probe light, on the other hand, passed through to the spectrometer with minimal attenuation since P2 and P5 were polarized in parallel. A 0.34-m effective focal length spectrometer with a 600-line/mm blazed grating was used. The spectrometer connected to a 25-mm 1024-channel linear reticon array detector, which in turn was interfaced to an optical multichannel analyzer (OMA). The spectrometer/OMA set-up produced a 1200-Å optical window, and its resolution was 2-3 Å.

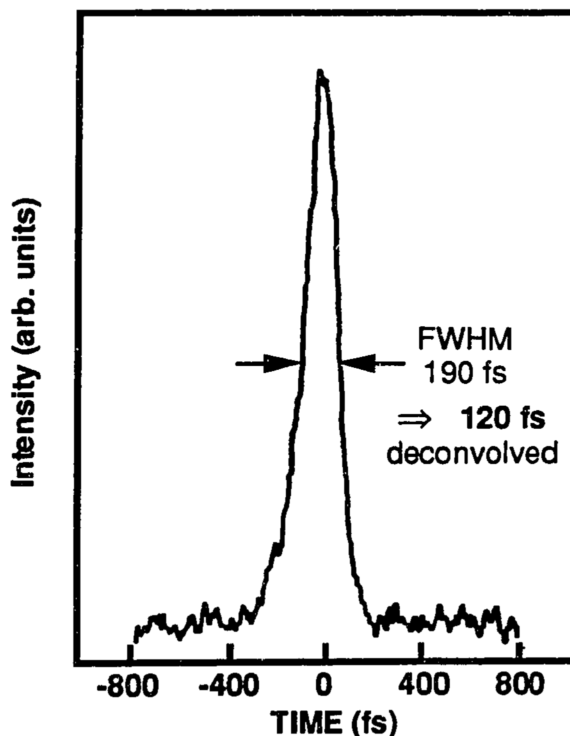

Figure 4.4 A typical cross-correlation trace of amplified pump pulse with filtered broad-band continuum probe pulse. FWHM is 120 fs, deconvolved.

4.2 Quasi-steady state spectroscopy

Two different methods were used to perform quasi-steady state spectroscopy on type-II QWs. As stated before, the quasi-steady-state in type-II QWs occurs on the order of one to ten nanoseconds after initial excitation because the carrier distributions require ~100 *ps* to reach the lattice temperature and the carrier lifetime is ~1 μs.

Nanosecond pump/nanosecond probe

A series of 7-ns pulses (λ = 530 and 578 nm) from the CVL were used to optically pump a dye laser. The laser wavelength was tuned to the He-Ne laser wavelength to mimic the cw excitation source. The fluorescence ($\lambda \approx$ 600–720 *nm*) from the DCM dye jet was collected with a microscope objective for use as a ns time-correlated broad-band probe. The pump and probe pulses were then routed to the cryostat in a similar fashion to that described above. The optical delay between the ns pump and probe pulses was measured with a fast GaAs photodiode.

Nanosecond pump/femtosecond probe

In the second set of nanosecond experiments the yellow laser line (λ = 578 *nm*) from the CVL was used as the excitation pulse, since only the green line (λ = 530 nm) was used in amplifying the femtosecond pulses from the CPM. Since the two laser lines from the CVL had perpendicular polarization, the 578-nm line was separated from the 530-nm line with a dicroic beam splitter. The fs continuum was generated in the same fashion described in Section 4.1. Again the optical delay was measured with a fast photodiode.

4.3 Differential transmission spectroscopy

The time-dependent spectra were obtained by constructing difference (or differential) transmission spectra (DTS). The DTS reveal saturation and shifts induced by the pump at a specific pump-to-probe delay. In the simplest case, only two transmission spectra are required to construct DTS:

$$DTS(\tau) = \frac{[T_{P+P}(\tau) - T_0]}{T_0} \tag{4.1}$$

where $T_{P+P}(\tau)$ is the transmission spectrum taken with both the pump and the probe present, and at a time delay between pump and probe given by τ. T_0 is the transmission spectrum taken without the pump present (i.e. linear transmission). The primary interest here is the nonlinearities near and below the unexcited band edge, and therefore, both the pump and the probe were mechanically shuttered [S1 and S2 in Fig. 4.3] in order to subtract the cw photoluminescence from the averaged pump-induced changes in the probe. An additional spectrum with only the pump present were taken in order to construct the DTS using

$$DTS(\tau) = \frac{[T_{P+P}(\tau) - P - T_0]}{T_0} \tag{4.2}$$

where P is the cw luminescence taken with only the pump present.

Since it is easier to observe shifts of a particular resonance in absorption spectra, the DTS was converted to absorption spectra using the linear transmission spectrum (T_0). The linear transmission spectrum is an exponential function of the absorption coefficient, α,

$$T_0 = \exp(-\alpha_0 L) \qquad (4.3)$$

where a perfect anti-reflection coating is assumed (i.e. R = 0). The nonlinear absorption spectrum is then given by

$$\alpha(t)L = -\ln[T(\tau)] = -\ln[DTS(\tau) + 1] - \ln[T_0] \qquad (4.4)$$

where L is the length of the absorbing material. Note that $\ln[T_0]$ is simply the linear absorption spectrum which can be taken independently. Each spectrum represents the integration of 3×10^5 pulses and the signal-to-noise ratio was greater than 5×10^3 (i.e. pump-induced changes in the transmission larger than 0.01% could be measured)..

4.4 Single-wavelength time scans

In cases where the temporal behavior of a certain spectral region is required, single-wavelength time scans (SWTSs) were performed using narrow-bandwidth interference filters (75-100 Å). The SWTSs were obtained with a lock-in amplifier and photomultiplier tube (PMT). Only the pump was chopped in this case. The probe light was spectrally filtered with a narrow band-pass interference filter after it passed through the sample. The light was then collected by a PMT mounted on the side exit port of the spectrometer. The PMT signal was fed directly to a lock-in amplifier and the data was acquired and stored using an IBM-compatible computer (with a 386 microprocessor).

The amplified femtosecond laser system described above is a versatile system which allows us to observe nonlinearities induced by a strong 100-fs pump pulse on time scales ranging from subpicosecond to nanoseconds over a wide spectral range.

5 Nonlinear Absorption: Quasi-Steady-State and Femtosecond Nonlinear Optical Properties of Type-II GaAs/AlAs Quantum Wells

In this chapter the complete temporal evolution of the optical nonlinearities in the absorption spectra of highly-optically-excited GaAs/AlAs type-II heterostructures is presented. These results are interpreted using simple physical arguments which arise from the well-known *e-h* plasma theory for bulk semiconductors [see e.g. Zimmermann, 1987; Chemla *et al.*, 1988; Schmitt-Rink *et al.*, 1989; Haug and Koch, 1990]. The spatial separation of *e* and *h* in type-II heterostructures allows the investigation of nonlinearities associated with a one-component hole plasma, the dynamics of which can be observed optically on subpicosecond to nanosecond time scales. In addition, the optical nonlinearities are controlled by using an applied electric field to vary the spatial distribution of electrons. The range of field strengths investigated includes the so-called band-alignment regime. In this regime, the optical nonlinearities are significantly changed.

Several time scales should be distinguished before discussing nonlinearities in type-II MQWs. In general, the non-thermal distribution of carriers created by a short optical pulse will thermalize among themselves through carrier-carrier scattering within a picosecond [i.e. the carriers can be described by distribution functions $f_{e,h}$ but with a hot carrier temperature]. Simultaneously, carriers scatter to the bottom of the bands via LO-phonon emission [~100 *fs*/LO-phonon; Shah, 1989]. In addition, in type-II QWs the

spatial transfer of photoexcited electrons from the GaAs layer to the AlAs layer occurs on a subpicosecond time scale (as discussed below). The absence of acoustic phonons at low lattice temperatures (k_BT << exciton binding energy) prevents the carrier distributions from reaching the ambient lattice temperature until hundreds of picoseconds after excitation. Finally, the radiative lifetime of the *e* and *h* is ~1 μs [Meynadier *et al.*, 1988; Wilson *et al.*, 1988]. The long radiative lifetime of the indirect transitions creates a "bottleneck" of carriers at the AlAs X-valley. Consequently, large densities of carriers can be created in type-II structures with moderate excitation intensities.

5.1 Quasi-steady-state absorption nonlinearities

Low-temperature linear (solid lines) and *nonlinear* (dashed lines) absorption and PL spectra for the (10/30) type-II sample are shown in Figure 5.1. The linear PL spectrum verifies the type-II band alignment: both the indirect (Γ-X) and direct (Γ-Γ) recombination peaks are observed. When optically excited ($n > 10^{11}$ cm^{-2}), both the indirect (Γ-X) PL and *hh*-absorption peaks shift to higher energies (see dashed curves in Fig. 5.1). The blue-shift of the indirect luminescence has already been discussed in Sec. 3.2.1. However, the physics behind the blue shift of the indirect PL and *hh* exciton are quite different since the macroscopic Hartree potential does not induce any significant net shifts in spatially direct transitions.

In order to study absorption nonlinearities of type-II QWs in quasi-equilibrium, nanosecond laser pulses ($E_{exc.} \approx 2.14$ *eV*, $\tau_{exc.} = 7$ *ns*) were used to excite carriers high in the band and 100-*fs* time-correlated broad-band continuum pulses to probe the samples [see Sec. 4.2]. Probing the system about a nanosecond after excitation allows the spatially separated *e* and *h* carrier distributions ample time to reach low lattice temperatures without significant recombination. Furthermore, the 8-*kHz* repetition rate of the copper-vapor laser

allows the type-II samples to fully recover to their unexcited state between excitation pulses.

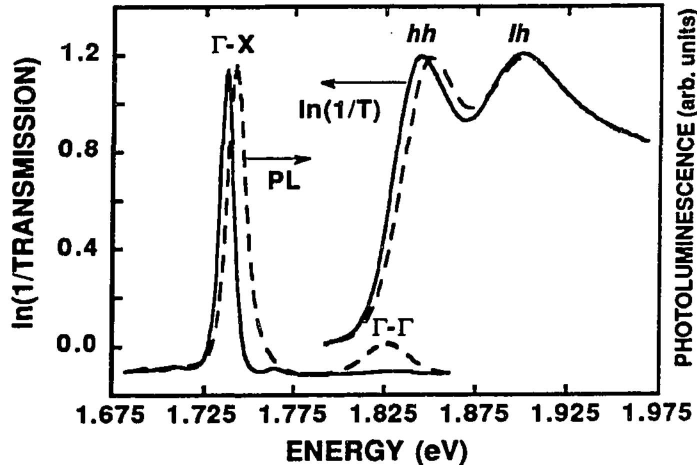

Figure 5.1. The blue shift of the absorption and photoluminescence (PL) spectra for the (10/30) GaAs/AlAs type-II sample. The linear spectra (I_{linear} = 1 W/cm^2) are in solid lines and the nonlinear spectra ($I_{exc.}$ = 10 kW/cm^2) are in the dashed lines. T = 15 K and $E_{exc.}$ = 1.96 eV. The indirect PL peak labeled Γ-X is due to the recombination of electrons confined to the AlAs X-point with holes confined to the GaAs Γ-point. The PL peak labeled Γ-Γ is due to direct recombination in the GaAs layer.

In Figure 5.2(a) the excitation-intensity-dependent absorption spectra are plotted for the (10/30) type-II structure at low temperature. The spectra show that the inhomogeneously broadened *hh*-exciton resonance shifts significantly toward higher energies and bleaches with increasing excitation intensity. In contrast, the *lh* exciton shifts to slightly lower energies and exhibits little reduction in oscillator strength for the intensities shown in Fig. 5.2(a). Finally, the optical gain is inhibited in type-II QWs: no evidence of optical gain is observed, even for carrier densities up to ~ 2x10^{12} cm^{-2}.

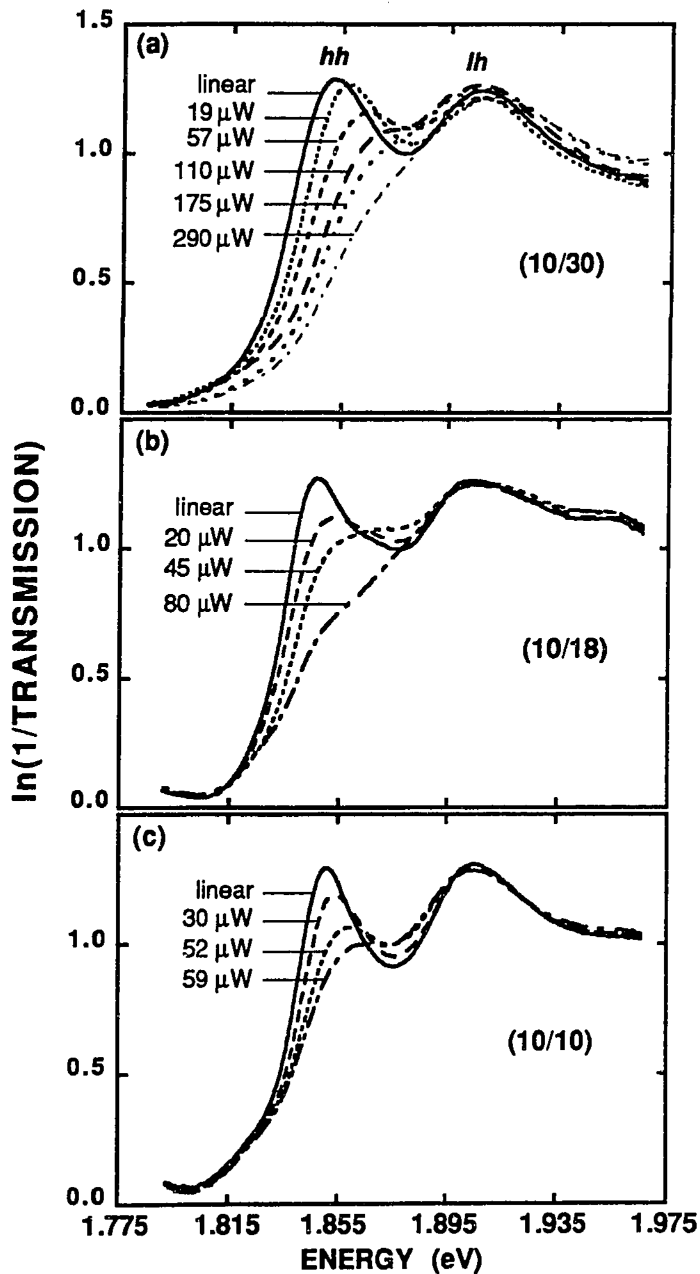

Figure 5.2. Experimental and excitation-intensity-dependent absorption spectra of the (a) (10/30), (b) (10/18), and (c) (10/10) type-II structures. The experimental conditions are: T = 30 K, $E_{exc.}$ = 2.14 *eV*, *f* = 8.2 *kHz*, $\tau_{exc.}$ = 7 *ns*. The carrier density for the spectrum labeled 110 μW is ~ 5×10^{11} cm^{-2}.

The dependence of the blue shift on the Γ-X splitting was investigated by repeating the experiment samples with 70 *meV* and 50 *meV* Γ-X splittings. These samples were nominally (10/18) and (10/10) GaAs/AlAs type-II MQWs. The dependence of the *hh* blue shift on the Γ-X splitting is summarized in Fig. 5.3. The blue shift decreases with the Γ-X splitting, thus suggesting that the blue shift arises from the spatial separation of electrons and holes. [However, as discussed in Section 3.2, the blue shift of the *hh* absorption peak cannot arise from the internal electric field induced by the space-charge layers.] The above results are corroborated by the electric-field-dependent data which are presented in Section 5.2.2.

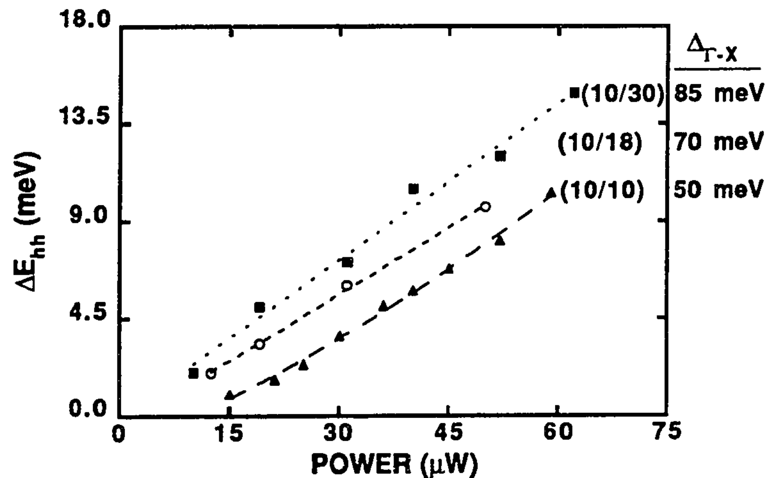

Figure 5.3. The blue shift of the heavy-hole exciton as a function of excitation intensity for the (10/30), (10/18), and (10/10) samples. The lines are drawn to aid the eye.

In a different experiment, nanosecond pulses were used for both the pump ($\lambda \approx$ 6320 Å) and probe [see Sec. 4.2]. As seen in Fig. 5.4, the results are very similar to those presented above. The calculated absorptive and dispersive changes for the spectra shown in Fig. 5.4. The maximum absorptive ($\Delta\alpha L$) and dispersive (Δn) changes were 0.98 and

-0.2, respectively, for an excitation intensity of 45 kW/cm^2 (see Fig. 5.5). A $\Delta n = -0.2$ corresponds to a $\pi/6$ phase shift for a 1-μm-thick structure (*i.e.* 0.25 μm total thickness of GaAs).† The changes in the refractive index were obtained using the Kramers-Kronig transformation of the differential absorption [see e.g. Jackson, 1972; Chemla *et al.*, 1984)]. In practice these spectra are summed over a finite energy range [≈ 620-720 nm for these spectra; see Fig. 5.5(a)] however, this is sufficiently large so that the absorption changes vanish at the endpoints. In Fig. 5.5(c) the linear absorption curve is superimposed with the maximum absorptive and dispersive changes. Such a plot is useful for finding the optimal operating point in devices such as light modulators. For example, the optimal operating wavelength is not at the maximum of $|\Delta n|$ since there is appreciable absorption at this wavelength (≈ 680 *nm*). Instead, the correct figure of merit is $\Delta n/\alpha$, consequently, it is preferable to operate at a slightly longer wavelength (690-700 nm) where absorption is smaller. One can see that there is a relatively narrow window for optimizing the quantum wells and the QCSE for such devices, thus demonstrating the importance of such measurements for design of the structures.

Room temperature application of the *hh* blue shift is unlikely since the blue shift quickly disappears for temperatures greater than ≈ 60 Kelvin. The nonlinear absorption changes at elevated temperature consist primarily of exciton bleaching with little or no shift. The effects responsible for the *hh* blue shift are discussed below, while the temperature dependence of the blue shift is discussed further in the next section.

---

† The propagation of optical field in the medium can be described by:

$$E \sim \exp\left(\frac{-2\pi k}{\lambda}\right)\exp\left[i\omega - ix\left(\frac{2\pi n}{\lambda}\right)\right]$$

where k is the extinction coefficient [Macleod, 1989, p.14]. Hence, a change in the refractive index of $\Delta n = -0.2$ over a thickness of $x = 0.25$ μm, for $\lambda = 680$ nm, the phase change is given by $2\pi(0.2)(0.25\ \mu m)/(0.680\ \mu m) \approx \pi/6$.

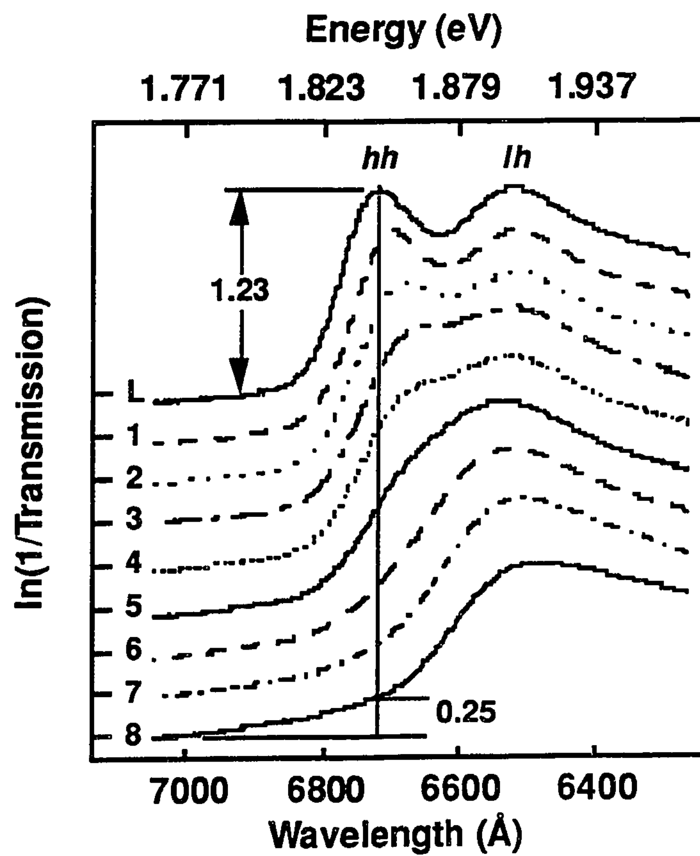

Figure 5.4. Excitation-intensity-dependent absorption spectra, α(I). L = linear spectra (I_{linear}= 1 W/cm^2), I_{1-8} = 5, 8, 10, 12, 15, 25, 35, and 45 kW/cm^2, respectively, T = 15 K and $E_{exc.}$= 1.96 eV.

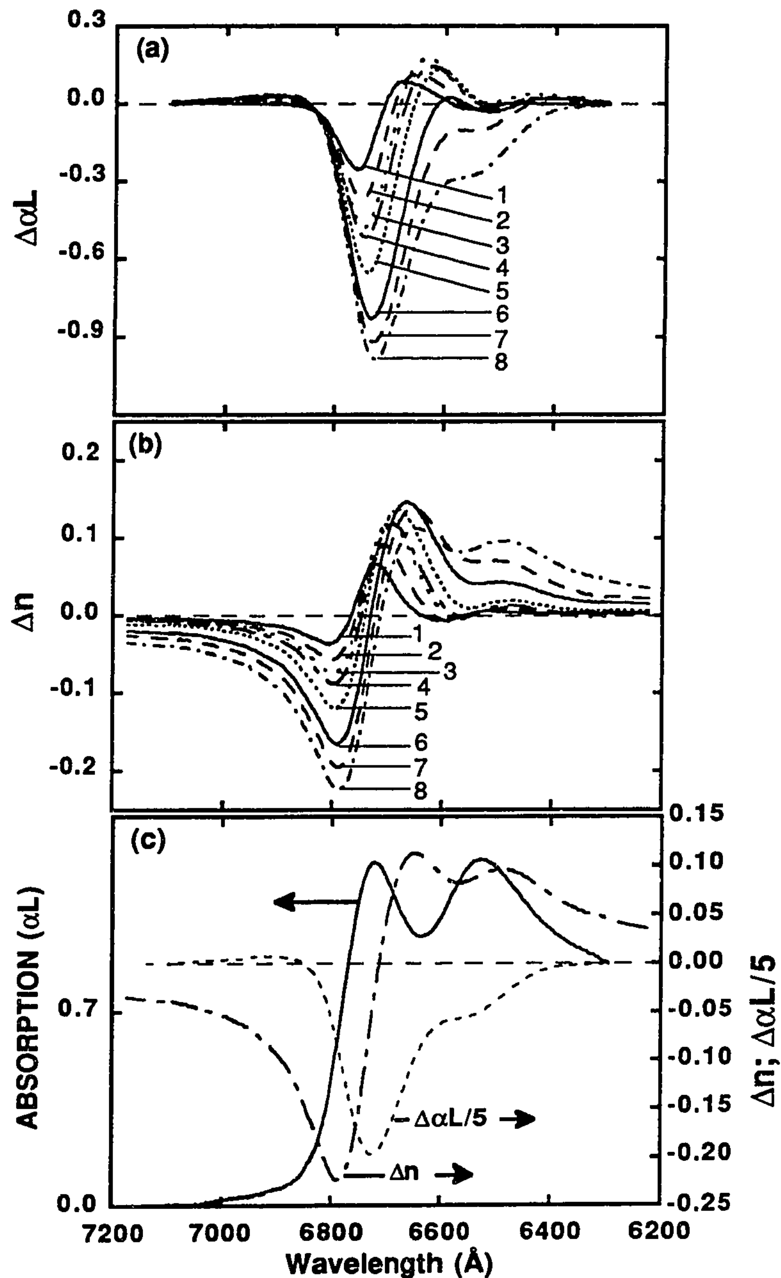

Figure 5.5. (a) Absorptive and (b) dispersive changes with respect to the linear spectrum. The curves labeled 1-8 correspond to the excitation intensities listed in Fig. 5.4. In (c) $\Delta\alpha L$ and Δn for excitation intensity of 45 kW/cm^2 are plotted along with the linear spectrum. Notice that $\Delta n = 0$ where $\Delta\alpha L$ reaches a minimum, which is a property of Kramers-Kronig transformations.

Discussion

In the structure considered here, it is possible to first rule out any significant contribution from the Hartree field to the absorption changes. This is done by solving the Schroedinger equation including the Hartree field for one particle energies. As already pointed out in Sec. 3.2.1, this difference is small if the GaAs layer is thin since the conduction and valence bands essentially shift in parallel as a function of the induced electric field. Thus, the local plasma effects, like Coulomb exchange and correlation must be taken into account.

Generally, in wide type-I QWs ($L_z > 100$ Å) or bulk semiconductors, increasing excitation first leads to bleaching of the exciton without any significant shift until at high densities, a gain region forms [see *e.g.* Zimmermann *et al.*, 1978; Shank *et al.*, 1983; Weber *et al.*, 1988; or Chapter 6]. The absence of a shift can be viewed as an exact cancellation of competing many-body effects. Recall from the discussion in Chapter 3 that the bandgap is reduced as a consequence of self-energy correction, $\Sigma(k)$, arising from exchange and correlation effects. However, a concomitant reduction in the *e-h* interaction reduces the binding energy of the exciton (δE_R). Thus, the renormalized transition energy can be written as

$$E_n = E_n{}^0 + \delta E_R + \Sigma_e(k) + \Sigma_h(k) \tag{5.1}$$

where $E_n{}^0$ is the unperturbed transition energy, and $\delta E_R + \Sigma_e(k) + \Sigma_h(k) \approx 0$ in bulk and type-I systems.††

In GaAs/AlAs type-II QWs, the absence of an electron plasma in the GaAs layer eliminates the contribution to bandgap shrinkage (BGR) from the electron band (i.e.

†† A blue shift of the exciton absorption in narrow type-I quantum wells has been observed and attributed to exciton-exciton interaction [see Sec. 3.1]. As we will show here, the blue shift of the *hh* exciton in our type-II structures is consistently explained by the many-body effects associated with the presence of a *hh* plasma in the GaAs layer without including exciton-exciton effects.

$\Sigma_{e,GaAs} \rightarrow 0$). Consequently, the reduction in the *hh*-exciton binding energy overcompensates the self-energy correction of the *hh* plasma (i.e. $|\delta E_R| > |\Sigma_{hh}(k)|$), and a net blue shift is observed. This picture is consistent with the observation of a diminishing blue shift with decreasing Γ-X splitting (in Fig. 5.3). As the Γ-X splitting is reduced, the spatial separation of the *e* and *hole* plasma becomes less ideal due to the increased overlap of the X-like electron wavefunction with the Γ-like hole wavefunction.

The above picture is only valid as long as there is a *hh* exciton (E_R^{hh} = 12-16 *meV*). More accurately, the competing effects consist of the exchange-correlation interactions and phase space filling (PSF). As discussed in Chapter 3, the energy shift due to PSF is an extremely strong effect at low temperatures ($E_F \sim n$; see eqn. 3.12), and as discussed in Chapter 6, PSF is greater than the reduction in the bandgap energy ($\Delta E_{gap} \sim n^{1/2}$; see eqn. 3.9) for the case of the 2d density of states. At high densities, the absorption edge in type-II QWs corresponds to the chemical potential of the *hh* plasma [see e.g. curves > 75 μW in Fig. 5.2; and curves 3-8 in Fig. 5.4]. Significant Coulomb-enhancement can lead to an absorption peak, known as the Mahan exciton.* It arises from the residual *e-h* correlation in combination with the sharpness of the Fermi edge. This absorption peak is analogous to loosely bound Cooper pairs in superconductors, and such Coulomb-enhancement peaks have been discussed for the case of n-type modulation-doped semiconductor QWs [see Schmitt-Rink *et al.*, 1989].

Comparison to theory

The results presented above have been modeled successfully by Binder, Galbraith, and Koch (1991) by a generalized Wannier equation. Numerical solutions to a generalized Wannier equation are presented in Fig. 5.6 [after Binder *et al.*, 1991]. The nonlinear spectra shown in Fig. 5.6 reflect changes associated with a low-temperature thermal

* The Mahan exciton is actually known from soft x-ray spectra of metals [see Mahan, 1967a, b].

(Fermi) distribution of holes in the absence of electrons. They exhibit good qualitative agreement with the nanosecond curves in Figs. 5.2 and 5.4. [In particular, notice the remarkable similarity between the spectrum calculated for $n = 0.4a_B^{-2}$ in Fig. 5.6 and the spectrum labeled 110 W in Fig. 5.2(a).] For all densities shown, the reduced *hh* bandgap is below the zero density *hh* exciton resonance. The *hh* chemical potential coincides with the onset of absorption for the type-II system. The renormalized bandgap is difficult to pinpoint in the absence of optical gain (see below). For the *lh* exciton the theoretical spectra exhibit a small red shift with relatively little loss in oscillator strength, also consistent with the experimental results. This shift is attributed to the long-range correlation effects of the *hh* plasma (i.e. generalized Coulomb-hole).[‡‡] Apart from the small red shift, fewer changes are observed than in the *hh* exciton since the PSF contributes more to the nonlinearities than screening [Schmitt-Rink *et al.*, 1989]. The rest of the discussion on temperature dependence is postponed until the femtosecond nonlinear spectra have been presented.

‡‡ Note that in the calculation by Binder *et al.* (1991) no occupation of the *lh* band is assumed, so that the bleaching of the *lh* exciton is a consequence of the long-range correlation effects.

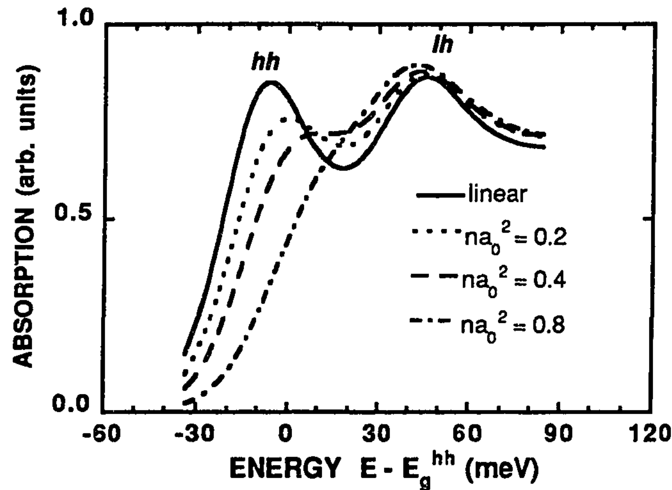

Figure 5.6. Theoretical absorption spectra for type-II quantum wells with GaAs layer thickness of 30 Å. The spectra are for the plasma densities $na_0^2 = 0.2$ (short-dashed line), 0.4 (long-dashed line), and 0.8 (dash-dot line). The linear spectrum is plotted in the solid line, and a_0 is the bulk-exciton Bohr radius. The plasma temperature is 30 *K*.

5.2 Femtosecond optical nonlinearities

5.2.1 Hole-plasma cooling in a heterogeneous Fermi gas

In the next set of experiments the temporal evolution of the *hh*-exciton blue shift is monitored by performing femtosecond pump-and-probe spectroscopy on the type-II MQW structures. A 6200-*Å*, 100-*fs*-duration pump pulse were used with a 100-*fs* duration time-correlated broad-band continuum probe pulse. In Fig. 5.7, the time-resolved absorption spectra of the (10/30) structure for various pump-to-probe time delays are presented. A small blue shift (≈ 4 *meV*) of the *hh* exciton is observed several hundred *femtoseconds* after excitation. The blue shift increases (> 15 *meV*) for the 200-*ps* spectrum as the quasi-

equilibrium state is approached. Notice the strong similarity between the 200-*ps* curve in Fig. 5.7(b) and the 110-μW curve in Fig. 5.2(a).

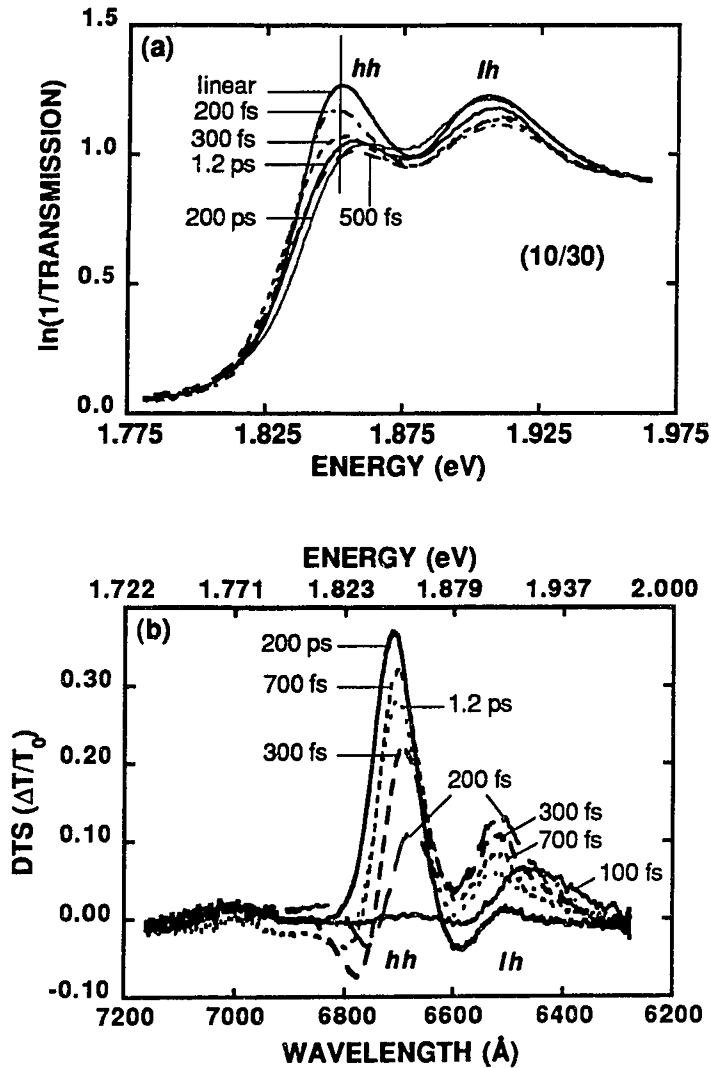

Figure 5.7. Femtosecond time-resolved absorption spectra for the (10/30) structure. $P_{exc.} \approx 10\ \mu W$ (corresponds to a density of ~$5\times10^{11}\ cm^{-2}$), $E_{exc.} = 1.99\ eV$, T = 30 *K*. The (a) full development of blue shift and (**b**) the corresponding differential transmission spectra (DTS).

Spatial Transfer of Electrons

Feldmann *et al.* (1989, 1990) reported a fast recovery of absorption in the spectral vicinity of the *hh* exciton, *lh* exciton, and the split-off band in type-II GaAs/AlAs superlattices. They attributed this subpicosecond absorption recovery to real-space charge transfer of electrons from the GaAs Γ-band to the AlAs X-band. In addition to the excitonic blue shift and saturation, a similar fast recovery of the *hh* and *lh* excitons is observed [see DTS in Fig. 5.7(b): compare curves taken between +200 *fs* and +1.2 *ps* in the vicinity of the *lh* exciton; and +700 *fs* and +1.2 *ps* in the vicinity of the *hh* exciton]. Moreover, a re-bleaching in the spectral vicinity of the *hh* exciton between ~1 *ps* and ~100 *ps* is observed. This can be seen by comparing the curves labeled +1.2 *ps* and +200 *ps* in Figs. 5.7(a) and (b).

The scattering rate between the GaAs Γ-state and the AlAs X-state is described by Fermi's Golden Rule:

$$\tau^{-1} \propto \sum |\langle \Psi_\Gamma | V_s e^{iqr} | \Psi_X \rangle|^2 \tag{5.2}$$

where V_s is the scattering potential, Ψ_Γ and Ψ_X are the respective wavefunctions of the initial state (Γ-like wavefunction) and final state (X-like wavefunction). However, the experimental results indicate that

$$\tau^{-1} \propto |\langle \Psi_i | \Psi_f \rangle|^2. \tag{5.3}$$

In other words, V_s is approximately independent of wavevector, q. The potential fluctuation due to interfacial roughness has been suggested as a possible mechanism for mediating the electron scattering [Feldmann, 1990]. A transfer rate diagram can be inferred from the observations presented here and the reports by Feldmann and co-workers (1990).

Of the three type-II samples examined, the fastest transfer rate was observed in the (10/10) sample (< 300 *fs*) and comparable transfer rates were observed in the (10/18) and (10/30) samples (~500 *fs*) [see Fig. 5.8].

Onset of hh blue shift

We attribute the delayed onset of the complete blue shift in our femtosecond spectra to the presence of a "hot" hole plasma. Initially, a non-thermal distribution of carriers is created high in the band. The carriers scatter quickly to within one LO-phonon of the band minima via LO-phonon emission. Simultaneously, thermal distributions of carriers are formed via carrier-carrier scattering. The absence of acoustic phonons at low temperatures prevents the *e* and *h* distribution functions from reaching the lattice temperature until hundreds of picoseconds after excitation. Therefore, immediately after the spatial transfer of electrons to the AlAs layer, ($\tau_{delay} \sim 1\ ps$) the nonlinearities are expected to be associated with a "hot" hole plasma. It is well known that PSF effects from a "hot" plasma is far less efficient than from a cold plasma [see Sec. 3.1]. Thus, the reduced PSF effects at high temperatures is nearly compensated by the concomitant reduction in the bandgap. As the temperature declines, the Fermi edge sharpens and PSF becomes more effective, which in turn shifts the Fermi edge to higher energy. The blue shift due to PSF begins to dominate the red shift from the BGR, and a large net blue shift is observed.

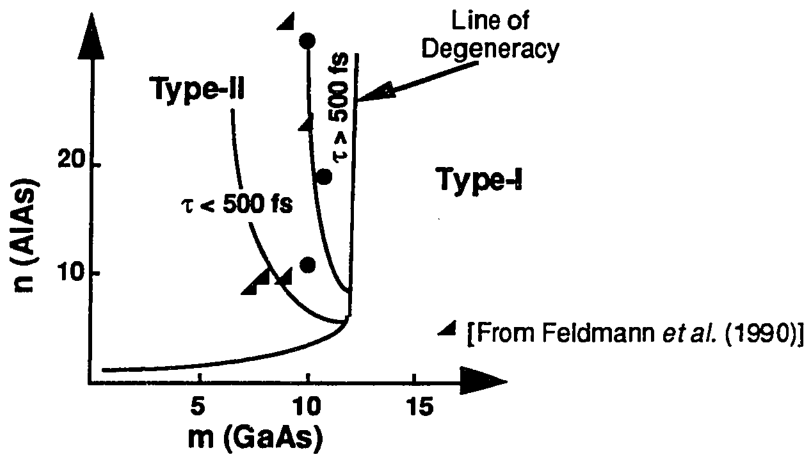

Figure 5.8. Transfer rate diagram. Solid circles show the three samples considered above.

Finally, the re-saturation of the *hh* exciton is consistent with the cooling of the holes. The absorption is initially decreased as photoexcited *e-h* pairs fill the available states according to the Pauli exclusion rule. As the electrons spatially transfer to the AlAs layer, the absorption increases as a result of the increased number of conduction-band states. At this point, the holes remain quite hot and only a fraction of the holes occupy the same phase space as the *hh* exciton. As the holes cool, the fraction of holes increases which occupy the same phase space as the exciton, and consequently, the exciton re-saturates and shifts to higher energy.

Comparison to theory

The fact that the carriers establish a near thermal distribution ~1 *ps* after excitation allows the use of a quasi-equilibrium theory to describe the observed optical nonlinearities. Binder *et al.* (1991) have successfully modeled our femtosecond data by assuming that immediately after the initial charge separation and thermalization (~1 *ps*), the *hh* plasma is still at an elevated temperature. Fig. 5.9 illustrates the effects of a high-temperature *hh* plasma. The inhomogeneously broadened 300-Kelvin spectrum of Fig. 5.9 bears strong

resemblance to the experimental spectra of Fig. 5.7 for times < 500 *fs*: the spectra exhibit no blue shift and strong saturation of the *hh* and *lh* excitons.

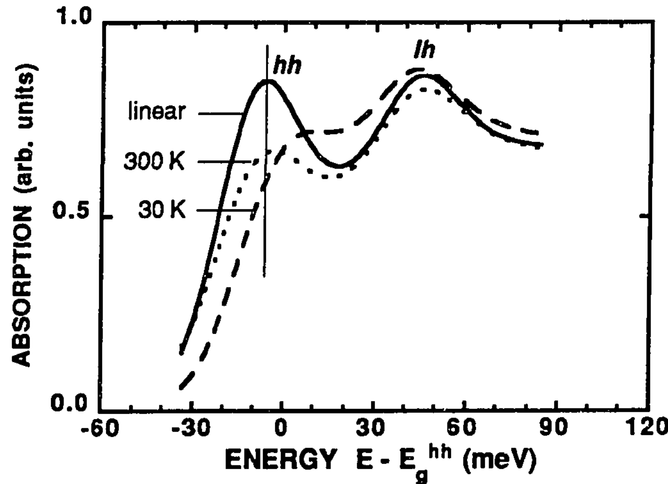

Figure 5.9. Theoretical temperature-dependent absorption spectra for a hole plasma n = 0.4 a_0^{-2}. T = 300 K (short-dashed line) and T = 30 K (long-dashed line). The linear spectrum and all other parameters are the same as in Fig. 5.6. [After Binder *et al.*, 1991.]

This analysis shows that at high densities, the observed exciton blue shift is in fact the Mahan exciton at the Fermi edge. The Mahan exciton is formally equivalent to loosely bound Cooper pairs in superconductors. Thus, as the temperature is increased, the Fermi edge is broadened, the effects of PSF are reduced, and the blue shift and the Mahan exciton disappear.

It is much more difficult to distinguish the low-density exciton peak from the Coulomb-enhancement peak if the spectra are inhomogenously broadened. Although this difficulty is shared by type-I and type-II MQWs, it is especially difficult in type-II systems due to the lack of optical gain below the quasi-chemical potential. This argument applies to the density range discussed here. In the next chapter the limit of extremely high densities is

investigated, where even in type-II structures, optical gain is possible due the enhanced X-Γ scattering.

In summary, the nonlinearities due to the spatial separation of photoexcited *e* and *h* plasmas has been investigated. The control of these nonlinearities by the application of an electric field is demonstrated in the next section.

5.2.2 Effects of a static longitudinal electric field

The application of an electric field perpendicular to the layers changes a structure from a type-II band alignment to a quasi-type-I band alignment. Electric-field-dependent time-resolved nonlinear absorption spectra are presented in Fig. 5.10: (a) at zero bias and (b) at the field corresponding to Γ-X alignment. At low field a blue shift of the *hh*-exciton peak is observed. In addition, a partial recovery of the absorption saturation which develops after several hundred femtoseconds (identical to the results presented in the previous section for intrinsic type-II MQWs). In contrast, at field strengths near the indirect-to-direct crossover region [*i.e.* $\Delta_{\Gamma\text{-}X} \approx 0$; see Fig. 2.5(b) and (c)], the *hh* blue shift disappeared, and a small transient red shift, which recovered after several hundred femtoseconds, appeared [Fig. 5.10(b)].

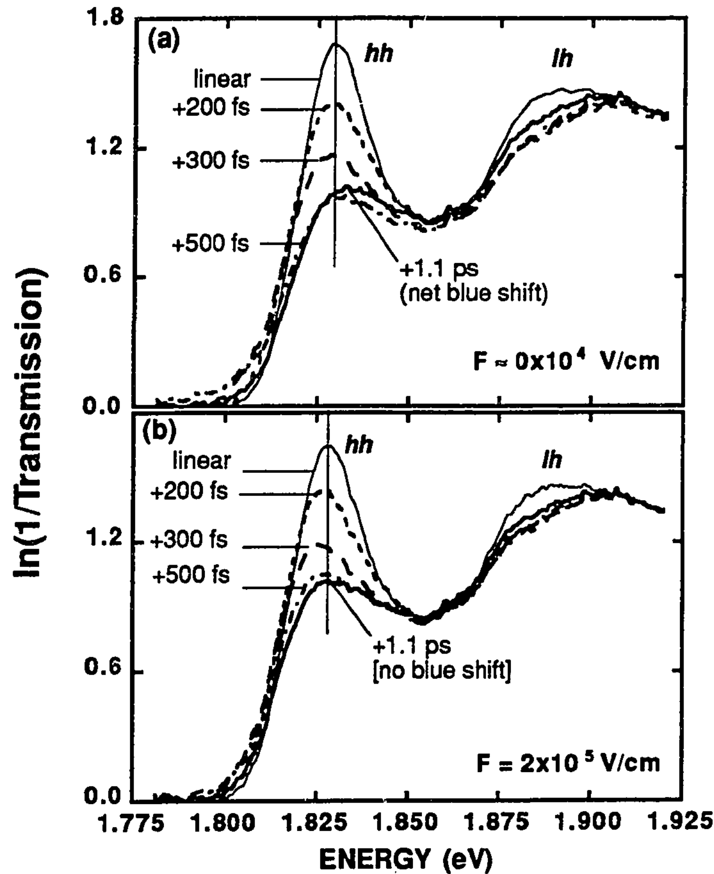

Figure 5.10. Transient nonlinear absorption spectra obtained from the p-i-n photodiode structure (a) flat-band ($\approx 0 \times 10^4$ V/cm; type-II), and (b) tilted-band (2×10^5 V/cm).

To illustrate the electric-field-dependent *hh* energy shift more clearly, the *hh*-exciton peak energy shift is plotted as a function of electric field for two pump/probe time delays in Fig. 5.11: (1) probe delayed +200 *fs* with respect to the pump (prior to interlayer electron transfer), and (2) probe delayed +500 *fs* (following interlayer electron transfer). The *hh*-exciton peak position was obtained by fitting each absorption spectrum, for a given applied field, using two Gaussians and two 2d continuum functions as described in Sec. 2.3. Fig. 5.11 clearly shows the decrease in the blue shift of the *hh* exciton as a function of

increasing axial electric-field amplitude and also shows the complete disappearance of the shift in the vicinity of the indirect-to-direct crossover. Note that the blue shifts in Fig. 5.11 are small compared to the shifts shown in Fig. 5.5 because these shifts occur at very early times (500 *fs*) and the full blue shift (> 15 *meV*) is not fully realized until the hole plasma reaches low temperature (~500 *ps*).

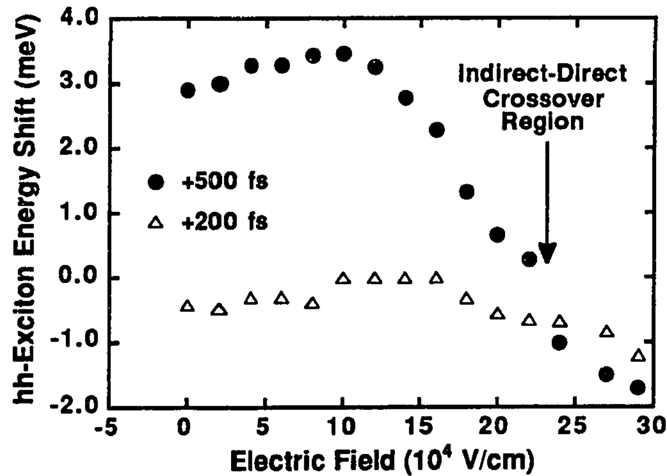

Figure 5.11. Field-dependent heavy-hole (hh) absorption-peak energy shift for +200 *fs* and +500 *fs* pump-to-probe delays. [Each point (*hh* energy shift) is taken with respect to the linear absorption spectrum at the corresponding field.]

Discussion

The interpretation of the data in the flat-band case is identical to that of regular type-II heterostructures. The situation is however more complicated when an electric field is applied. With a DC electric field present, quasi-equilibrium is in principle not possible because the field induces a current, thereby depleting the carrier density in the intrinsic region. However, on a picosecond time scale, the most important effect of the field is not a macroscopic carrier drift or diffusion but merely the deformation of the square quantum

wells into triangular wells[§] and a shift of the relative position of energy levels in adjacent layers. This shift manifests itself clearly in the luminescence data. As discussed in Sec. 2.4, the quantum-confined Stark effect is small, even at F ~ 3×10^5 V/cm, because the GaAs layer is very thin (30 Å) and the total potential drop across the thin GaAs layer is relatively small (~100 *meV*). The situation at this field strength is quite different for the electrons which reside in the AlAs X-valley. Since the AlAs layer is thick, the potential drop is ~300 *meV*, which is essentially the same as the entire confining potential (GaAs X-valley to AlAs X-valley). Consequently, the electrons will no longer be strongly localized in the AlAs layer, even if they have been scattered from the Γ to the X level. Also, the spatial extent of the X-like electron wavefunction in the GaAs layer will increase with decreasing Γ-X splitting. In general, one can conclude that the influence of the electrons on the absorption spectra increases with increasing electric field. Furthermore, one would expect the effect of these electrons on the absorption to occur on the same time scale as the charge separation (~500 *fs*) in a regular type-II structure. In the case near the indirect-to-direct crossover region, the electron wavefunctions have an appreciable part in the adjacent GaAs layer. We assert that in this case the electrons contribute to long-range Coulomb correlation effects but have no contribution to the PSF in the GaAs layer.

Comparison to Theory

The above arguments have led to a simple, numerically tractable model that can account for the reduced charge separation, which is assumed to be the main effect of the E-field. This model is a modification of the one reported previously by Binder *et al.* (1991). It consists of one layer (i.e. the GaAs layer) containing a plasma of electrons and holes, which are in thermal equilibrium. The plasma temperature is assumed to be larger than the lattice temperature when modeling the situation for times before the plasma reaches the

[§] The deformation of the wells changes the allowed stationary states, which in turn removes the coupling between AlAs X-states.

lattice temperature. The result of the numerical solution for the excitonic polarization is presented in Fig. 5.12 [after Binder, 1991b; Fu *et al.*, 1992]. The case where the electrons have the same density as the holes but contribute to only the correlation effects is presented. At a high electron temperature (300 K) the electron correlation effects contribute to a red-shift in the *meV* range [Fig. 5.12(b)]. A slight cooling of the carriers to 200 *K* leads to an increased bleaching and the disappearance of the red shift. Hence, this simple model qualitatively explains the experimental data.

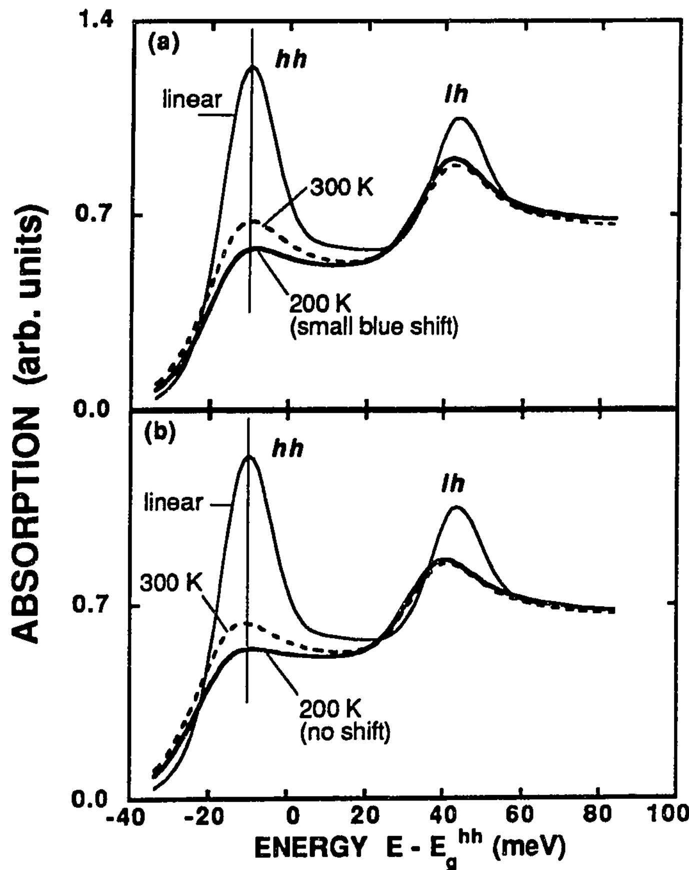

Figure 5.12. Computed *hh* and *lh* exciton spectra for the case of (a) type-II system with $n_h = 0.8\ a_B^{-2}$, $n_e = 0$, where a_B is the exciton Bohr Radius and $T_{e,h} = 300\ K$ (dashed line); same at $T_{e,h} = 200\ K$ (heavy solid line), and the case (b) where electrons contribute to correlation only with $n_e = n_h$ for $T_{e,h} = 300\ K$ (dashed line) and $T_{e,h} = 200\ K$ (heavy solid line). [After Binder *et al.* (1992)]

For a quantitative analysis, one would have to take into account many other effects. If the electric field is not perfectly normal to the layer, it could accelerate (and hence heat) the carriers in the plane of the layers. Also, a more realistic QW structure calculation and a theoretical description of the tunneling probabilities (i.e. the motion perpendicular to the layers) should be taken into account. One might also expect an effect of the electric field on the spatial inhomogeneity due to well-width fluctuation (i.e. interfacial roughness) since the field presents a force on the carriers toward one interface (see Sec. 2.4). Furthermore, one might investigate the influence of the electrons at the Γ-point, which give rise to the luminescence signal in Fig. 2.5(c). The luminescence signal is not sufficient to estimate the ratio of electrons at Γ versus X since the short lifetime of the Γ-like electrons always dominates the signal. This discrepancy led us to investigate absorption changes of the sample at voltages up to 3×10^5 V/cm for longer optical delays. When the plasma starts to cool down, the Γ-like electrons should recombine much faster (~500 *ps*) and the absorption spectra should recover on a similar time scale and the formation of excitons should be observed [see Chapter 6]. Since a relatively fast recovery of the absorption spectra (< 500 *ps*) was not detected (even at the highest voltage), the Γ-valley is not likely to be strongly populated by electrons at any time.

Summary

The optical nonlinearities in the absorption spectra of type-II MQWs has been presented. Although the Hartree potential created by the spatial separation of electrons and holes in type-II structures leads to shifts in the indirect transition energies, the direct transitions are relatively unaffected because the primary potential drop occurs between layers. However, the absorption spectrum is profoundly changed by the single-component hole plasma. A blue shift of the *hh* absorption peak is observed, which we identify as a

Coulomb-enhancement peak at the hole quasi-chemical potential. The blue shift develops fully only after the hole distribution reaches low lattice temperature. A hot plasma temperature causes strong reduction of the Pauli blocking and hence, reduces the blue shift. Consequently, a time delay in the full development of the blue-shift in the femtosecond measurements is observed. The primary effect of an electric field perpendicular to the layers is an effective reduction in the Γ-X splitting. The blue-shift of the *hh*-exciton on a 0.5-1.0 *ps* time scale in the zero-field case is reduced and turned into a transient red shift at field strengths that correspond to a Γ-X alignment (i.e. $\Delta_{\Gamma X} \approx 0$).

6 Optical Gain and Ultrafast Nonlinear Response in Narrow GaAs/(Al,Ga)As Quantum Wells

In this chapter, the spectral and temporal behavior of optical gain in narrow type-I QWs is compared to optical gain in narrow type-II QWs. First, the time-resolved spectra which show the development and decay (recovery) of optical gain (absorption) in narrow type-I MQWs are presented. In Section 6.2 the gain in type-II systems is compared with that in type-I systems. In addition, the ability to control the gain magnitude with an applied longitudinal electric field is demonstrated in Section 6.2. Finally, the power dependence, temperature dependence, and spatial dependence of the ultrafast decay of the gain is investigated.

6.1 Gain in narrow GaAs/(Al,Ga)As type-I quantum wells

The condition for optical gain in a type-I structure is satisfied when the *e* and *h* quasi-chemical potentials are pushed above the conduction band minimum and below the valence band maximum [see e.g. Yariv, 1989]. Femtosecond optical gain measurements were performed on a 55-period type-I GaAs/$Al_{0.45}Ga_{0.55}As$ MQW structure grown by MBE. The 24-Å GaAs wells were isolated by 100-Å $Al_{0.45}Ga_{0.55}As$ barriers. Again, anti-reflection coating and substrate removal were performed before transferring the sample onto a sapphire substrate in a cryostat where both low temperature (≈ 30 K) and room temperature data were taken.

In Fig. 6.1(a) time-dependent absorption spectra show the development of gain in the type-I MQW sample. Initially, strong spectral hole burning (not shown) is observed in the continuum states at the pump energy (well above the *lh*-exciton absorption peak energy). This is a consequence of state filling by the non-thermal photoexcited carriers, similar to that originally addressed by Oudar *et al.* (1985). Saturation and broadening of the *hh* exciton and complete saturation of the *lh* exciton occurs at 600 *fs*. A transient increase in the absorption on the low-energy side of the *hh* exciton (see curve labeled "+900 *fs*" near 1.72 *eV*) is observed around 0.8-0.9 *ps* after excitation. Between +900 *fs* and +1.5 *ps* the onset and rapid increase of the gain amplitude and bandwidth is observed. Immediately after +1.5 *ps*, decay of the gain is observed, followed by a recovery of the absorption spectrum including the formation of excitons [see curves labeled 1.8–50 *ps*; Fig. 6.1(b)].[§]

In Fig. 6.1(b), the magnitude of the gain decays by more than half of its maximum value between +1.5 *ps* and +3.0 *ps*, and then requires an additional +50 *ps* to completely recover. This is indicative of a multi-component decay of the gain. [A similar ultrafast nonlinear response is observed in the gain region of type-II QWs.] Between +3.0 *ps* and +50 *ps* an exponential decay due to stimulated emission [time constant of $\approx$ 10 *ps*; see Fig. 6.2] [Dubard *et al.*, 1987]. The discussion of the ultrafast nonlinear response of the gain (< 500 *fs*) is postponed until later in this chapter.

[§] The blue shift of the *hh* and *lh* exciton resonance has been previously reported and attributed to exciton-exciton interactions [see Sec. 3.1].

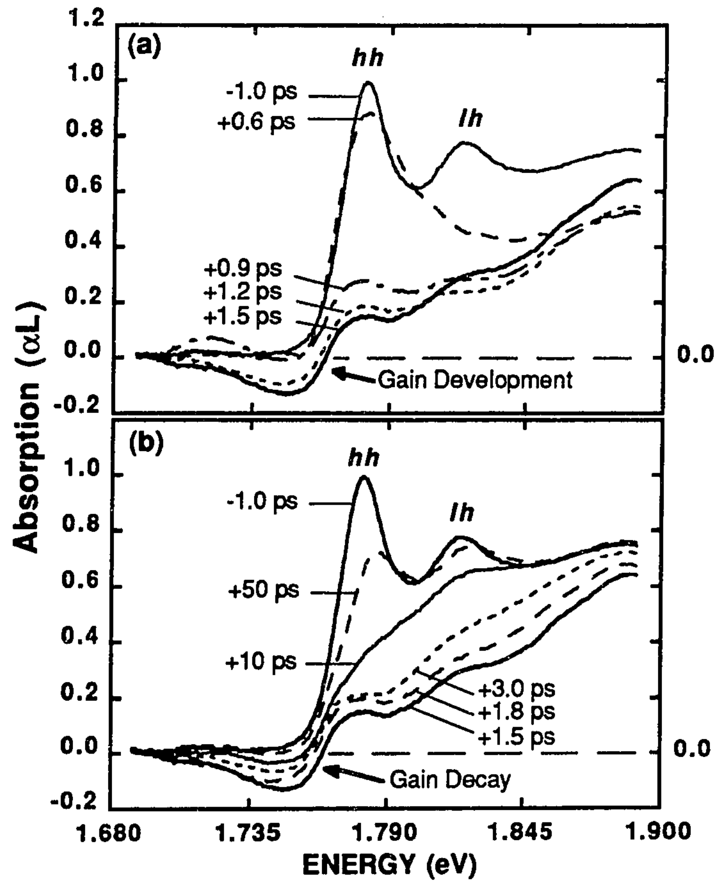

Figure 6.1. Time-resolved absorption/gain spectra showing the (a) development and (b) decay (recovery) of the gain (absorption) spectra in type-I QWs.. ($T = 30\ K$, $\lambda_{exc.} = 6200\ Å$, $P_{exc.} = 110\ \mu W$.)

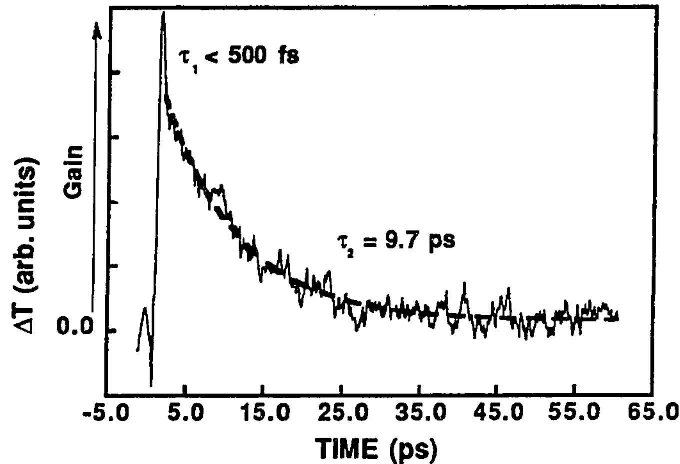

Figure 6.2. Single-wavelength time scan showing the time constant for stimulated emission. (T = 30 *K*, λ_{probe} = 7100 Å, $P_{exc.}$ = 110 μW).

Discussion

We attribute the transient increase in absorption below the unexcited bandgap [+900-*fs* curve in Fig. 6.1(a)] to the onset of bandgap renormalization. As the hot carriers reach the bottom of the unexcited bandgap, the Coulomb exchange-correlation effects shift the bandgap to lower energy. Immediately thereafter, the state filling of the lowest lying states becomes complete and gain is observed. Shank *et al.* (1983) observed excitonic broadening and enhanced absorption below the unexcited bandgap ~1.5 *ps* after photoexcitation of 200-Å GaAs/(Al,Ga)As MQWs. However, optical gain was never observed at the same excitation intensity (corresponding to $n \sim 5\text{x}10^{11}\ cm^{-2}$). Furthermore, they did not report any transient absorption at densities where they observed significant gain [Shank *et al.*, 1979, 1983].

Complete suppression of the reflectance allows us to obtain a good estimate of the carrier density from the gain bandwidth ($n \approx 4\text{x}10^{12}\ cm^{-2}$ for a gain bandwidth of ≈ 75

meV).[§§] For GaAs QWs gain bandwidth does *not* exactly correspond to the sum of the e and h quasi-chemical potential energies because the effective mass of the e and h are not equal (though they are fairly close at $\mathbf{k} = \mathbf{0}$: $m_e^* = 0.067m_o$ and $m_h^* = 0.087m_o$). Only in an ideal semiconductor, where $m_h = m_e$, does the gain bandwidth corresponds exactly to the sum of the two quasi-Fermi levels.

The gain spectra in Fig. 6.1 provide practical information for GaAs-laser designs. Although the band gap renormalization is significant (~ 60 *meV*), the maximum gain amplitude occurs about 25 *meV* below the unperturbed *hh*-exciton peak energy. In practice, only linear cw luminescence and absorption spectra are available for material characterization. Thus, a good "rule of thumb" for laser-cavity design is to design the lasing wavelength approximately 25-30 *meV* below the *hh*-absorption peak. For luminescence the cavity should be designed for lasing 10-15 *meV* below the direct PL peak.[*]

[§§] The residual reflectance ($R \leq 0.01$) was removed by modeling the reflectance of the imperfect anti-reflection coating [see Macleod, 1989] and the absorption spectra [see Sec. 2.3] simultaneously. This is valid as long as the reflectance, R is much less than the absorbance, A (i.e. $R << A$).

[*] There is typically a 10-15 meV Stokes shift between our *hh*-absorption and PL peaks.

6.2 Gain in type-II GaAs/AlAs quantum wells

Optical gain is inhibited in type-II QWs because the electrons become spatially separated from the holes. The condition for gain in type-II heterostructures [see Fig. 6.3] is difficult to satisfy because the AlAs X-valley lies energetically below the GaAs Γ-valley. Of course, the extremely long lifetime of the indirect (Γ-X) transition prohibits optical gain via the Γ-X transition. Electrons must first occupy all the states in the AlAs X-valley which lie below the GaAs Γ-band minimum before satisfying the condition for gain, hence, it is somewhat difficult to observe gain in type-II QWs.†

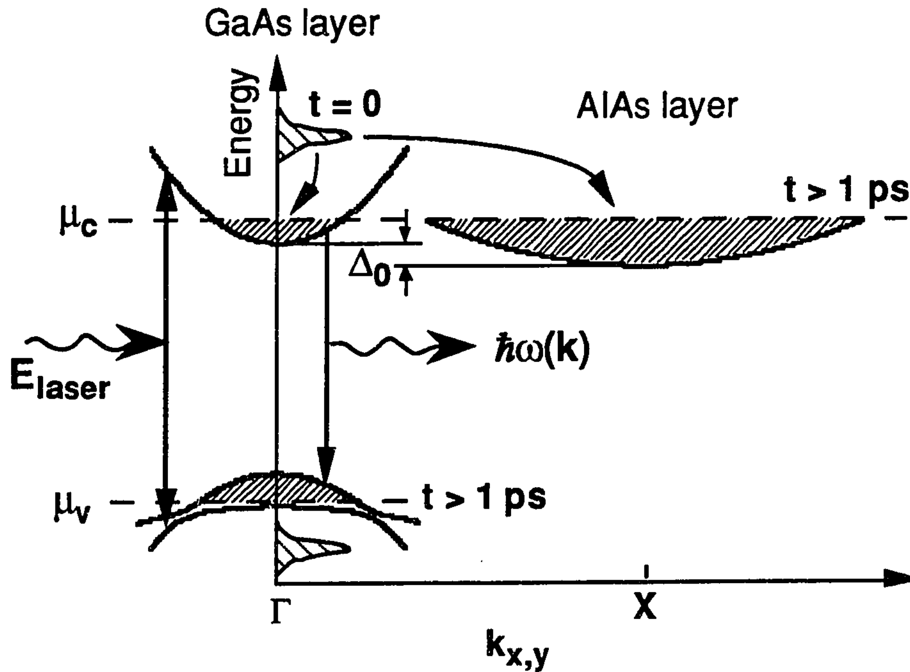

Figure 6.3. Condition for gain in type-II quantum wells.

† Jung *et al.* (198-) have reported evidence of stimulated emission in the luminescence from *nipi* structures, which also support spatially separated *e* and *h* plasmas.

6.2.1 Effects of AlAs X-valley "reservoir"

The loss of carriers to the AlAs X-valley is substantial, and consequently, a significantly higher gain threshold in type-II systems is expected. However, recall from Sec. 3.2.1 that the Γ-X splitting is reduced by the Hartree potential at high carrier densities. The gain threshold was measured by systematically decreasing the pump intensity while monitoring the gain amplitude with a photomultiplier tube and lockin amplifier (same set-up used to acquire single wavelength time scans; also see Sec. 4.3). [Identical measurement on the type-I sample was made to verify the threshold density.] The gain-threshold density in the type-II MQW samples was determined to be approximately 3×10^{12} cm^{-2}. This is about a factor of 2-3 less than what one would expect if the reduction in the Γ-X splitting due to the Hartree potential were not taken into account.

A comparison of the gain/absorption spectra for the type-I and type-II MQWs is shown in Fig. 6.4. The spectra were taken under identical conditions, although the results are dramatically different. In both cases, the gain reaches a maximum about +1.5 *ps* after excitation [compare curves labeled "+1.5 *ps*" in Fig. 6.4], however, the gain amplitude and bandwidth are significantly larger in the type-I system.** The bandwidth of 100 *meV* in the type-I sample corresponds to $n \sim 5.4 \times 10^{12}$ cm^{-2}. Since the gain bandwidth of the type-II sample is about half as broad, approximately 2.7×10^{12} cm^{-2} electrons were lost to the AlAs X-valley. This is quite consistent with the gain measurement. The most dramatic difference appears in the curves taken +150 *ps* after initial excitation. The +150-*ps* curve for the type-II sample still exhibits a small but appreciable amount of gain (bandwidth ≈ 25 *meV*). In contrast, the gain in the type-I system has decayed completely by ~50 *ps* [from Fig. 6.1(b)], and by +150 *ps* the absorption has recovered, and formation of excitons is clearly observed [see Fig. 6.4(a)]. The loss of carriers from the Γ-valley to the X-valley is

---

** The "bump" in the type-I spectra is most likely an artifact from an imperfect anti-reflection coat.

consistent with the observation of higher gain threshold, smaller gain amplitude, smaller gain bandwidth, and the persistence of the gain to longer times in type-II (compared to type-I) structures.

Because the rate for indirect recombination is several orders of magnitude longer than the rate for direct recombination, the X-valley acts as a "reservoir" for the electrons. From the time-resolved gain/absorption spectra in the type-I sample [Fig. 6.1], it is apparent that ~50 *ps* after the carriers are created, the quasi-chemical potential for the electrons drops to a point just below the Γ-band minimum. However, the long-lifetime states in the X-valley are still completely full. Therefore, electrons can scatter (e.g. via acoustic phonon scattering) back to the Γ-valley and recombine directly. This slow process for depleting the X-valley effectively increases the lifetime of gain to times beyond ~150 *ps* in the type-II superlattices. Note that the zero-crossing point in the spectrum, labeled +150 *ps* in Fig. 6.4(b), corresponds to only the hole quasi-chemical potential, whereas in a type-I or bulk sample the zero-crossing point corresponds to approximately the sum of the electron and hole quasi-chemical potentials (assuming $m^*_e \approx m^*_h$ which is not the case for $E_F > 20\ meV$). Finally, the power-dependent spectra taken at +150 ps (for the type-II sample) are consistent with the above results: At lower carrier densities ($n \sim 5\text{x}10^{11}$ – $1\text{x}10^{12}\ cm^{-2}$) the blue shift and saturation of the *hh* exciton is observed, corroborating the results presented in Chapter 5 (i.e. phase-space filling by a cold hole plasma). At high carrier densities ($n > 10^{12}\ cm^{-2}$) the absorption spectra were strongly saturated although gain was not observed until $n(\tau{=}0) \sim 3\text{x}10^{12}\ cm^{-2}$.

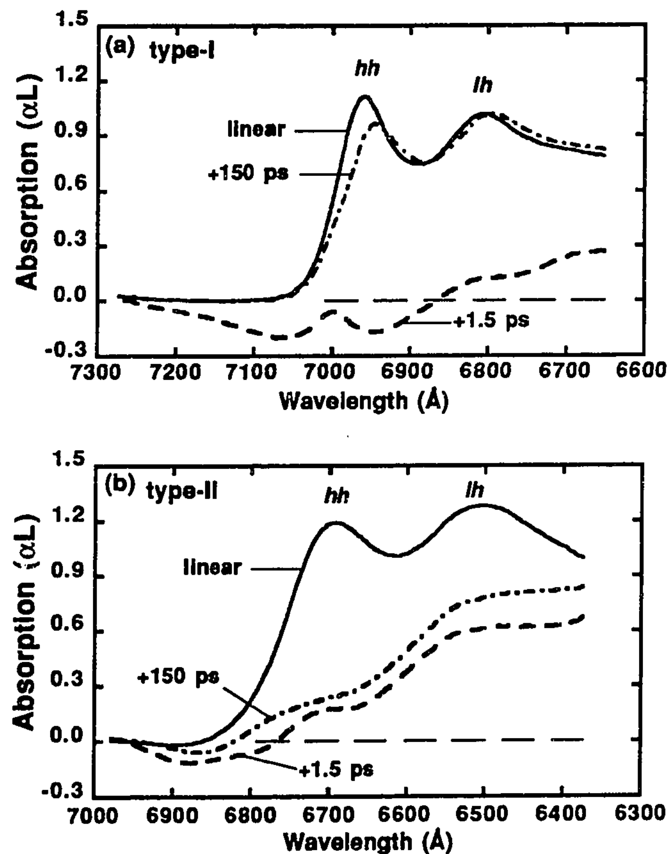

Figure 6.4. Time-resolved absorption/gain spectra for (a) type-I and (b) type-II quantum wells. ($T = 30\ K$, $\lambda_{exc.} = 6200\ \AA$, $P_{exc.} = 150\ \mu W$.)

At room temperature the gain threshold for the type-II sample was lower than at low temperature. Furthermore, the room-temperature gain threshold was not significantly higher (within 30%) than the gain threshold for the type-I sample. This is not surprising since the increased thermal energy in the lattice effectively decreases the Γ-X splitting significantly, and consequently, the law of mass action distributes the electrons more evenly between the AlAs X-valley and the GaAs Γ-valley. The room-temperature linear PL exhibited significant overlap of the direct and indirect luminescence peaks.

6.2.2 Effects of a static longitudinal electric field

In the following gain measurement the role of the AlAs X-valley is investigated. The dependence of the Γ-X splitting on an applied electric field is essentially linear, especially at high fields (see Sec. 2.4). First, the gain measurements described above were repeated on the type-II MQW *p-i-n* photodiode to verify its type-II behavior. In the following experiment, a lockin-amplifier and photomultiplier tube (see Sec. 4.3) were employed to measure the transmission (optical gain) at a single wavelength and optical delay (i.e. where the maximum gain was observed: $\lambda = 6900$ Å, $\Delta\lambda = 100$ Å, and $\tau_{delay} = 1.5$ *ps*) as a function of applied electric field. As the electric field changed the type-II band alignment to the "quasi-type-I" band alignment, the gain magnitude increased linearly with the applied electric field for a pump-to-probe delay of +1.5 *ps* [see Fig. 6.5(a)]. In contrast, when the pump-to-probe delay was set to +100 *ps*, the gain magnitude decreased by about a factor of two as the band alignment changed from type-II to "quasi-type-I" [see Fig. 6.5(b)]. Of course, the band alignment at high fields is not truly type-I. If the band alignment for the *p-i-n* photodiode were truly type-I at high fields, then absolutely no gain would be observed at +100 *ps*. Nevertheless, the electric-field-dependent gain data is consistent with the comparison of gain in type-I and type-II MQWs [in Fig. 6.4]: gain bandwidth and amplitude is larger in the quasi-type-I (high-field) case, but the gain lifetime is longer in the type-II (low-field) case.

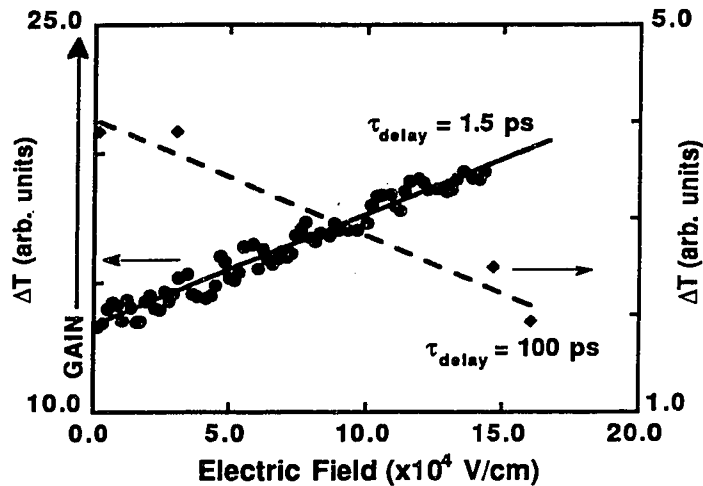

Figure 6.5. Gain (transmission) as a function of applied electric field. The left axis corresponds to (**a**) 1.5 *ps* optical delay (solid line) and the right axis corresponds to (**b**) 100 *ps* delay (dashed line). [T = 30 *K*, λ_{probe} = 6900 *Å*, $\Delta\lambda_{probe}$ = 100 *Å*, $P_{exc.}$ = 150 μW, $\lambda_{exc.}$ = 6200 *Å*.]

6.3 Ultrafast nonlinear optical response

Thus far, the discussion has primarily addressed the spectral behavior of the gain by analyzing absorption spectra at preset pump-to-probe delays. To better analyze the temporal behavior of the gain region, single-wavelength time scans (SWTSs; i.e. lockin detection of the transmitted probe pulses) have been performed on the gain region. [See Sec. 4.3 for the experimental configuration.] A strong power dependence in the low-temperature SWTSs is observed [in Fig. 6.6]. At high power [see curve labeled "150 μW"

(incident power) in Fig. 6.6] a two-component decay of the gain is observed for pump-to-probe delays up to +3.0 *ps*. The sharp negative dip around 0.8 *ps* in the SWTSs corresponds to the increased absorption below the band edge in Fig. 6.1(a) [see curve labeled +0.9 *ps*]. Between +1.5 *ps* and +2.0 *ps* an ultrafast (≈ 500 *fs*), non-exponential decay of the gain is observed. A ≈ 40% reduction of the power results in the complete disappearance of the ultrafast gain decay component, indicating a strong nonlinear dependence of the decay on carrier density [see curve labeled "90 μW" in Fig. 6.6]. Analysis of several power-dependent scans revealed that the time constant has a super-linear dependence on power [i.e. carrier density; see inset].

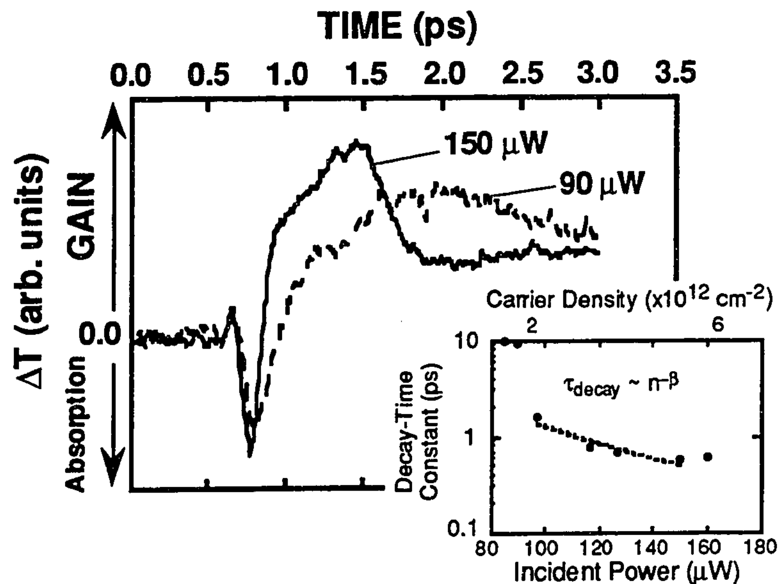

Figure 6.6. Power-dependent single-wavelength time scans. Inset: Decay constant vs. power (or carrier density). $\beta \approx 1.8 \pm 0.5$. [T = 30 K, λ_{probe} = 7100 Å.]

The same behavior at room temperature is observed with the exception that the onset of the ultrafast decay of the gain was delayed [see Fig. 6.7(a)]. At room temperature the unperturbed bandgap is ≈ 90 *meV* lower than at low temperature. Consequently, the

carriers have additional energy to dissipate before reaching the bottom of the room-temperature bandgap.

SWSTs were also performed at the *hh*- and *lh*-exciton wavelengths. The results of SWTSs ($\tau_{delay} < 5\ ps$) were again similar for both type-I and type-II heterostructures: Similar effects were observed above as below the bandgap with the exception that no increase in absorption was observed above the band-edge [see Fig. 6.7(b)].

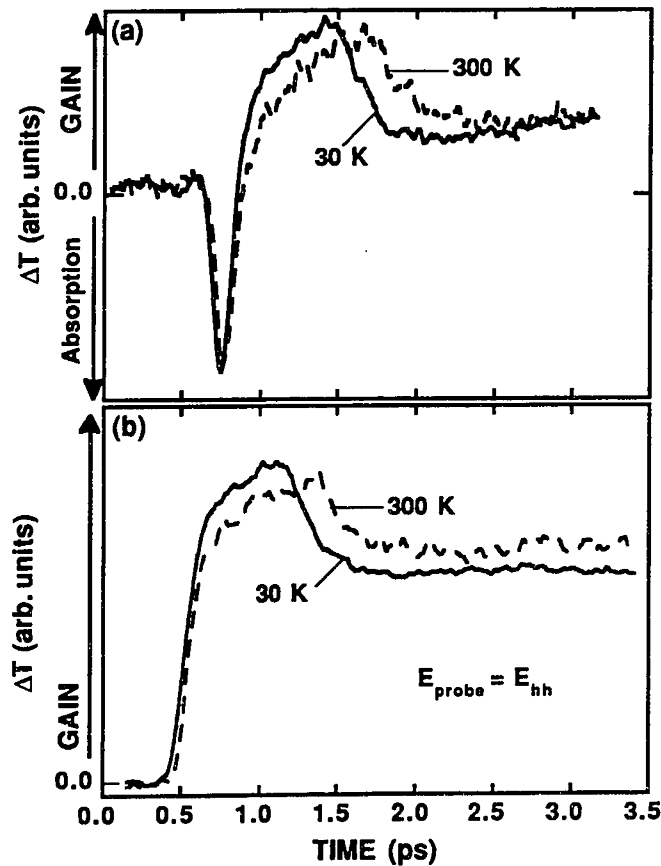

Figure 6.7 Temperature-dependent single-wavelength time scans (**a**) below [probe wavelengths for the 30-*K* (solid line) and the room-temperature (dashed line) scans are λ = 7100 *Å* and λ = 7350 *Å*, respectively] and (**b**) above the unexcited bandgap.

Possible mechanisms

As mentioned above, analysis of the power-dependent SWTSs (two of which are presented in Fig. 6.6) indicate a super-linear dependence of the ultrafast decay on carrier density. In addition, the quasi-chemical potentials of the electrons and holes must be quite high for the ultrafast decay to appear. The similarity of the SWTSs performed above and below the unexcited bandgap suggests that the ultrafast decay mechanism occurs for all wavenumbers (k). The data also suggest that the mechanism is insensitive to temperature, which eliminates phonon-mediated processes.

Electron-hole scattering is one possible mechanism which would be consistent with all of the above observations. Since the carrier densities are quite high, the effects of a non-parabolic valence band would have to be taken into account (see below). Especially in the case of the type-II QWs where the ultrafast decay of the gain/absorption is observed only when large densities of e and h are present in the GaAs layer. Another possible mechanism which may occur on an ultrafast time scale is spatial plasma expansion [for example, photon recycling]. Other carrier loss mechanisms such as Auger recombination [see e.g. Sugimura, 1982] and carrier diffusion [see e.g. Mahler *et al.*, 1988] typically take place on much longer time scales (100 picoseconds to microseconds).

Spatially-resolved time scans

To explore the spatial dependence of the gain region, a separate set of experiments were performed to measure the gain dynamics as a function of pump-probe spatial overlap. The temporal gain dynamics were measured as a function of spatial separation between 100-μm diameter pump and 20-μm diameter probe pulses.†† In Fig. 6.8, the SWTSs are plotted for increasing pump-probe spatial separation. These SWTSs show the disappearance of the ultrafast decay component of the gain (see Fig. 6.8). A similar

†† In all of the prior experiments the probe and pump were both approximately 100 μm. In the following experiment the probe was focused down to ≈ 20 μm while the pump beam diameter was held at 100 μm.

behavior is observed in type-II MQWs.‡ These observations are similar to the power-dependent SWTS data presented and discussed above in Fig. 6.6. Thus, we conclude from the spatially-dependent data that the observed ultrafast decay does not arise from in-plane plasma expansion which would manifest itself in a delay in the onset of gain for increasing pump-to-probe separation.

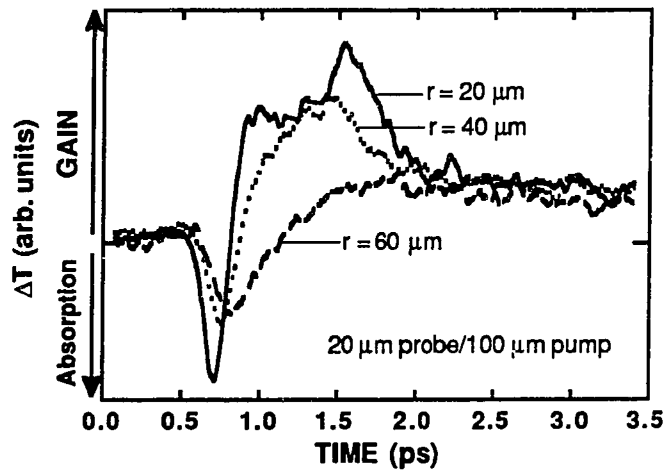

Figure 6.8. Single-wavelength time scans as a function of spatial overlap of the pump (100-μm diameter) and probe (20-μm diameter). The distance from the center of the pump to the center of the probe is denoted as r.

Enhanced e-h scattering

Ultrafast nonlinear optical response in the gain region has been investigated theoretically by solving the semiconductor Bloch equations for bulk GaAs by Paul, Binder, and Koch (1991). The semiconductor Bloch equations encompass all the relevant many-body effects for a two-band semiconductor. Solutions to the semiconductor Bloch

‡ If the spatial expansion were due to some kind of photon-assisted plasma expansion (i.e. photon recycling), the increased index change due to the increased Al content in the barriers of type-II samples would enhance this effect. This does not appear to be the case, hence this is consistent with our spatially-resolved scans.

equations modeling bulk GaAs have revealed that the gain development in bulk GaAs is similar that observed in GaAs QWs [Koch *et al.*, 1991].

Detailed calculations using the above model revealed that *e-h* scattering enhanced by the disparity in the electron versus hole potentials can lead to a significant reduction of the gain magnitude without any carrier loss. In the numerical model a non-thermal distribution of carriers are created within one LO-phonon of the band minima. The carriers thermalize through intraband *e-e* and *h-h* scattering. The holes cool much faster than the electrons because heavy-mass holes ($m_h^* = 0.45m_o$ and $m_e^* = 0.067m_o$ for bulk GaAs) "see" a much shallower potential than the light-mass electrons. In fact, the holes were found to reach an intermediate temperature which was lower than their final temperature [Paul, 1991]. The holes subsequently re-heat via interband *e-h* scattering. The enhanced *e-h* scattering reduces the phase-space filling and consequently, reduces the gain amplitude. Gain spectra computed by Paul, Binder, and Koch (1991) for bulk GaAs are presented in Fig. 6.9(a). The "0-ps" spectrum represents the spectrum for a non-thermal distribution of carriers created within a LO phonon of the conduction-band minimum and valence-band maximum. The calculated spectra exhibit a decrease both in gain bandwidth and amplitude with increasing time without any carrier loss. Fig. 6.9(a) and Fig. 6.9(b) show qualitative agreement with Fig. 6.1(b) and Fig. 6.7(a), respectively.

The model shows that an ultrafast gain decay can arise from a redistribution of carriers in the bands (*i.e.* there is no carrier loss). The theory, however, does not account for the experimentally observed absorption enhancement just before the onset of gain. However, the model assumes that the carriers are created within one LO phonon of the band minima while the carriers were created several LO-phonons above the *hh* exciton in these experiments. As suggested above, the enhanced absorption is possibly a consequence of carriers becoming "bottlenecked" one LO-phonon above the band extrema. Alternatively, general excitonic broadening could possibly account for the above

observation. Additional refinement of the model, such as inclusion of non-parabolic band-structure effects and LO-phonon scattering will likely be required to accurately model transient absorption behavior.

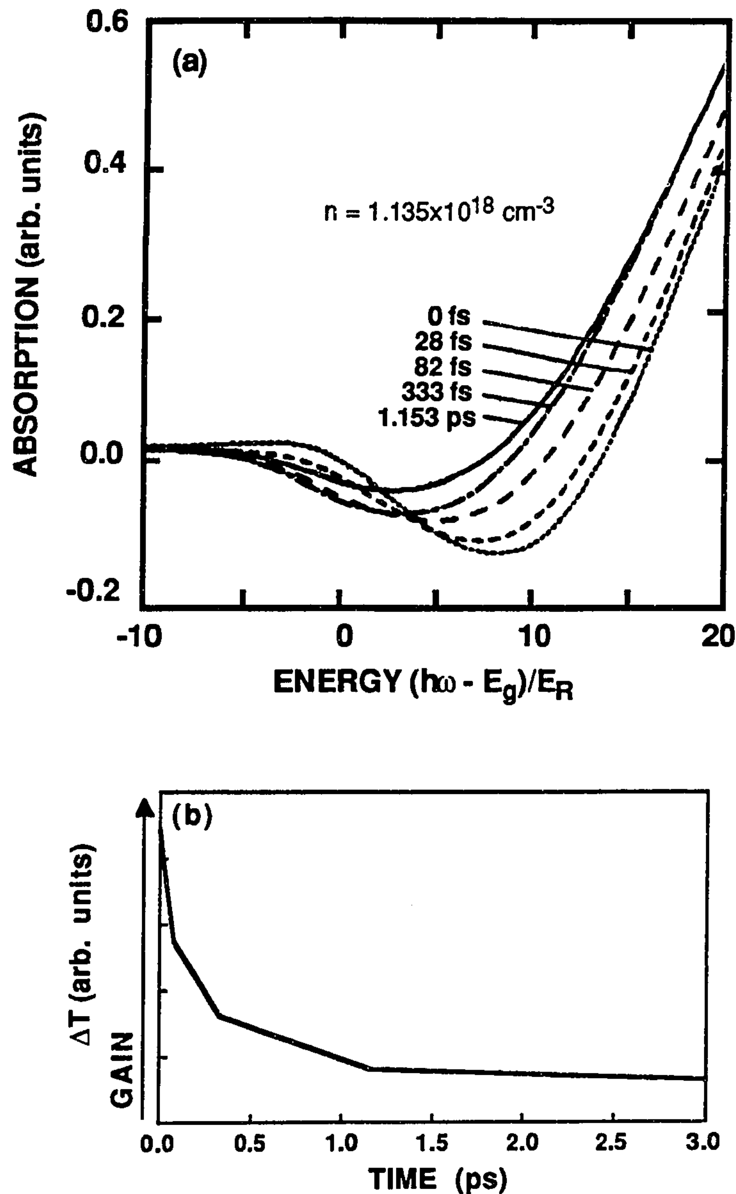

Figure 6.9. Solutions to the semiconductor Bloch equations. (a) The time-dependent gain/absorption spectra for bulk GaAs. [After Paul, Binder, and Koch.] (b) The single-wavelength time scan corresponding to the spectra shown in (a).

The key condition for the above theoretical result is the relatively shallow hole potential. The *hh* potential in QWs becomes nonparabolic and relatively shallow for even small values of $\boldsymbol{k} \neq \boldsymbol{0}$ [Chang and Schulman, 1983; Bastard and Brum, 1986]. As the wavevector, $\boldsymbol{k}$, increases, the valence band becomes non-parabolic, the dispersion begins to resemble that of bulk GaAs (i.e. $m_{transverse,hh} = 0.45 m_o$), and $k_{\mathrm{Fermi},hh} >> k_{\mathrm{Fermi},e}$. The quasi-Fermi level of the holes is sufficiently high in the QWs to place the holes in a non-parabolic, shallow potential [$E_{\mathrm{Fermi}} \geq 10\text{-}20\ meV$; see Bastard and Brum, 1986].***

Summary

Significant gain in type-II quantum wells has been observed at high excitation intensities. The temporal and spectral behavior of gain in GaAs/(Al,Ga)As type-I and type-II MQWs has been presented. The loss of electrons from the GaAs Γ-point to the lower-lying AlAs X-valley in type-II structures results in a higher gain threshold, but a longer gain lifetime because the X-valley acts as a "reservoir" for the electrons. Control of the gain magnitude has been demonstrated through the use of an applied electric field. Finally, the ultrafast (< 500 *fs*) decay of the gain and absorption in both type-I and type-II systems approximately 1.5 *ps* after excitation has been observed and attributed enhanced electron-hole scattering.

*** This argument is used to explain the higher efficiency of (In,Ga)As/(Al,Ga)As QW lasers. The strain in the (In,Ga)As material system increases the splitting of the *hh* and *lh* bands, thus preventing the holes from occupying the *lh* band which has a large transverse effective mass (i.e. larger density of states).

7 Conclusion and Future Work

In summary, the linear and nonlinear optical properties of type-II QWs have been presented. A novel, direct measurement of the quantum-confinement energy shifts in the valence band independent of the energy shifts in the conduction band using only linear spectroscopic techniques has been described. This spectroscopic technique is generally applicable to type-II heterostructures that exhibit photoluminescence from spatially indirect transitions.

In contrast, only a qualitative understanding of the nonlinear optical properties exists at this time. Nonlinearities caused by the spatial separation of photoexcited e and h plasmas has been presented. Although the spatial separation occurs on a subpicosecond time scale, the long lifetime of carriers in type-II QWs has allowed the observation of nonlinearities associated with a single-component hole plasma. The long lifetime allowed the carriers to thermalized to much deeper localized states than is possible in bulk or type-I QWs, consequently, revealing effects unobservable in type-I systems. Finally, control of the nonlinearities in type-II structures has been demonstrated through the application of an electric field.

At extremely high densities both type-I and type-II QWs exhibit an ultrafast nonlinear optical response. Electron-hole scattering enhanced by the non-parabolicity of the valence band has been suggested as a possible mechanism. The threshold for optical gain in type-II QWs is higher than in type-I QWs, however, the X-valley (in type-II QWS) extends the lifetime of the gain by acting as a "reservoir" for electrons. Furthermore, control of the gain magnitude has also been demonstrated by using an electric field to vary

the distribution of electrons between the GaAs and AlAs layers. One possible extension of this work is, of course, device applications where a reverse bias could provide a large number of electrons in a short amount of time. Another extension of the optical gain experiments would be to bring in a third optical beam for spectral hole burning of the gain region to study side-mode build-up.

The large *e-h* plasma densities and long lifetime suggests droplet formation at lower temperatures ($T \leq 5$ K) similar to that observed in Si and Ge. At much lower densities the formation of indirect excitons, which obey Bose statistics, combined with the long radiative lifetime could offer a system favorable toward the observation of Bose condensation.

A natural extension of the above work would be to study type-II structures in 1d (quantum wire) or zero-dimension (quantum box). For example, the transport properties of a single-component plasma should be studied.

REFERENCES

Adachi, S., 1985, "GaAs, AlAs, and $Al_xGa_{1-x}As$: Material parameters for use in research and device applications," *J. Appl. Phys.* **58**, pp. R1-R29.

Bandara, K. M. S. V., D. D. Coon, Byung-Sung O, Y. F. Lin, M. H. Francombe, 1988, "Exchange interactions in quantum-well subbands," *Appl. Phys. Lett.* **53**, pp. 1931-3.

Bastard, G., 1981, "Superlattice band structure in the envelope-function approximation," *Phys. Rev. B* **24**, pp. 5693-7.

Bastard, G. and Brum, J. A., 1986, "Electronic states in semiconductor heterostructures," *IEEE J. Quant. Electron.* **22**, pp. 1625-44.

Bastard, G., 1988, *Wave Mechanics Applied to Semiconductor Heterostructures* (Les Ulis Cedex, France: les editions de physique).

Binder, R., S. W. Koch, M. Lindberg, N. Peyghambarian, W. Schaefer, 1990, "Ultrafast Adiabatic Following in Semiconductors," *Phys. Rev. Lett.* **65**, pp. 899-902.

Binder, R., I. Galbraith and S. W. Koch, 1991, "Theory of band-edge nonlinearities in type-I and type-II quantum well structures," *Phys. Rev. B* **44**, pp. 3031-41.

Binder, R. and Koch, S. W., 1992, "Transient Redshift in Γ-X Aligned Type-II GaAs/AlAs Quantum Wells," unpublished.

Bleuse, J., G. Bastard, and P. Voisin, 1988, "Electric-Field-Induced Localization and Oscillatory Electro-Optical Properties of Semiconductor Superlattices," *Phys. Rev. Lett.* **60**, pp. 220-3.

Bor, Z. and Racz, B., 1985, "Group velocity dispersion and its application to pulse compression and travelling-wave excitation," *Optics Communications* **54**, pp. 165-70.

Boykin, T. B., J. P. A. van der Wagt, and J. S. Harris, 1991, "Tight-Binding Model for GaAs/AlAs Resonant Tunnel Diodes," *Phys. Rev. B* **43**, pp. 4777-84.

Casey, H. C. Jr. and Panish, M. B., 1978, *Heterostructure Lasers Part B: Materials and Operating Characteristics* (San Diego: Academic Press).

Chang, Y. C. and Schulman, J. N., 1983, "Modification of optical properties of GaAs-$Ga_{1-x}Al_xAs$ due to band mixing," *Appl. Phys. Lett.* **43**, pp. 536-8.

Chemla, D. S., 1985, "Two-Dimensional semiconductors: Recent Development," *J. Lumin.* **30**, pp. 502-19.

Chemla, D. S. and Miller, D. A. B., 1985, "Room-temperature excitonic nonlinear-optical effects in semiconductor quantum well structures," *J. Opt. Soc. Am. B* **2**, pp. 1155-73.

Chemla, D. S., D. A. B. Miller, and S. Schmitt-Rink, 1987, "Generation of Ultrashort Electrical Pulses through Screening by Virtual Population in Biased Quantum Wells," *Phys. Rev. Lett.* **59**, pp. 1018-21.

Chemla, D. S., D. A. B. Miller, and S. Schmitt-Rink, 1988, "Nonlinear Optical Properties of Semiconductor Quantum Wells," in *Optical Nonlinearities and Instabilities in Semiconductors*, edited by H. Haug (New York: Academic Press Inc.), pp. 83-120.

Chemla, D. S., D. A. B. Miller, P. W. Smith, A. C. Gossard, W. Wiegmann, 1984, "Room Temperature Excitonic Nonlinear Absorption and Refraction in GaAs/AlGaAs Multiple Quantum Well Structures," *IEEE J. Quantum Electron.* **QE-20**, pp. 265-275.

Dawson, P., C. T. Foxon and H. W. van Kesteren, 1990, "Nature of the Lowest Electron State in GaAs/AlAs Type-II Quantum Wells as a Function of AlAs Thickness," *Semicond. Sci. Technol.* **5**, pp. 54-9.

Danan, G., B. Etienne, F. Mollot, and R. Planel, A. M. Jean-Louis,m F. Alexandre, B. Jusserand, G. Le Roux, J. Y. Marzin, H. Sarary, and B. Sermge, 1987a, "Optical Evidence of the Direct-to-Indirect-Gap Transitions in GaAs-AlAs Short-Period Superlattices," *Phys. Rev. B* **35**, pp. 6207-12.

Danan, G., F. R. Ladan, F. Mollot, and R. Planel, 1987b, "Longitudinal Electric Field Effects on GaAs-AlAs Type-II Superlattices," *Appl. Phys. Lett.* **51**, pp. 1605-7.

Deveaud, B., A. Regreny, J-Y. Emery, and Chomette, 1986, "Photoluminescence study of interface defects in high-purity GaAs-GaAlAs superlattices," *J. Appl. Phys.* **59**, p. 1633-40.

Dingle, R., W. Wiegmann, and C. H. Henry, 1974, "Quantum states of confined carriers in very thin AlGaAs-GaAs heterostructures," *Phys. Rev. Lett.* **33**, pp. 665-8.

Dingle, R., 1975, "Confined Carrier Quantum States in Ultrathin Semiconductor Heterostructure," *FestkÔrperprobleme XV*, edited by H. J. Queisser, (Braunschweig: Pergamon Vieweg) pp. 21-48.

Dohler, G. H., 1985, "Doping Superlattices," in *The Technology and Physics of Molecular Beam Epitaxy*, edited by E. H. C. Parker (New York: Plenum Press) pp. 233-274.

Dubard, J., J. L. Oudar, F. Alexandre, D. Hulin and A. Orszag, 1987, "Ultrafast absorption recovery due to stimulated emission in GaAs/AlGaAs MQWs," *Appl. Phys. Lett.* **50**, pp. 821-3.

Drummond, T. J., E. D. Jones, H. P. Hjalmarson, and B. L. Doyle, 1986, *Inst. Phys. Conf. Ser.* **83**, pp. 331-3.

Duggan, G., 1985, "A critical review of heterojunction band offsets," *J. Vac. Sci. Tech. B* **3**, pp. 1224-9.

Eisenstein, G., J. M. Wiesenfeld, M. Wegener, G. Sucha, D. S. Chemla, S. Weiss, G. Raybon, and U. Koren, 1991, "Ultrafast gain dynamics in 1.5 μm multiple-quantum-well optical amplifiers," *Appl. Phys. Lett.* **58**, pp. 158-60.

Elliot, R. J., 1957, "Intensity of Optical Absorption by Excitons," *Phys. Rev.* **108**, pp. 1384-9.

Ezis, A., L. L. Liou, K. Ikossi-Anastasion, K. R. Evans, C. E. Statz, R. L. Jones, 1989, "A high gain (Ga,Al)As/GaAs heterostructure bipolar transistor with an equilibrium depleted spike-doped base," *IEEE Electron Device Letters* **10**, pp. 168-70.

Feldmann, J., R. Sattmann, E. O. Göbel, J. Kuhl, J. Hebling, K. Ploog, R. Muralidharan, P. Dawson, and C. T. Foxon, 1989, "Subpicosecond Real-Space Charge Transfer in Type-II GaAs/AlAs Superlattices," *Phys. Rev. Lett.* **62**, pp. 1892-5.

Feldmann, J., J. Nunnenkamp, G. Peter, E. O. Göbel, J. Kuhl, K. Ploog, P. Dawson, and C. T. Foxon, 1990, "Experimental Study of the Γ-X Electron Transfer in Type-II (Al,Ga)As/AlAs Superlattices and Multiple-Quantum Well Structures," *Phys. Rev. B* **42**, pp. 5809-12.

Finkman, E., M. D. Sturge, M. C. Tamargo, 1986, "X-point excitons in AlAs/GaAs superlattices," *Appl. Phys. Lett.* **49**, pp. 1299-1301.

Finkman, E., M. D. Sturge, M. H. Meynadier, R. E. Nahory, M. C. Tamargo, D. M. Hwang, and C. C. Chang, 1987, "Optical Properties and Band Structure of Short-Period GaAs/AlAs Superlattices," *J. Lumin.* **39**, pp. 57-74.

Fork, R. L., O. E. Martinez, and J. P. Gordon, 1984, "Negative dispersion using pairs of prisms," *Optics Letters* **9**, pp. 150-2.

Fu, W. S., G. R. Olbright, A. Owyoung, J. F. Klem, R. M. Biefeld, and G. R. Hadley, 1990, "Electron/hole energy shifts in narrow GaAs/AlAs quantum wells: Inhomogeneous broadening due to half-monolayer well-width fluctuations," *Appl. Phys. Lett.* **57**, pp. 1404-6.

Fu, W. S., G. R. Olbright, G. E. Poirier, R. P. Bryan, A. Paul, R. Binder, S. W. Koch and J. S. Harris, Jr., 1991, "Femtosecond Gain Dynamics in Semiconductors," in *Quant. Opto.-Elect. Conf. Technical Digest* **7**, (Optical Society of America, Washington, D.C.) pp. 144-6.

Fu, W. S., J. S. Harris, R. Binder, S. W. Koch, J. F. Klem, and G. R. Olbright, 1992, "Nonlinear optical properties and ultrafast response of GaAs/AlAs type-II quantum wells," to be published in *IEEE J. Quantum Electron., Special Issue on Ultrafast Optics and Electronics*, **28** (October).

Gigase, Y. B., C. S. Harder, M. P. Kesler, H. P. Meier, B. V. Zeghbroeck, 1990, "Threshold reduction through photon recycling in semiconductor lasers," *Appl. Phys. Lett.* **57**, pp. 1310-2.

Hall, K. L., Y. Lai, E. P. Ippen, G. Eisenstein, U. Koren, "Femtosecond gain dynamics and saturation behavior in InGaAsP multiple quantum well optical amplifiers," 1990, *Appl. Phys. Lett.* **57**, pp. 2888-90.

Haug, H. and Koch, S. W., 1990, *Quantum Theory of the Optical and Electronic Properties of Semiconductors* (Singapore: World Scientific).

Haug, H. and Schmitt-Rink S., 1984, "Electron Theory of the Optical Properties of Laser-Excited Semiconductors," *Prog. Quantum Electron.* **9**, pp. 3-100.

Hulin, D., A. Mysyrowicz, A. Antonetti, A. Migus, W. T. Masselink, H. Morkoc, H. M. Gibbs, N. Peyghambarian, 1986, "Well size dependence of exciton blue shift in GaAs multiple-quantum well structures," *Phys. Rev B* **33**, pp. 4389-92.

Ihm, J., 1987, "Effects of the Layer Thickness on the Electronic Character in GaAs-AlAs Superlattices," *Appl. Phys. Lett.* **50**, pp. 1068-70.

Jackson, J. D., 1975, *Classical Electrodynamics*, Second ed. (New York: Wiley & Sons, Inc.).

Jewell, J. L., 1991, "Microlasers," *Scientific America* **265**, pp. 56-62.

Jung, H., G. H. Dohler, E. O. Gobel, and K. Ploog, "Optical gain in GaAs doping superlattices," *Appl. Phys. Lett.* **43**, 40-2 (1983).

Kadanoff, L. P. and Baym, G., 1976, *Quantum Statistical Mechanics* (New York: W. A. Benjamin Inc.)

Kesler, M. P. and Ippen, E. P., 1987, "Subpicosecond gain dynamics in GaAlAs laser diodes, *Appl. Phys. Lett.* **51**, pp. 1765-7.

Klingshirn, C. and Haug, H., 1981, *Phys. Rev.* **70**, 315.

Knox, W. H., D. S. Chemla, D. A. B. Miller, J. B. Stark, S. Schmitt-Rink, 1989, "Femtosecond ac Stark Effect in Semiconductor Quantum Wells: Extremely Low- and High-Intensity Limits," *Phys. Rev. Lett.* **62**, pp. 1189-92.

Knox, W. H., M. C. Downer, R. L. Fork, and C. V. Shank, 1984, "Amplified Femtosecond Optical Pulses and Continuum Generation at 5-kHz Repetition Rate," *Opt. Lett.* **9**, pp. 552-4.

Knox, W. H., C. Hirlimann, D.A.B. Miller, J. Shah, D. S. Chemla, and C. V. Shank, 1986, "Femtosecond Excitation of Nonthermal Carrier Populations in GaAs Quantum Wells," *Phys. Rev. Lett.* **56**, pp. 1191-4.

Kugler, S., 1988, "Generation-recombination noise in the saturation regime of MODFET Structures," *IEEE Trans. of Electron Devices* **35**, pp. 623-8.

Lee, Y. H., A. Chavez-Pirson, S. W. Koch, H. M. Gibbs, S. H. Park, J. Morhange, A. Jeffery, N. Peyghambarian, L. Banyai, A. C. Gossard, and W. Wiegmann, 1986, "Room Temperature Optical Nonlinearities in GaAs," *Phys. Rev. Lett.* **57**, pp. 2446-8.

LePore, J. J., 1980 "An Improved Technique for Selective Etching of GaAs and $Ga_xAl_{1-x}As$," *J. Appl. Phys.* **51**, pp. 6441-2.

Lin, W. Z., L. G. Fujimoto, E. P. Ippen, and R. A. Logan, 1987, "Femtosecond carrier dynamics in GaAs," *Appl. Phys. Lett.* **50**, pp. 124-6.

Lindberg, M. and Koch, S. W., 1988, "Effective Bloch Equations for Semiconductors," *Phys. Rev. B* **38**, 3342.

Livescu, G., D. A. B. Miller, D. S. Chemla, M Ramaswamy, T. Y. Chang, N. Snuer, A. C. Gossard, and J. H. English, 1988, "Free Carrier and Many-Body Effects in Absorption Spectra of Modulation Doped Quantum Wells," *IEEE J. Quantum Electron.* **QE-24**, pp. 1677-84.

Macleod, H. A., 1989, *Thin Film Optical Filters*, Second Edition (New York: McGraw-Hill).

Mahan, G. D., 1967a, "Excitons in Degenerate Semiconductors," *Phys. Rev.* **153**, pp. 882-9.

Mahan, G. D., 1967b, "Excitons in Metals: Infinite Hole Mass," *Phys. Rev.* **163**, pp. 612-7.

Mahler, G., T. Kuhn, A. Forchel and H. Hillmer, 1988, "Optical Decay and Spatial Relaxation," *Optical Nonlinearities and Instabilities in Semiconductors*, edited by H. Haug, (New York: Academic Press Inc.) pp. 159-80.

Mendez, E. E., F. Agullo-Rueda, and J. M. Hong, 1988, "Stark localization in GaAs-GaAlAs superlattices under an electric field," *Phys. Rev. Lett.* **60**, pp. 2426-9.

Mendez, E. E., G. Bastard, L. L. Chang, and L. Esaki, 1982, "Effect of an electric field on the luminescence of GaAs quantum wells," *Phys. Rev. B* **26**, pp. 7101-3.

Meynadier, M.- H., R. E. Nahory, J. M. Worlock, M. C. Tamargo, J. L. de Miguel, and M. D. Sturge, 1988, "Indirect-direct anticrossing in GaAs/AlAs superlattices induced by an Electric Field: Evidence of Γ-X splitting," *Phys. Rev. Lett.* **60**, pp. 1338-41.

Miller, D. A. B., D. S. Chemla, T. C. Damen, A. C. Gossard, W. Wiegmann, T. H. Wood and C. A. Burrus, 1984, "Band-Edge Electroabsorption in Quantum Well Structures," *Phys. Rev. Lett.* **53**, pp. 2173-6.

Miller, D. A. B., D. S. Chemla, T. C. Damen, A. C. Gossard, W. Wiegmann, T. H. Wood and C. A. Burrus, 1985, "Electric Field Dependence of Optical Absorption Near the Band Gap of Quantum Well Structures," *Phys. Rev. B* **32**, pp. 1043-60.

Miller, R. C. and Kleinman, D. A., 1985, "Excitons in GaAs Quantum Wells," *J. Lumin.* **30**, pp. 520-7.

Miller, R. C., D. A. Kleinman, and A. C. Gossard, 1984, "Energy gap discontinuity and effective masses for GaAs-AlGaAs quantum wells," *Phys. Rev. B* **29**, pp. 7085-7.

Miller, R. C., D. A. Kleinman, W. T. Tsang, and A. C. Gossard, 1981, "Observation of the excited level of excitons in GaAs quantum wells," *Phys. Rev. B* **24**, pp. 1134-6.

Moore, K. J., P. Dawson and C. T. Foxon, 1986, *Phys. Rev. B* **34**, 6022.

Moore, K. J., P. Dawson and C. T. Foxon, 1987, "Optical Studies of Type-I and Type-II Recombination in GaAs-AlAs Quantum Wells," *Journal de Physique*, supplement au n∞11, Tome **48**, pp. C5-525-8.

Morrow, R., 1987, "Establishment of an effective-mass Hamiltonian for abrupt heterojunction," *Phys. Rev. B* **35**, pp. 8074-9.

Mysyrowicz, A., D. Hulin, A. Antonetti, A. Migus, W. T. Masselink, and H. Morkoc, 1986, "Dressed Excitons in a Multiple-Quantum-Well Structures: Evidence for an Optical Stark Effect with Femtosecond Response Time," *Phys. Rev. Lett.* **56**, pp. 2748-51.

Olbright, G. R., 1987, "Femtosecond Dynamics and Nonlinear Effects of Electron-Hole Plasma in Semiconductor Doped Glasses," **Ph.D. Dissertation** (University of Arizona, Tucson).

Olbright, G. R., J. F. Klem, A. Owyoung, T. M. Brennan, R. Binder, S. W. Koch, 1990a, "Many-body Effects in the Luminescence of Highly Excited Indirect Superlattices," *J. Opt. Soc. Am. B* **7**, pp. 1473-80.

Olbright, G. R., W. S. Fu, J. Klem, T. E. Zipperian, R. Binder and S. W. Koch, 1990b, "Femtosecond Optical Nonlinearities in GaAs/AlAs Type-II Superlattices," in *Ultrafast Phenomena VII*, edited by C. Harris, E. Ippen and A. H. Zewail (New York: Springer-Verlag), pp. 1358-60.

Olbright, G. R., W. S. Fu, A. Owyoung, J. F. Klem, R. Binder, I. Galbraith and S. W. Koch, 1991a, "CW and Femtosecond Optical Nonlinearities in Type-II Quantum Wells," *Phys. Rev. Lett.* **66**, pp. 1358-61.

Olbright, G. R., W. S. Fu, J. F. Klem, H. M. Gibbs, G. Kithrova, R. Pon, B. Fluegel, K. Meissner, N. Peyghambarian, R. Binder, I. Galbraith and S. W. Koch, 1991b, "Nonlinear Optical Properties of Type-II Quantum Wells," *Phys. Rev. B* **44**, pp. 3043-53.

Oudar, J. L., D. Hulin, A. Migus, A. Antonetti, and F. Alexandre, 1985, "Subpicosecond Spectral Hole Burning Due to Nonthermalized Photoexcited Carriers in GaAs," *Phys. Rev. Lett.* **55**, pp. 2074-7.

Paul, A., R. Binder, S. W. Koch, 1991, "Ultrafast Optical Response in Highly Excited GaAs," private communications.

Peyghambarian, N., H. M. Gibbs, and J. L. Jewell, A. Antonetti, A. Migus, D. Hulin, and A. Mysyrowicz, 1984, "Blue Shift of the Exciton Resonance Due to Exciton-Exciton Interactions in a Multiple-Quantum-Well Structure," *Phys. Rev. Lett.* **53**, pp. 2433-6.

Peyghambarian, N., S. W. Koch, M. Lindberg, B. Fluegel, and M. Joffre, 1989, "Dynamic Stark Effect of Exciton and Continuum States in CdS," *Phys. Rev. Lett.* **62**, pp. 1185-8.

Pezeshki, B., S. M. Lord, T. B. Boykin, J. S. Harris, Jr., 1991 "AlGaAs/AlAs Quantum-Well Modulator for 6328-Å Operation," *Elect. Lett.* **27** pp. 1971-3.

Pezeshki, B., S. M. Lord, T. B. Boykin, B. L. Shoop, and J. S. Harris, Jr., "Electro-Absorption in GaAs/AlAs Quantum Wells," 1992, submitted for publication.

Reitze, D., 1990, private communications.

Ruden, P. and DÔhler G. H., 1983, *Phys. Rev. B* **27**, pp. 3538-46.

Saeta, P., J. F. Federici, R. J. Fischer, B. I, Greene, L. Pfeiffer, R. C. Spitzer, and B. A. Wilson, 1989, "Γ to X transport of photoexcited electrons in type-II GaAs/AlAs multiple quantum well structures," *Appl. Phys. Lett.* **54**, pp. 1681-3.

Schaefer, W., R. Binder, and K. Schuldt, 1988, *Z. Physik B* **70**, 145.

Schmitt-Rink, S., D. S. Chemla and D. A. B. Miller, 1985, *Phys. Rev. B* **32**, 6601.

Schmitt-Rink, S., D. S. Chemla, and D.A.B. Miller, 1989, "Linear and nonlinear optical properties of semiconductor quantum wells," Adv. Phys. **38**, pp. 89-188.

Shah J., 1989, "Photoexcited Hot Carriers: From CW to 6 fs in 20 Years," *Solid State Electronics* **32**, pp. 1051-6.

Shank, C. V., R. L. Fork, R. F. Leheny, and J. Shah, 1979, "Dynamics of Photoexcited GaAs Band-Edge Absorption With Subpicosecond Resolution," *Phys. Rev. Lett.* **42**, pp. 112-5.

Shank, C. V., R. L. Fork, B. I. Greene, C. Weisbuch, and A. C. Gossard, 1982, "Picosecond Dynamics of Highly Excited Multiquantum well structures," *Surface Science* **113**, pp. 108-11.

Shank, C. V., R. L. Fork, R. Yen, J. Shah, B. I. Greene, A. C. Gossard and W. Weisbuch, 1983, "Picosecond Dynamics of Hot Carrier Relaxation in Highly Excited Multi-Quantum Well Structures," *Solid State Commun.* **47**, pp. 981-3.

Shinada, M. and Sugano, S., 1966, "Interband optical transitions in extremely anisotropic semiconductors. I: Bound and unbound exciton absorption," *J. Phys. Soc. Japan* **21**, pp. 1936-46.

Shindo, K., 1970, *J. Phys. Soc. Japan* **29**, 287.

Speriosu, V. S. and Vreeland, T. Jr., 1984, "X-ray rocking curve analysis of superlattices," *J. Appl. Phys.* **56**, pp. 1591-8.

Stern, F. and Woodall, J. M., 1974, "Photon recycling in semiconductor lasers," *J. Appl. Phys.* **45**, pp. 3904-9.

Sugimura, A., 1982, "Band-to-Band Auger effect in Long Wavelength Multinary III-V Alloy Semiconductor Lasers," *IEEE J. of Quantum Electron.* **QE-18**, pp. 352.

Tai, K., A. Mysyrowicz, R. J. Fischer, R. E. Slusher, and A. Y. Cho, 1989, "Two-Photon Absorption Spectroscopy in GaAs Quantum Wells," *Phys. Rev. Lett.* **62**, pp. 1784-7.

Tanaka, S., T. Kuwata, T. Hokimoto, H. Kobayashi and H. Saito, 1983, "Picosecond dynamics of optical gain due to electron-hole plasma in GaAs under near band-gap excitation," *J. Phys. Soc. Japan* **52**, pp. 677-10.

Tanaka, M. and Sakaki, H., 1987, "Atomistic Models of Interface Structures of GaAs-$Al_xGa_{1-x}As$(x = 0.2-1) quantum wells grown by interrupted and uninterrupted MBE," *J. Crys. Growth* **81**, pp. 153-8.

van Kesteren, H. W., E. C. Cosman, P. Dawson, K. J. Moore, and C. T. Foxon, 1989, "Order of the X conduction-band valleys in type-II GaAs/AlAs quantum wells," *Phys. Rev. B* **39**, pp. 13426-33.

Vinter, B., 1977, "Many-Body Effects in n-type Si inversion layers. II. Excitation to higher subbands," *Phys. Rev. B* **15**, pp. 3947-58.

Weber, C., C. Klingshirn, D. S. Chemla, D. A. B. Miller, J. E. Cunningham, C. Ell, 1988, "Gain measurements and bandgap renormalization in GaAs/$Al_xGa_{1-x}As$ multiple quantum well structures," *Phys. Rev. B* **38**, pp. 12748-52.

Weisbuch, C., R. Dingle, A. C. Gossard, and W. Wiegmann, 1981, "Optical characterization of interface disorder in GaAs-$Ga_{1-x}Al_xAs$ multiple quantum well structures," *Solid State Commun.* **38**, pp. 709-12.

Wilson, B. A., C. E. Bonner, R. C. Spitzer, P. Dawson, K. J. Moore, and C. T. Foxon, "Recombination Mechanisms in Type-II (GaAs/AlAs) Heterostructures," 1988, *J. Vac. Sci. Technol. B* **4**, pp. 1156-60.

Wilson, B. A., P. Dawson, C. W. Tu, and R. C. Miller, 1986, "Optical evidence of staggered band alignments in (Al,Ga)As/AlAs multiple quantum-well structures," *J. Vac. Sci. Technol. B*, **4**, pp. 1037-40.

Wolford, D. J., T. F. Kuech, T. W. Steiner, J. A. Bradley, M. A. Gell, D. Ninno, and M. Jaros, 1988, *Superlattices and Microstructures* **4**, pp. 525-35.

Yamanishi, M., 1987, "Field-induced optical nonlinearities due to virtual transitions in semiconductor quantum well structures," *Phys. Rev. Lett.* **59**, pp. 1014-7.

Yariv, A., 1989, *Quantum Electronics*, Third Edition (New York: Wiley).

Zimmermann, R., K. Lilimann, W. D. Kraeft, D. Knemp, R. Roepke, 1978, "Dynamical Screening and Self-Energy of Excitons in the Electron-Hole Plasma," *Phys. Stat. Sol. B* **90**, pp. 175-85.

Zimmermann, R., 1987, *Many-Particle Theory of Highly Excited Semiconductors* (Berlin: Teubner Texte zur Physik; 18).